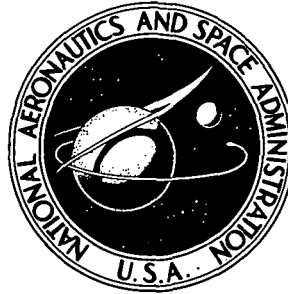


N 73-28178



NASA TECHNICAL NOTE

NASA TN D-7240

REVISED

CASE FILE
COPY

NASA TN D-7240

RETRIEVAL OF DISPERSIVE AND CONVECTIVE
TRANSPORT PHENOMENA IN FLUIDS USING
STATIONARY AND NONSTATIONARY
TIME DOMAIN ANALYSIS

by J. Briscoe Stephens and Robert M. St. John

*George C. Marshall Space Flight Center
Marshall Space Flight Center, Ala. 35812*

1. Report No. NASA TN D-7240 (REVISED)		2. Government Accession No.		3. Recipient's Catalog No.	
4. Title and Subtitle RETRIEVAL OF DISPERSIVE AND CONVECTIVE TRANSPORT PHENOMENA IN FLUIDS USING STATIONARY AND NONSTATIONARY TIME DOMAIN ANALYSIS				5. Report Date August 1973	
				6. Performing Organization Code	
7. Author(s) J. Briscoe Stephens and Robert M. St. John*				8. Performing Organization Report No. M-106	
9. Performing Organization Name and Address George C. Marshall Space Flight Center Marshall Space Flight Center, Alabama 35812				10. Work Unit No.	
				11. Contract or Grant No.	
12. Sponsoring Agency Name and Address National Aeronautics and Space Administration Washington, D.C. 20546				13. Type of Report and Period Covered Technical Note	
				14. Sponsoring Agency Code	
15. Supplementary Notes Prepared by Aero-Astroynamics Laboratory, Science and Engineering * University of Oklahoma, Norman, Oklahoma					
16. Abstract <p>Simultaneously occurring dispersive and convective components of fluid kinematics are obtained by a time domain analysis of optically retrieved temporal histories of the transport phenomena.</p> <p>Utilizing triangulation of collimated optical fields of view from two radiometers to obtain the temporal histories of the intensity fluctuations associated with the transport phenomena has enabled investigators to retrieve the local convective transport by employing correlation statistics. The location of the peak in the covariance curve determines the transit time from which the convection velocity is calculated; whereas, the change in shape of the peak in the covariance curve determines the change in average frequency of the wave packet from which the dispersion velocity is calculated. Thus, our two-component analysis requires the maximum possible enhancement of the delineation for the transport. The convection velocity is the result of a fixed reference frame calculation; whereas, the dispersion velocity is the result of a moving reference frame calculation. This moving reference frame is constrained to move along the common streamline at the convection velocity.</p> <p>The transport probability has been developed as an estimate of whether the transport phenomena have been measured along the common stream, and also provides an indication of whether the period of stationarity is sufficient to provide adequate information enhancement. The time information is suppressed by the utilization of a fourth-order autocovariance curve. This moving frame delineation is analyzed in the time domain with the wave packet algorithm for the dispersion parameters. The effectiveness of these models is demonstrated on empirical data sets obtained in glow discharge investigations, cold jet experiments, and air quality investigations.</p>					
17. Key Words (Suggested by Author(s)) Correlation Analysis Fourier Analysis, Statistical Time Domain Analysis Environmental Transport Analysis Glow Discharge Jet Exhaust				18. Distribution Statement	
19. Security Classif. (of this report) Unclassified		20. Security Classif. (of this page) Unclassified		21. No. of Pages 105	
				22. Price* \$3.00	

* For sale by the National Technical Information Service, Springfield, Virginia 22151

ACKNOWLEDGMENTS

The empirical facet of this research was conducted under the direction of Dr. Fritz R. Krause, Flight Data Statistics Office, Marshall Space Flight Center, Huntsville, Alabama. For his inspiration, understanding aid, and excellent advice during the course of this project and the subsequent report, I wish to express to Dr. Krause my deepest gratitude.

I also wish to thank Dr. J.M. Canfield, Physics Department, University of Oklahoma, Norman, Oklahoma, who provided the conceptual insight that led to the wave packet formulation for turbulence transport, and to Dr. M.Y. Su, Northrop Services, Inc., Huntsville, Alabama, for his illuminating review of this report.

This research was performed as a part of the Graduate Cooperative Training Program at Marshall Space Flight Center. I wish to acknowledge the outstanding support of Mark L. Russell who coordinates this program, and to express my appreciation to the Aero-Astroynamics Laboratory for its active participation in this program. I owe a debt of gratitude to Evelyn Carter for preparing the illustrations and to Sara Hightower for editing this report.

To the many others whose names do not appear in this acknowledgments but whose advice and encouragement have contributed to the successful completion of this report, I express my deepest gratitude.

TABLE OF CONTENTS

Section	Page
I. BACKGROUND	1
A. Introduction	1
B. Fluid Model	2
C. Fundamental Averaging Techniques	6
II. COVARIANCE OF SEPARATED PROBES	10
A. Introduction	10
B. Accumulative Covariance Technique	10
C. Transit Time and Coherence Time	14
D. Statistical Error and Period of Stationarity	17
E. Probability of Retrieving Information About Transport Phenomena	22
III. WAVE DESCRIPTION OF THE TRANSPORT PHENOMENA	25
A. Introduction	25
B. Wave Description of the Covariance Curve	25
C. The Wave Packet Interpretation for the Covariance Curve	33
D. Classification of Covariance Curves	35
E. Separation of Convective and Dispersive Transport Phenomena ..	47
IV. APPLICATIONS TO REMOTELY SENSED DATA	52
A. Introduction	52
B. The Crossed-Beam Test Arrangement	52
C. Ion and Electron Transport in the Glow Discharge	58
D. Convective and Dispersive Transport in a Supersonic Jet Shear Layer	66
E. Convection and Dispersion in the Atmosphere	73
V. SUMMARY AND CONCLUSIONS	79
APPENDIX: THE ENERGY DENSITY WAVE NUMBER SPECTRUM	81
REFERENCES	96

LIST OF ILLUSTRATIONS

Figure		Page
1.	Space-fixed control surface in a flowing fluid	3
2.	The notation of the time series	7
3.	The first two moments about the mean	8
4.	A one-event, two-dimensional physical model	15
5.	Phaser diagram for coherence	16
6.	Accumulative quantized covariance	18
7.	Accumulative error curve	20
8.	Accumulative error curve from cold jet data (Fisher's, Johnson's)	21
9.	Accumulative error curve for a nonstationary process	22
10.	Probability of commonality	24
11.	Graphical relation between input spectrum and energy density spectrum	26
12.	Autocovariance curve in time domain	26
13.	Energy density spectrum of a narrowband process	27
14.	Spectrum of the wave packet algorithm	29
15.	Autocorrelation curves for moving striations	34
16.	Covariance curve from the wave packet algorithm	36
17.	Schematic representation of the envelope for the spectrum from narrowband and broadband processes	38
18.	Flow diagram of spectral decomposition program	39
19.	Autocovariance curves of narrowband and broadband processes	41

LIST OF ILLUSTRATIONS (Continued)

Figure		Page
20.	Transform of square input with integral spacing	42
21.	Compressed bandwidth	43
22.	Broadband folding	44
23.	Broadband folding at average frequency	45
24.	Wave packet algorithm fit of elliptical envelope	48
25.	Wave packet algorithm fit of broadband process	49
26.	Retrieval of convective and dispersive transport	50
27.	Schematic cross section for the crossed-beam monitoring system in a turbulent flow	53
28.	Crossed-beam test configuration for the cold jet	57
29.	Experimental setup for glow discharge	58
30.	Forward-moving striation	59
31.	Backward-moving striation	61
32.	Separation of electron and ion transport	62
33.	Data reduction block diagram for MLTCOR	63
34.	Ion striation model	64
35.	Electron packet flow in the glow discharge	67
36.	Convection and dispersion velocities for electron flow	68
37.	Space-time correlation curves for cold air jet	69
38.	Typical energy density spectrum for cold air jet	71

LIST OF ILLUSTRATIONS (Concluded)

Figure		Page
39.	Prediction of lateral scales in cold jet	72
40.	Atmospheric crossed-beam detection system for clear-air turbulence. . . .	73
41.	Crossed-beam and anemometer comparisons	74
42.	Crossed-beam test arrangement for fan system.	76
43.	Smoke-plume convection and dispersion transport	77
44.	Remote mapping of high stack emissions.	78
A-1.	Atmospheric energy density spectrum	94

LIST OF TABLES

Table		Page
1.	Mapping of Algorithm Deviation Residue for an Average Frequency of 5 Hz.	47
A-1.	Spectrum from 0.125 to 12.5 Hz	90
A-2.	Spectrum from 12.625 to 25.0 Hz	91
A-3.	Spectrum from 25.125 to 37.5 Hz	92
A-4.	Spectrum from 37.625 to 50.0 Hz	93

RETRIEVAL OF DISPERSIVE AND CONVECTIVE TRANSPORT PHENOMENA IN FLUIDS USING STATIONARY AND NONSTATIONARY TIME DOMAIN ANALYSIS

SECTION I. BACKGROUND

A. Introduction

New algorithms have been developed which permit the separation and consistent interpretation of the simultaneously occurring kinematics — convection and dispersion — associated with stationary and nonstationary fluid transport.

The separation of the fluid kinematics of the transport process poses both an experimental and an analytical problem. The experimental problem is to retrieve sufficiently detailed local information for a field description of the scalar quantities without introducing probe interference on the field or the modes of transport. The solution utilized was to remotely sense by optical means — that is, using radiometers — a local flow field by crossed-beam triangulation. The temporal information thus retrieved contains the signature of the space-time variations of the transmission coefficients (absorption, scattering, and emission)[1].

The analytical problem is to extract a description of the transport kinematics in terms of the field parameters that are related to the accepted description of turbulence flows. A description of the convective component of the transport can be retrieved from the temporal histories of the fluctuations by using two radiometers and cross-correlating these histories. This cross-correlation results in the average temporal relationship between events occurring at two different points along the streamline. This transit time is used in conjunction with the transit distance — the distance along the streamline between the points of observation — to calculate the convection speed. This experimental and analytical procedure is called the crossed-beam correlation technique.

Fluid transport investigations with the crossed-beam correlation technique have been conducted in cold jet flows [2], in tropospheric turbulence flows [3], in glow discharges [4], and in combustion processes [5]. The analysis used to interpret these experimental results accounted for only the convective component of the transport. Consequently, an incomplete description was obtained in that it failed to account for the dispersive transport component. This analysis also failed to afford a systematic classification procedure and failed to establish the probability for the transport retrieval occurring along a common streamline.

The description developed here compresses the temporal fluctuations into a wave packet; whereas, the presently accepted description uses an infinitely long wave description. A wave packet is recognized by its finite coherence length, whose value can be determined

from correlation analysis. The key to the separation of transport phenomena is the recognition that the characteristics of the wave packet obtained from the finite data record contain the signature of the component of the transport phenomena as viewed in a moving reference frame. The accumulative time averages obtained from the summation of piecewise estimated statistical averages will provide results that differ according to the sensitivity of the accumulation procedure for the various transport phenomena. Analysis of data sequences in terms of the characteristics of the wave packet and the temporal averages of the accumulative procedures results in enhanced signatures for the desired separation of the simultaneous but different transport phenomena.

Section II reviews the ordinary correlation techniques used for stationary data and includes additional criteria that have been developed for the recognition and processing of nonstationary data in a fixed reference frame. Section III illustrates the transformation of the covariance curve into a wave packet description in a moving reference frame. When the convection signature is suppressed, the covariance curve is then fitted with an algorithm that affords a wave packet description of the experimental time histories from more than one probe. The parameters obtained for this wave packet afford a systematic classification procedure of the process in terms of a bandwidth-frequency ratio. The rate of change of the average frequency in the moving frame gives the signature whereby the dispersion is calculated. This unique description affords separation of the components associated with the transport phenomena.

In Section IV, this change analysis is applied to data obtained from both laboratory and field test experiments, representing stationary and nonstationary ensembles, respectively. Since dispersion tends to make any data record nonstationary for large scale waves, a discussion of nonstationary data is mandatory. Considering all data that have been evaluated, the effectiveness of the proposed methods is then assessed from an evaluation of all the results.

B. Fluid Model

An analysis of the turbulent transport process which describes the coupling between the mean transport and the turbulent fluctuations enables us to demonstrate the need for a semiempirical, statistical technique in the investigation of fluid transport. Our fluid model (Fig. 1) assumes a flowing turbulent fluid that is both inhomogeneous and stationary. The inhomogeneities are primarily a result of velocity and density fluctuations in the fluid generated by the shear stresses associated with the transport process. The density, ρ , and the center of mass velocity, \vec{v} , can be described in terms of a mean component, $(-)$, and a fluctuating component, $(-)'$, as

$$\rho(t) = \bar{\rho} + \rho(t)' \quad (1)$$

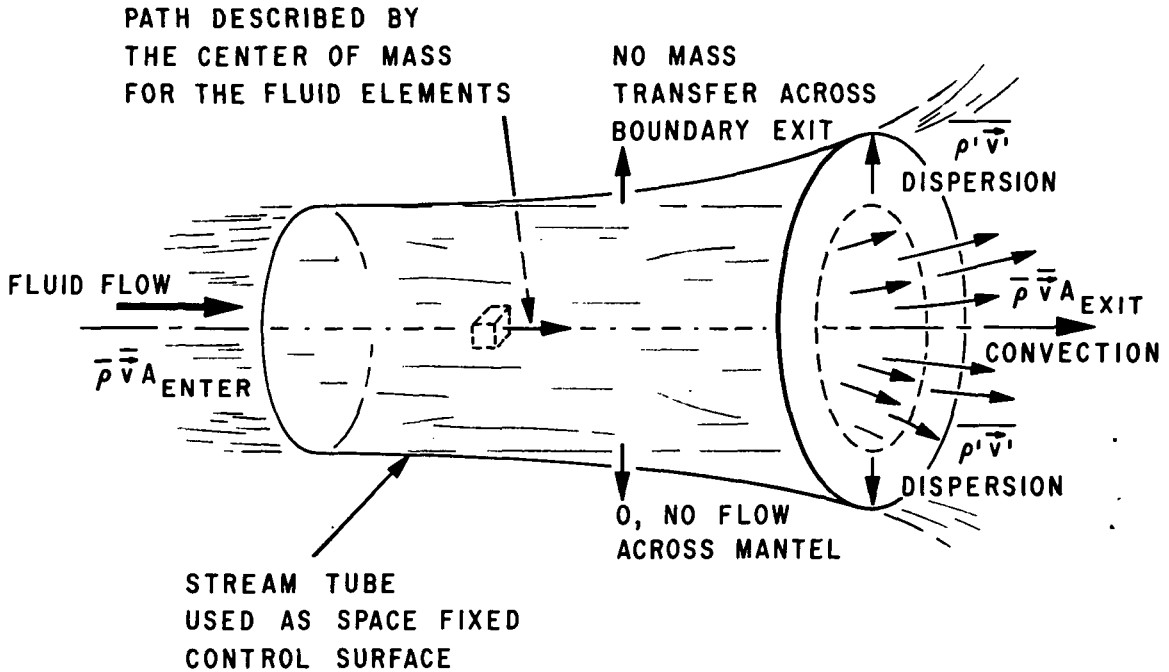


Figure 1. Space-fixed control surface in a flowing fluid.

and

$$\vec{v}(t) = \vec{\bar{v}} + \vec{v}(t)'. \quad (2)$$

The condition of stationarity implies that the mean values are independent of time. This description is applicable to multicomponent fluid transport such as that associated with moving striations in a glow discharge – the shear layer formed by the exhaust of an air jet, and the atmospheric transport phenomena – all of which will be considered later as the empirical results of convection and dispersion are evaluated.

To analytically establish the significance of a description for the fluid transport involving both a convective and dispersive component of transport, we must first define a space-fixed control surface. The control surface is assumed to lie along the axis of a streamline, where the streamline is defined to be the path of the center of mass which is generated by the motion of a small fluid volume. While this discussion will be limited to the motion of the center of mass, this streamline can be defined more generally so that it includes any conservative property [6]. The control surface will be the stream tube in the flow selected such that the mass average flux across the mantle is zero. This directly implies that:

1. The mass flux entering one end of the control surface is exiting at the other end.

2. In an expanding flow, the area of the exit of the tube is greater than the area of the entrance.

In addition, we can assume that within the stream tube, a local isotropy exists.

The continuity equation for the fixed system is

$$\frac{\partial \rho}{\partial t} = \text{div } \rho \vec{v} . \quad (3)$$

This equation, when written for the stream tube in terms of the mean and fluctuating components, becomes

$$\int_V \int \int \frac{\partial [\bar{\rho} + \rho(t)']}{\partial t} dV = \int_V \int \int \sum_{j=1}^3 \frac{\partial}{\partial x_j} [\bar{\rho} + \rho(t)'] [\bar{v}_j + v(t)']_j dV . \quad (4)$$

When the time average is taken, the last equation reduces to

$$\int_V \int \int \frac{\partial \bar{\rho}}{\partial t} dV = \int_V \int \int \text{div} \left(\bar{\rho} \bar{\vec{v}} + \overline{\rho' \vec{v}'} \right) dV , \quad (5)$$

since the mean component is time-independent and the time average of the fluctuating component is zero. This follows since

$$\overline{\rho'} = \frac{1}{T} \int_0^T \rho' (t) dt = 0 , \quad (6)$$

$$\overline{\rho' \vec{v}'} = \frac{1}{T} \bar{\vec{v}} \int_0^T \rho' (t) dt = 0 , \quad (7)$$

and

$$\overline{\overline{\rho} \vec{v}'} = \frac{1}{T} \overline{\rho} \int_0^T \vec{v}'(t) dt = 0, \quad (8)$$

if we assumed a self-stationary flow. By utilizing Gauss' theorem, the right side of the continuity equation for the mean motion, equation (5), can be rewritten as the stream tube surface integral:

$$\int_V \frac{\partial \overline{\rho}}{\partial t} dV = \int_S \overline{\rho} \vec{v} dS + \int_S \overline{\rho'} \vec{v}' dS. \quad (9)$$

Consider now the significance of the terms of this equation.

Term 1

$$\int_V \frac{\partial \overline{\rho}}{\partial t} dV = 0, \quad (10)$$

since the flow is constant.

Term 2

$$\int_{S_{\text{end}}} \overline{\rho} \vec{v} dS. \quad (11)$$

The term is the flux of the time-averaged to volume concentrations which are convected with the time-averaged mass velocity \vec{v} in the stream tube. By definition of the stream tube, the mass transport from this term across the mantle is zero. The integral over one end of the stream tube represents the flow measured by a probe in a fixed reference frame and will be referred to as convection.

Term 3

$$\int_S \left[\frac{1}{T} \int_0^T \rho'(t) \vec{v}'(t) dt \right] d\vec{S}. \quad (12)$$

The average longitudinal component of this term is zero, since the backward expansion of a small fluid element will be cancelled by the forward expansion of the next small fluid element as a result of the time averaging. This is why a probe, which is a space-fixed observer, in the flow cannot measure this fluctuating longitudinal transport. The transverse component is the dispersive transport which results in the lateral expansion of the stream tube. This term represents the covariance between the convecting and convected properties as measured simultaneously at the same spot by both a space-fixed observer and an observer moving with the convected fluid.

This dispersive term in the continuity equation for the mean motion is the term that has remained analytically unsolved [7]. The new approach introduced in this report to solve the problem is the employment of empirical information retrieved by a remote optical detection system which monitors the density fluctuations, and it is coupled with new statistical correlation techniques to extract the dispersive information. When the cross-covariance curves are obtained for two path lengths along a common streamline, the change in the wave packet represents the signature for the mean longitudinal fluctuations of the mass transport as seen by the moving observer. Since we are assuming local isotropy, this mass transport is the dispersion. To verify that the measurements are taken from probes on a common streamline, it is necessary to calculate the transport probability.

Before discussing this probability calculation, it is necessary to define our basic statistical techniques. To begin, we will examine the single-probe averaging techniques, which are fundamental to this information retrieval analysis.

C. Fundamental Averaging Techniques

The averaging techniques are used to establish probe moments. The single-probe averages used are the mean and variance, and the two-probe average used is the covariance curve. Although N-probe averages do exist, they are beyond the scope of this investigation. Our immediate attention will be focused on an evaluation of the first and second moments for single-probe averages.

Assume that the behavior of a physical parameter in the fluid model can be expressed as the time history of the amplitude fluctuation, $x(t)$, of this parameter. This temporal history is thus a function of the running parameter t (Fig. 2), the relative time. The range of the relative time is from zero to T . The interval between discrete samples is given by the sampling interval, Δt , such that

$$T = N \Delta t, \tag{13}$$

where the integer N is the total number of discrete samples in the data record. For easier analysis and manipulation, the total data record can be subdivided into equal time segments, ΔT , called pieces, such that

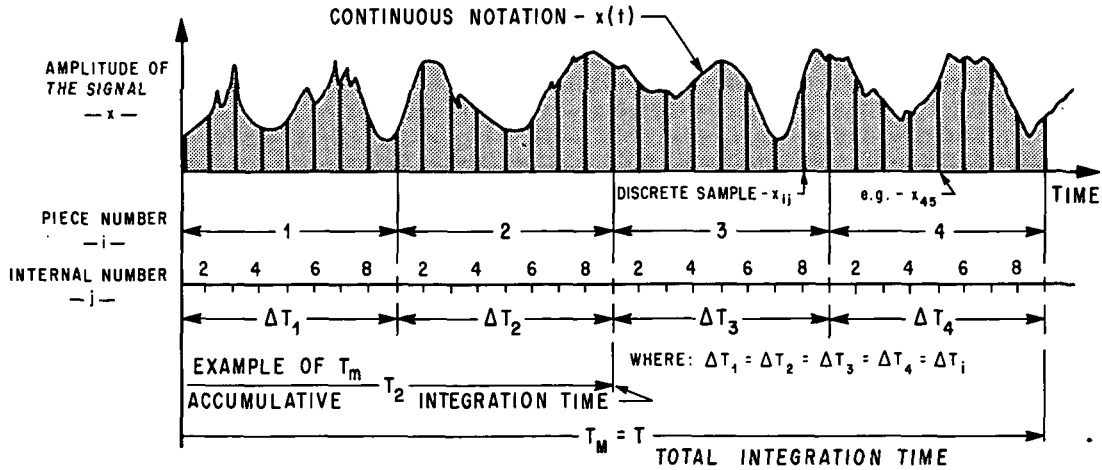


Figure 2. The notation of the time series.

$$T = T_M = M \Delta T, \quad (14)$$

where the integer M is the total number of pieces available in the data record. This piecewise subdivision of the total data record not only affords more computational flexibility, but this piecewise subdivision also affords an opportunity to apply statistical techniques for information enhancement and analysis. In fact, this piecewise analysis is the cornerstone in the evaluation of nonstationary data records. Each piece of data record contains n discrete samples, such that

$$N = M n \quad (15)$$

or

$$\Delta T = n \Delta t. \quad (16)$$

The accumulative results of a summation of a number of pieces of the data are signified by the subscripted lower case m . For example, T_m means the interval time from the start of the data record to the end of the m th piece, or N_m is the number of data points from zero to the end of the m th piece of data. The accumulative result will be precisely contrasted to the piecewise result, which is given by the subscript i .

The first two moments of the single probe averages are schematically shown in Figure 3. The first moment \bar{x}_i is

MEAN AND VARIANCE

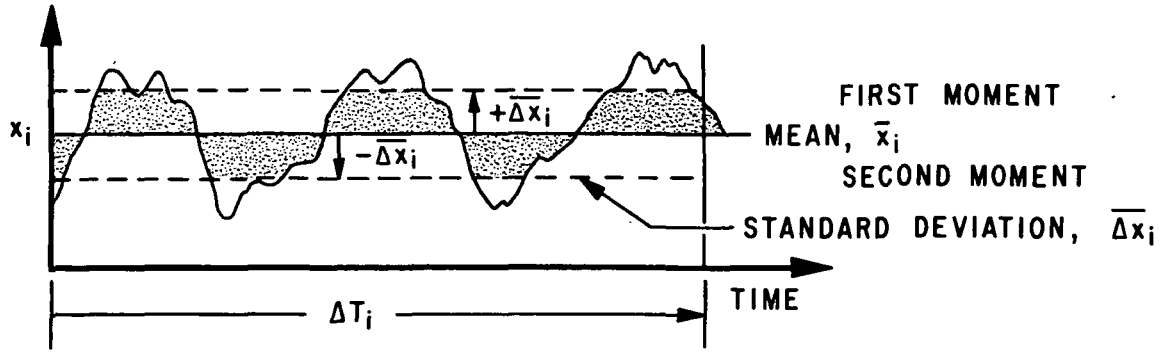


Figure 3. The first two moments about the mean.

$$\bar{x}_i = \frac{1}{\Delta T} \int_{(i-1)\Delta T}^{i\Delta T} x_i(t) dt, \quad (17)$$

which is known as the mean value of the i th piece of data record. The integral is used here as a shorthand notation for the summation when the summation represents a continuous sum. In electrical terms, \bar{x}_i is the dc component of the time series, and $[x_i(t) - \bar{x}_i]$ is the ac component of the time series.

The second moment $\overline{x_i^2}$ is

$$\overline{x_i^2} = \frac{1}{\Delta T} \int_{(i-1)\Delta T}^{i\Delta T} x_i(t)^2 dt, \quad (18)$$

which is the mean-squared value of the i th piece of data record.

The mean-squared deviation about the mean, $\overline{(\Delta x)_i^2}$, is

$$\overline{(\Delta x)_i^2} = \frac{1}{\Delta T} \int_{(i-1)\Delta T}^{i\Delta T} [x_i(t) - \bar{x}_i]^2 dt, \quad (19)$$

commonly known as the variance. The square root of the variance is the standard deviation (or the rms value of the ac-coupled signal). This gives a measure of the dispersion of the data about the mean.

We now introduce some subtleties in notation to show how the mathematical manipulation is carried out between the different pieces of the data record. If we use a direct summation of data points, then the double bar notation is used; e.g.,

$$\overline{\overline{x^2}}_m = \frac{1}{T} \int_0^T x(t)^2 dt. \quad (20)$$

If the results of the individual pieces are summed, the notation is

$$\langle \overline{x^2} \rangle_m = \frac{1}{m} \sum_{i=1}^m \overline{x_i^2}. \quad (21)$$

Usual methods of time series analysis assume that the accumulative average should approach a limiting value, a condition referred to as self-stationarity. Section II introduces a two-probe test of stationarity which is sensitive to the signatures associated with convection and dispersion rather than with the level of activity.

SECTION II. COVARIANCE OF SEPARATED PROBES

A. Introduction

The one-probe averages just discussed will now be extended to a two-probe average known as the covariance curve. It will be demonstrated how the coherence length and the transit times are retrieved from the covariance delineations. In addition, techniques to establish the confidence level of the covariance curve along with the period of stationarity are discussed. These concepts are then extended so that we can obtain the probability of retrieving the transport phenomena for a common streamline.

B. Accumulative Covariance Technique

Correlation techniques are employed to compare the measurements from two probes which are separated in space and in time. In this technique, the average product at a time delay between two time series results from one time series being advanced or delayed in starting time relative to the other time series. Hence, the correlation curve gives a comparative measure of the degree of similarity as a function of time delay [8,9].

To accomplish the above product integration, the total data record is subdivided into pieces in the manner discussed in Section I (Fig. 2). Each piece of the data record affords a piecewise product mean value as a function of time delay. These values are usually normalized with the geometric mean of the mean-square value. The result of such normalization is called the piecewise correlation coefficient. We have

$${}_{\tau}^{xy}\bar{R}_i = \frac{1}{\Delta T \sqrt{\overline{x_i^2} \overline{y_i^2}}} \int_0^{\Delta T} x_i(t + \tau) y_i(t) dt, \quad (22)$$

where the presubscripts x and y of the correlation coefficient signify that this is the cross correlation of the i th piece of the x and y data records. The presubscript τ refers to the functional dependence on time delay; τ , and the postsubscript i refers to the i th piece of the data record whose length is ΔT . The R signifies the correlation coefficient over this i th interval. The terms $\overline{x_i^2}$ and $\overline{y_i^2}$ are the mean-square values of the i th interval, equation (18).

When a data record is correlated with itself, the correlation is called an autocorrelation. The piecewise autocorrelation coefficient, ${}_{\tau}^{xx}\bar{R}_i$, for the i th piece of the x data record at the time delay τ is

$$\overline{R_i}^{\tau} = \frac{1}{\Delta T \overline{x_i^2}} \int_0^{\Delta T} x_i(t + \tau) x_i(t) dt, \quad (23)$$

which has a maximum value of one at zero time delay. That is, when $\tau = 0$, there is an exact match between the data record and itself. The unnormalized autocorrelation coefficient is the mean-squared value at $\tau = 0$.

The correlation function [equation (22)] has an inherent limitation. When there is a large mean value associated with either (or both) the x and y data records, then the small fluctuations are swamped out by this large constant mean. When the swamping effect exceeds the dynamic range of the systems, the meaningful intelligence cannot be retrieved.

This swamping effect associated with the correlation coefficient can be surmounted by computing the correlation coefficient about the mean of the data records. This form of correlation coefficient is referred to as a piecewise cross-covariance coefficient, $\overline{R_i}^{\tau xy}$, and is defined as

$$\overline{R_i}^{\tau xy} = \frac{1}{\Delta T \sqrt{(\Delta x)_i^2} \sqrt{(\Delta y)_i^2}} \int_0^{\Delta T} [x_i(t + \tau) - \overline{x_i}] [y_i(t) - \overline{y_i}] dt, \quad (24)$$

where the autocovariance coefficient is

$$\overline{R_i}^{\tau xx} = \frac{1}{\Delta T (\Delta x)_i^2} \int_0^{\Delta T} [x_i(t + \tau) - \overline{x_i}] [x_i(t) - \overline{x_i}] dt. \quad (25)$$

The unnormalized autocovariance coefficient at $\tau = 0$ is the variance.

The traditional time average is a straight time integration over the entire data record [8]. For self-stationary data, this straight time integration is more meaningful since the average is approaching its limiting value as more information is processed. However, very often the boundary conditions for the experiment cannot be controlled by

the investigator, and the time integration becomes ambiguous because of the changes in boundary conditions which can prohibit the averages from reaching asymptotic values with an increase in integration time. Accumulative covariance techniques, where the data set is subdivided into segments, provide an opportunity to recognize and account for these changes in boundary conditions.

Sometimes a short segment of the data completely dominates the data record and prevents an intelligent evaluation of the experimental results. Such domination can be reduced by a simple quantization technique where each segment of the data record is normalized relative to itself [10,11]. This quantization affords only an estimate for the accumulative covariance. The choice of the mean value and the normalization factor provides the different accumulative covariance estimates. This discussion uses the following definitions for the accumulative covariance techniques:

1. Sequential covariance where the means and the variances refer to the time integration over all the preceding record; i.e.,

$$\frac{xy}{\tau}_m = \frac{1}{m\Delta T} \sum_{i=1}^m \frac{1}{\sqrt{\overline{(\Delta x)}_m^2} \sqrt{\overline{(\Delta y)}_m^2}} \int_0^{\Delta T} [x_i(t - \tau) - \bar{x}_m] [y_i(t) - \bar{y}_m] dt , \quad (26)$$

where m is the accumulative total of pieces that have been processed.

2. Quantized covariance where the means and variances are recomputed for each segment of the data record before accumulation; i.e.,

$$\langle \frac{xy}{\tau} \rangle_m = \frac{1}{m} \sum_{i=1}^m \frac{xy}{\tau}_i . \quad (27)$$

The piecelength of the data segment of the quantized covariance acts as a low frequency filter which suppresses the information associated with frequencies of periods greater than the piecelength. This is not true for the sequential covariance, since the time averages are not restricted to intervals less than the total accumulative integration time. If a specific reference is not made to the accumulative technique used, it implies that both techniques afford equivalent results.

In Section I (Fig. 2), the interval between samples was defined to the Δt , where

$$\Delta \tau \approx \Delta t. \quad (28)$$

The maximum time delay, τ_m , will be one-third the piecelength.

To select the piecelength of a data segment, let us examine the effect of piecelength duration on a cosine wave. The resultant autocorrelation curve of a cosine wave obtained over the finite interval ΔT is

$$\overline{R_{\tau}} = \cos (2\pi f \tau) - E, \quad (29)$$

where the truncation error, E , is obtained directly from a table of integrals as

$$E = \frac{2 \sin^2 2\pi f \Delta T \sin 2\pi f \tau}{\sin 4\pi f \Delta T + 4\pi f \Delta T} \quad (30)$$

This term could introduce as much as 12.7 percent distortion in the amplitude of the correlation curve. We would like to remove this distortion caused by the truncation error, because this truncation distortion introduces a distortion in the wave packet description. Let us examine the conditions necessary for no, or at least minimum, truncation distortion. When the integration time, ΔT , is infinite, no distortion exists; but the data of interest in this discussion are always of finite duration, rendering this condition unattainable. When the integration time is

$$\Delta T = \frac{n}{2f}, \quad n = 1, 2, 3, \dots, \quad (31)$$

again no distortion exists. The infinite integration time and the multiple period integration times are the limits of integration normally found in statistics texts [8,9].

Since random processes normally involve data with a finite bandwidth, the multiple period integration time is not directly applicable. The problem is that the integration time can be selected to eliminate only the distortion from a single frequency, thereby leaving a degree of distortion in the remaining frequencies in the bandwidth. The solution is to select a multiple period of the mean energy-bearing frequency to reduce the principal distortion. As just pointed out, the truncation error can be reduced by increasing the integration time; therefore, the distortion caused by the bandwidth can be reduced by selecting a relatively large multiple of the period of the mean energy-bearing

frequency. Analysis shows that, when n is eight, the maximum truncation error is less than 2 percent. Thus, the duration of the piecelength should be at least four times the period associated with the mean energy-bearing frequency to minimize the truncation error introduced in narrow and broadband data.

C. Transit Time and Coherence Time

The covariance curve contains the signatures for the transit time and the coherence time. The transit time is that time required by the transport phenomenon to pass between the two points of observation [12]. The coherence time is that period of observation for which the transport can be treated as belonging to the same wave packet [13].

To demonstrate the concept of transit time, the elementary model is illustrated in Figure 4 [14]. The data collection system is an optical detection system [15] comprising two independent units (Fig. 4a). Each unit has a photodetector which receives collimated radiation modulated by events occurring at the point where the beam and the streamline intersect. These modulations form the temporal history of the intensity fluctuations. To illustrate the operation of this system, a test object is moved along the streamline to produce the sequential temporal histories of the intensity fluctuations (Fig. 4b). A correlation of these two time histories provides a covariance curve that indicates the temporal relationship between the x and y data records as the x data recorder is advanced or delayed in time (Fig. 4c). By inspection of the covariance curve, we observe that the maximum correlation between the temporal histories is 2 seconds – the time required for the phenomenon to traverse the distance along the streamline between the beams. Utilization of this transit distance accompanied by a knowledge of the transit distance between the two beams thus affords us the convection speed of the test object.

While this example of transit time retrieval is rudimentary, it is the conceptual basis of correlation statistics and illustrates the principle applied in complex data records containing both dispersive and convective information. A more typical data record that can be expected in this work is the initial example given in Figure 2.

The coherence time is obtained from the covariance delineation. The coherence time, which is a direct result of the application of the uncertainty principle [13], is readily obtained from a covariance phase diagram (Fig. 5). This is a plot of the covariance and the time derivative of the covariance as a function of time delay. The time delay corresponding to the first radial minimum of the phase diagram is defined as the coherence time. The rate of radial decay is a measure of the damping of the covariance and is directly related to the bandwidth-frequency ratio. That is, the phase diagram shows that the greater the bandwidth-frequency ratio, the shorter the piecelength required to obtain a wave packet description. We observe that the coherency time for a periodic process is infinite. In practice, some data sets must be truncated; therefore, the maximum

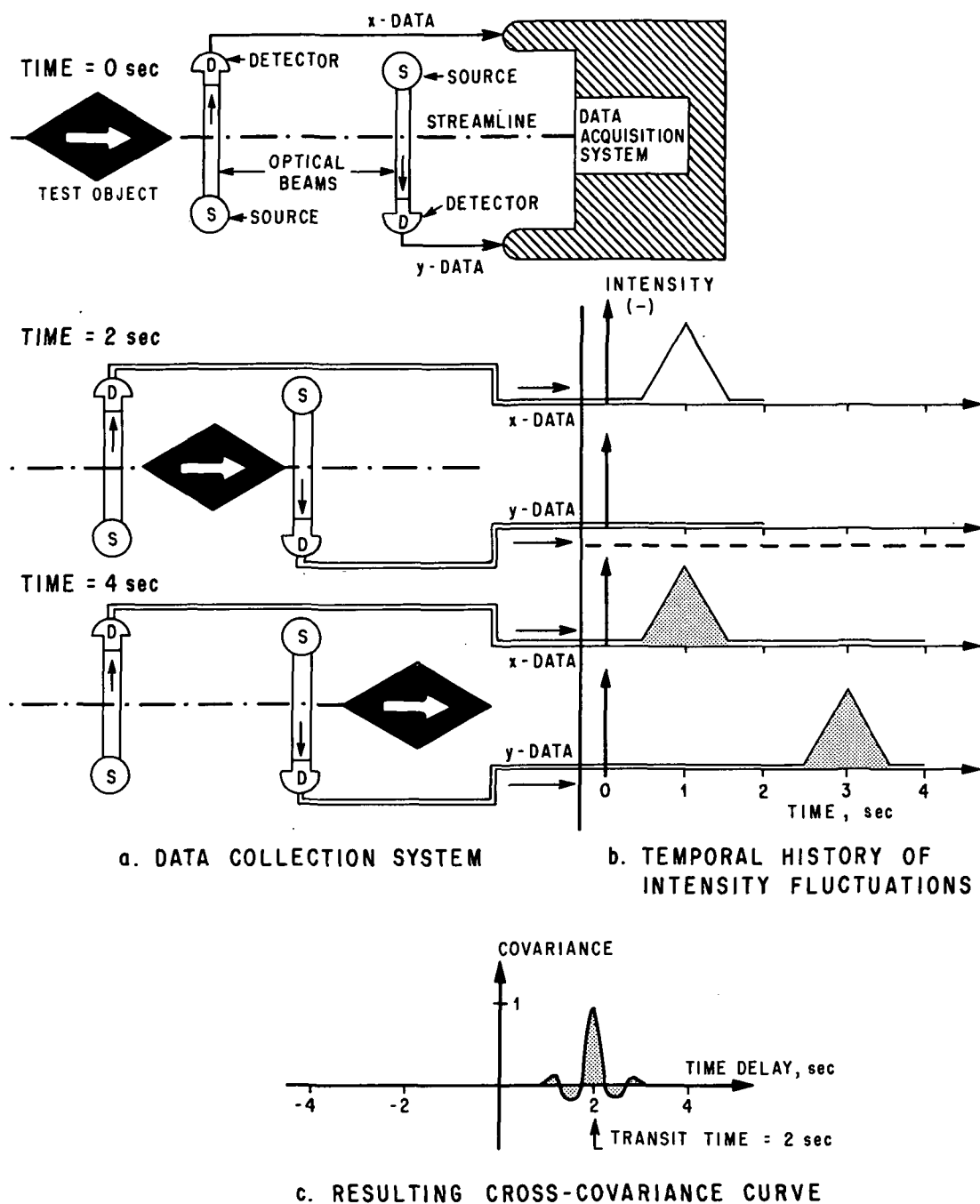


Figure 4. A one-event, two-dimensional physical model.

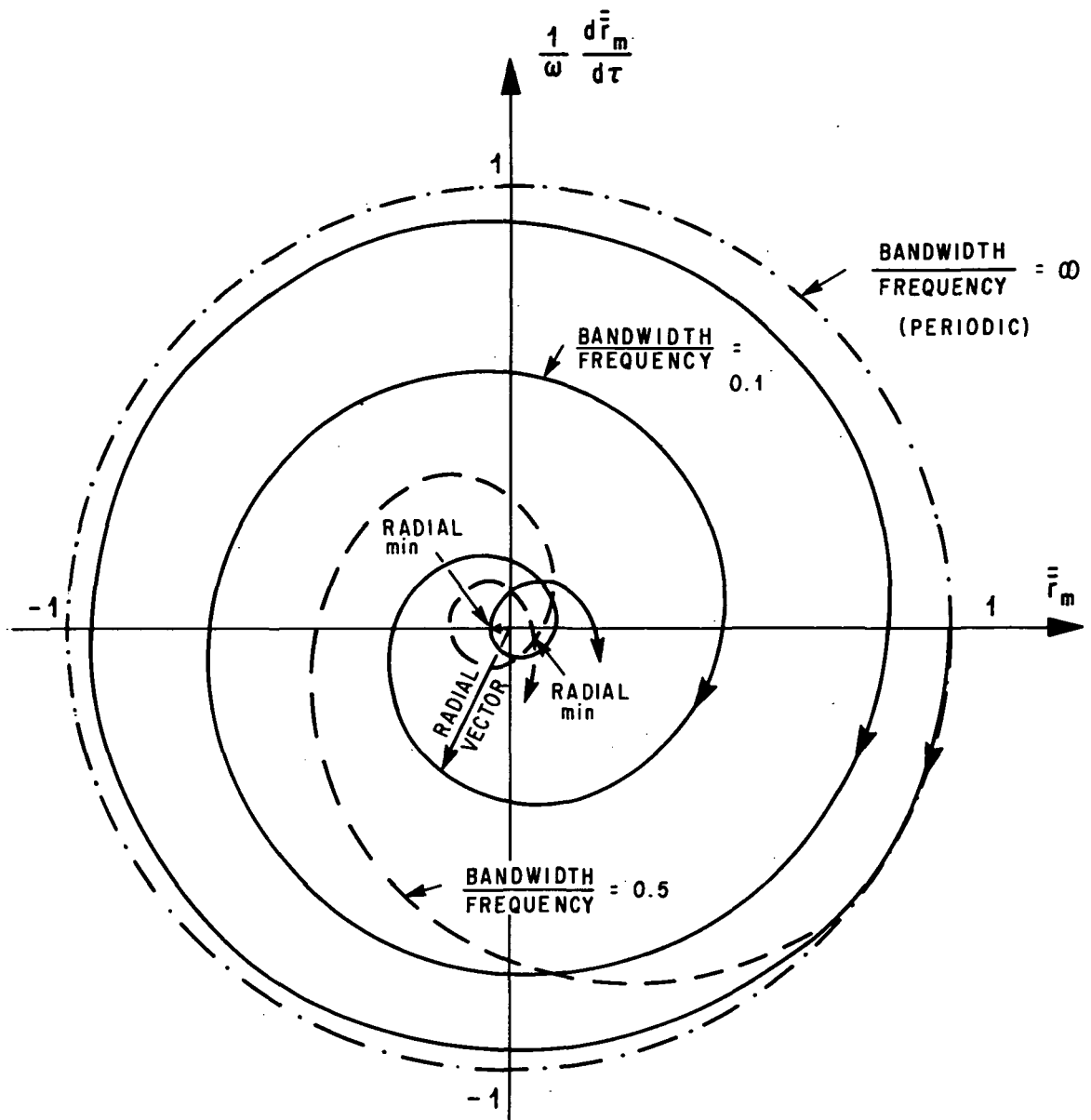


Figure 5. Phaser diagram for coherence.

piecelength will be set at four times the period associated with the mean frequency, unless the coherence time is less than half that value. In that case, the piecelength can be reduced to twice the coherency time without an information distortion.

D. Statistical Error and Period of Stationarity

To facilitate the evaluation of the covariance curve and to establish the stability of the data set, it is necessary to utilize a set of statistical criteria. These criteria will now be developed.

The sequential covariance curve is the basis for testing the stability of the boundary conditions. The first class of stability test is the statistical error of the accumulative covariance that is produced as a result of the deviations of the covariance coefficient, at a particular time delay, between the different pieces of record. The statistical error is

$$\langle \Delta \langle \frac{xy}{\tau} \rangle \rangle_m = \sqrt{\frac{1}{m} \sum_{i=1}^m \left[\frac{xy}{\tau}_i - \langle \frac{xy}{\tau} \rangle_m \right]^2} \quad (32)$$

The confidence interval, $\langle \delta \langle \frac{xy}{\tau} \rangle \rangle_m$, can then be written as

$$\langle \delta \langle \frac{xy}{\tau} \rangle \rangle_m = \langle \Delta \langle \frac{xy}{\tau} \rangle \rangle_m t_{P,m} \quad (33)$$

where $t_{P,m}$ is the "student's t" coefficient for a probability level, P , with m pieces [15]. The normal distribution would be used when there are more than 30 pieces of data record.

Briefly, let us examine the significance of this criterion with regard to the evaluation of the stability of the covariance curve. Assume that we have a set of piecewise covariance curves which contain some undesirable signal (noise). When these piecewise covariance curves are averaged together, we obtain the quantized accumulative covariance curve, together with the confidence limits, as shown in Figure 6. Only those parts of the covariance curve that are greater than the confidence limits are statistically significant to the probability level selected. Equations (32) and (33) are providing an estimate of the reproducibility of a covariance coefficient at a particular time delay. Since the noise has a low reproducibility compared to the information bearing signal, the noise lies below the confidence level and is thereby rejected.

A second type of stability test is based on averaging the statistical error, from the accumulative averages, over the time delay range. The accumulative error,

$$\overline{\langle \Delta \langle \frac{xy}{\tau} \rangle \rangle_m} = \sqrt{\frac{1}{2\tau_m m} \sum_{\tau=-\tau_m}^{\tau_m} \langle \Delta \langle \frac{xy}{\tau} \rangle \rangle_m^2} \quad (34)$$

QUANTIZED COVARIANCE

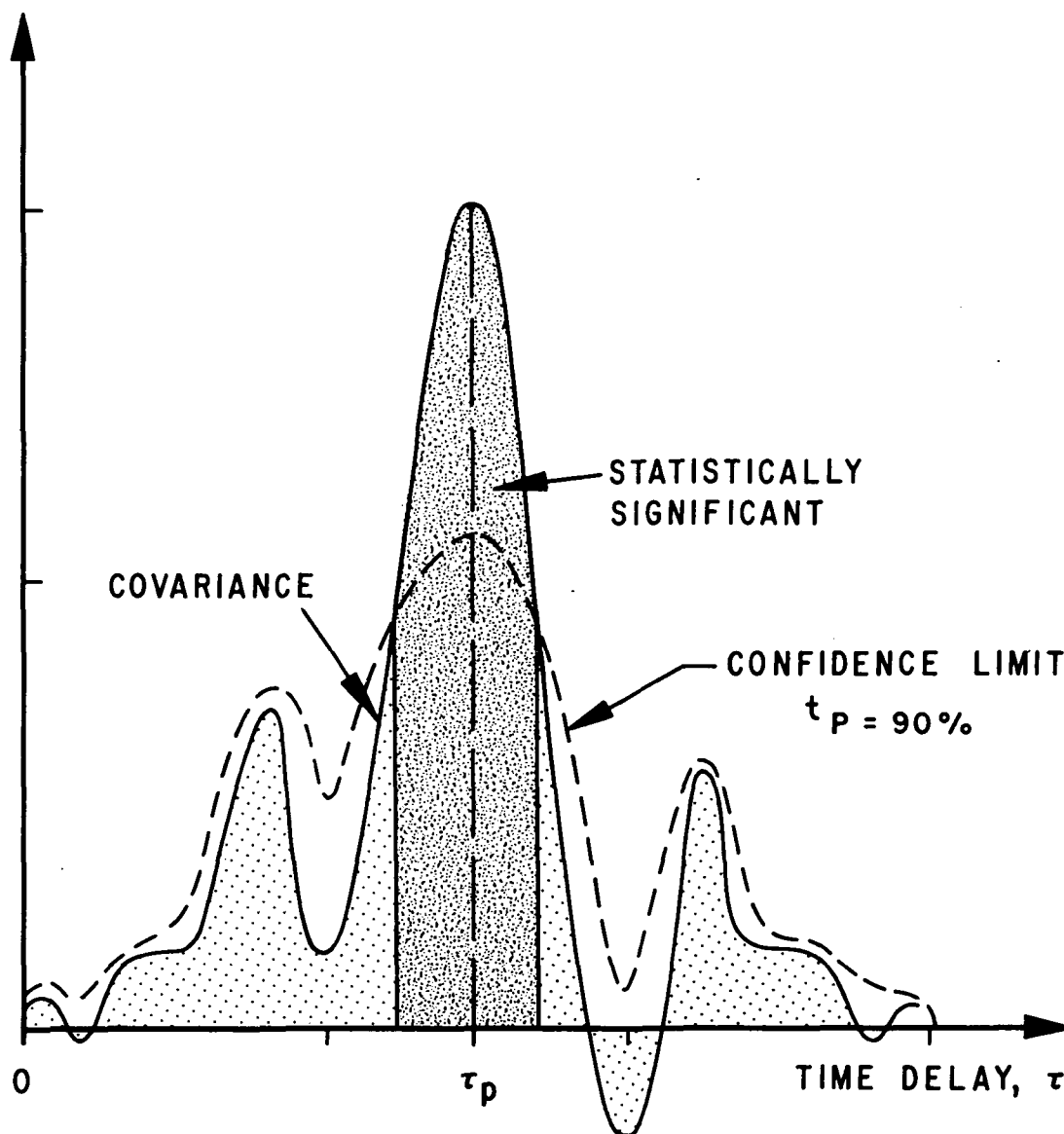


Figure 6. Accumulative quantized covariance.

implies that the average piecewise variance of the piecewise covariance curve is converging at the rate of $1/m$ with the variance of the accumulative covariance curve. This convergence can also be interpreted in terms of the bandwidth in the following manner. The variance about the mean of the piecewise covariance curve can be written in terms of the power spectrum as

$$\overline{\overline{\Delta \langle xy \rangle_r}}_i = \int_0^T \overline{\langle S^2(f) \rangle} e^{-i2\pi f \tau} df, \quad (35)$$

where we are assuming a boxcar spectral distribution where all frequencies have the same amplitude. The limits of integration of this integral can be reduced to the effective bandwidth, B_{eff} . This means that there are just $1/B_{\text{eff}}$ realizations per piece. Since the data record is T long, there are T realizations resulting from averaging. Thus, the rate of the convergence between the variance of the piecewise covariance and the accumulative covariance for stationary data is $1/B_{\text{eff}}T$. In terms of the accumulative error, which is the square root of the variance, the rate of convergence is $1/\sqrt{B_{\text{eff}}T}$. When the accumulative error is plotted as a function of the inverse of the square root of integration time, we should obtain a straight line for a stationary process, whose slope is the square root of the inverse effective bandwidth (Fig. 7). This has been demonstrated rigorously by Jayroe and Su [11].

The accumulative error can also be plotted as a function of integration time to determine the integration time needed to retrieve the enhanced covariance curve. When the accumulative error stops decreasing as a function of integration time, then we are no longer enhancing the accumulative averages. At that point, we can terminate the integration. The period of enhancement can be clearly distinguished in the cold jet data shown in Figure 8, where we observe that the integration of additional data did not significantly enhance the results after 3 seconds of integration. The bottom diagram in Figure 8 clearly shows how stationary the boundary conditions were in this experiment.

An important question still remains with regard to stationarity: "When does the data record become too nonstationary to correlate?" The statistical nonstationarity of the data does not imply it is meaningless. Consider, for example, the atmospheric wind velocity. Generally, over a 24-hour period the wind velocity is nonstationary, but for short intervals of time it is stationary. Thus, it is desirable to know when to create a new ensemble, since we are interested in isolating changes in environmental conditions that would result in a nonstationary data record. The chi-square test enables us to establish the limits of stationarity for the accumulative error [10]. The limits of stationarity are

$$\frac{\sqrt{\chi^2_{.1}}}{m\sqrt{B \Delta T}} \leq \overline{\overline{\Delta \langle xy \rangle_r}}_m \leq \frac{\sqrt{\chi^2_{.9}}}{m\sqrt{B \Delta T}}. \quad (36)$$

The envelope defined by these chi-square limits (Fig. 9) sets the region of stationarity such that, when the accumulative error is within this envelope, the data record can be

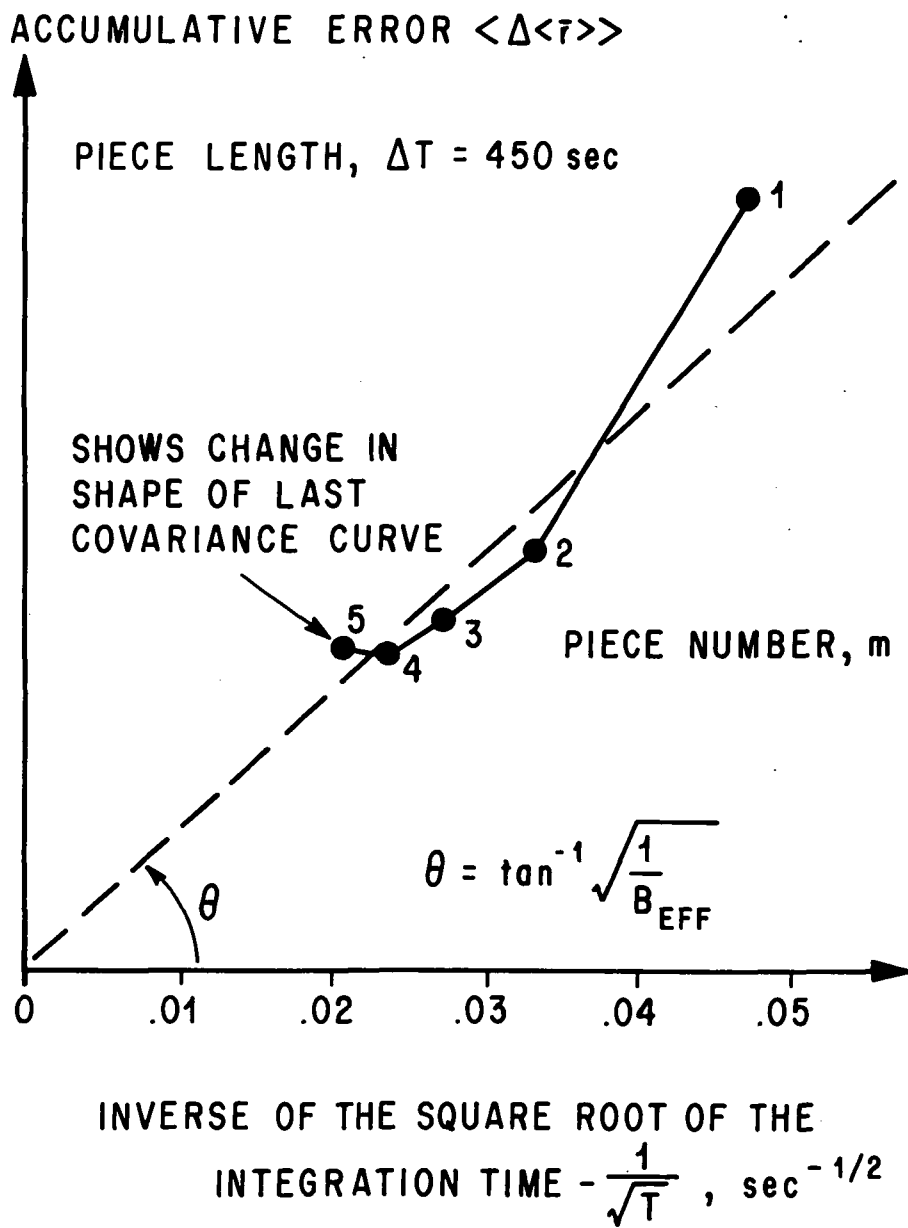


Figure 7. Accumulative error curve.

considered analytically stationary. It is important to recognize that this is simply a restriction on the amount of variation of the bandwidth that can be tolerated.

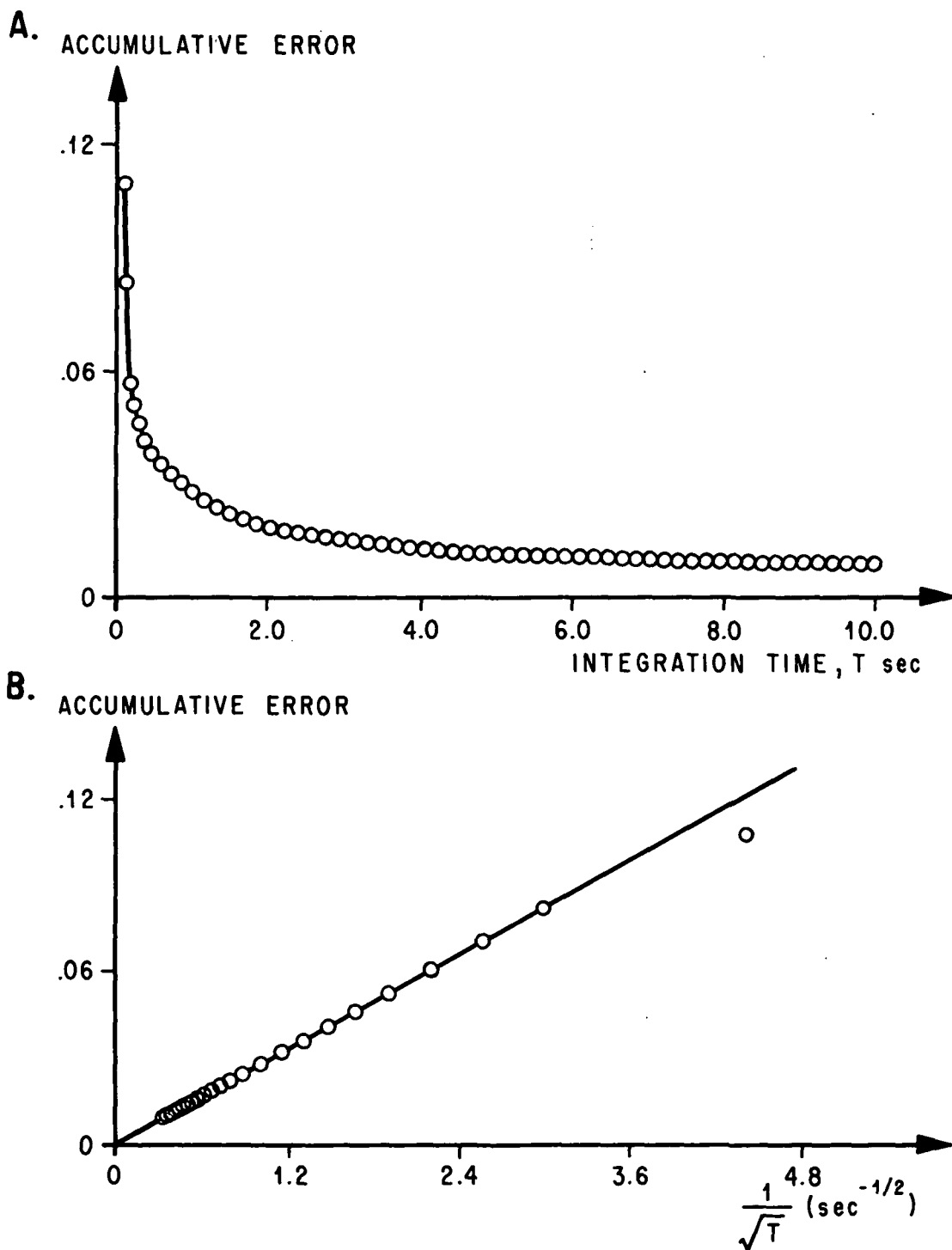


Figure 8. Accumulative error curve from cold jet data
(Fisher's, Johnson's).

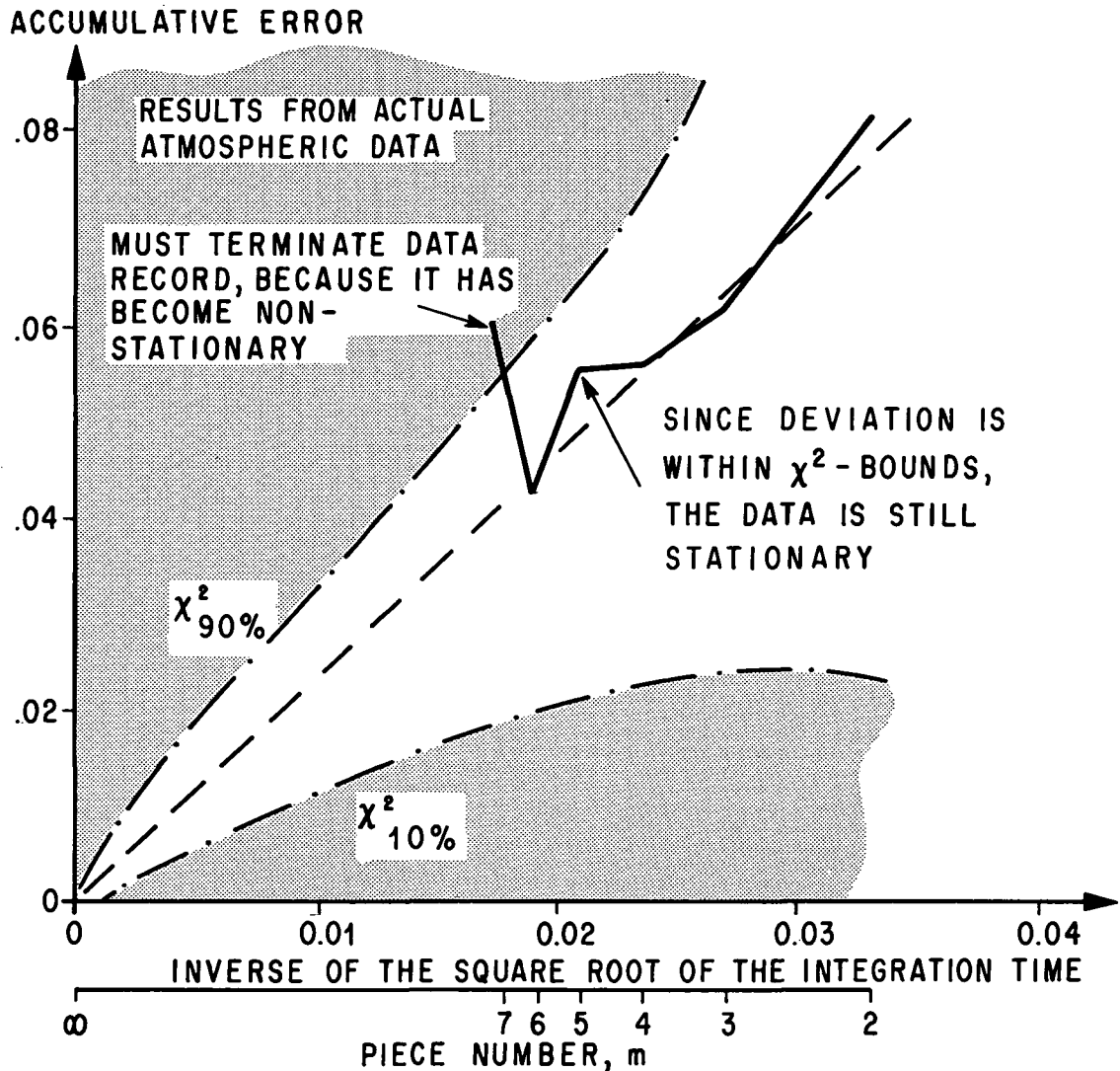


Figure 9. Accumulative error curve for a nonstationary process.

E. Probability of Retrieving Information About Transport Phenomena

Utilizing the statistical tests that were just discussed, criteria will be established whereby an estimate can be obtained for the probability of retrieving significant transit time information concerning the local transport phenomena.

The retrieval of transport information requires the detection of the common information contained in the temporal fluctuations from two spatially separated probes. The criterion of commonality requires the two signals to always maintain the same sign

over the period of integration. The probability of transport retrieval is thus identical with the probability that the accumulative covariance exhibits commonality and exceeds its statistical error. The degree of commonality between the average product can be treated as student's t distributed if the data set is stationary, which is to say that this distribution applies only to processes which belong to the same population as indicated by the chi-squared test. Under these conditions, the probability of retrieving the transport information can be computed directly from the student's t distribution [16].

The degree of commonality is obtained for the student's t from the ratio of the accumulative covariance and its statistical error, which is

$$\tau^t_{P,m} = \frac{\langle \tau^{\overline{xy}}_r \rangle_m}{\langle \Delta \langle \tau^{\overline{xy}}_r \rangle \rangle_m} \quad . \quad (37)$$

The probability of commonality associated with this student's t is then given by

$$\tau^P_{t,m} = \frac{2 \Gamma \left\{ \frac{m}{2} \right\}}{\sqrt{\pi(m-1)} \Gamma \left\{ \frac{m-1}{2} \right\}} \int_0^{\tau^t_{P,m}} \left[1 + \frac{x^2}{\left(\frac{m-1}{2} \right)} \right]^{-m/2} dx \quad , \quad (38)$$

where $\Gamma \left\{ \right\}$ is the gamma function [17]. The probability of commonality can now be plotted as a function of time delay (Fig. 10) and subdivided in accordance with geometric constraints into an information region and a noise region. The commonality probability because of noise, P_{noise} , is the maximum probability that exists in the noise region. The probability of transport retrieval, P_{trans} , is

$$P_{\text{trans}} = \frac{P_{\text{imf}}}{P_{\text{imf}} + P_{\text{noise}}} \quad , \quad (39)$$

where P_{imf} is the maximum information commonality probability. The probability of transport retrieval must be

$$P_{\text{trans}} \geq 50\% \quad (40)$$

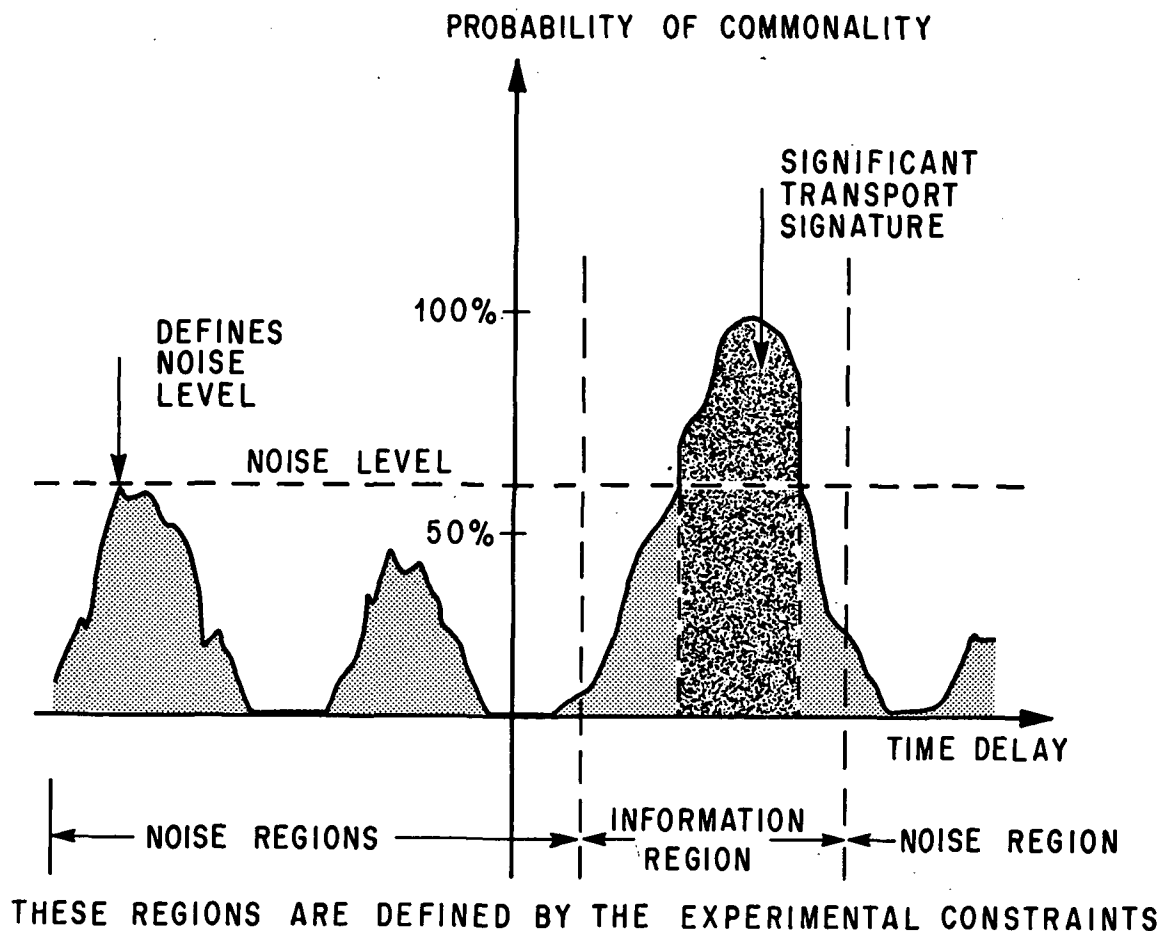


Figure 10. Probability of commonality.

for the transport signature to be significant. This now affords an interval estimator for selection of the significant transit time signature by providing the probability that the common information from the two probes is obtained from the same streamline.

SECTION III. WAVE DESCRIPTION OF THE TRANSPORT PHENOMENA

A. Introduction

Experiments using correlation analysis [2-5,18] clearly show that the covariance curve contains signatures of the transport phenomenon, which cannot be retrieved or interpreted using the traditional time-series analysis. To extend the analysis, it is necessary to augment these analytical techniques with a new three-parameter wave description of the covariance curve.

This description enables us to determine how the parameters of the wave packet are described in the covariance curve and thereby to develop a systematic classification procedure for the different kinds of turbulent transport processes. The wave description permits an interpretation of the covariance curve which separates the transport phenomenon into a convective component and dispersion component.

B. Wave Description of the Covariance Curve

The wave description will be obtained from a new wave packet algorithm, which will provide a three-parameter description of the signature associated with the fluctuations in the fluid transport. In the crossed-beam correlation technique, fluctuations are essential, in that their signature affords a time-dependent information element that enables us to retrieve the convection kinematics. The frequency description of the covariance delineations provides a field description of the affluence of the fluctuations present in the wave packet which, as was shown in Section I, are the signature of the dispersive kinematics. Before developing the wave description, the limitations of the Fourier frequency spectrum with regard to transport analysis will be considered.

The covariance curve can be transformed from the time domain to the frequency domain using the Fourier analysis procedures outlined in the appendix. To demonstrate the effectiveness of this transformation, we can construct a covariance curve by the superposition theorem, which represents a wave packet, so that we know the input spectrum. For this example, suppose we obtain the covariance curve of our wave packet by superimposing 21 cosine functions of equal amplitudes which are equal frequency intervals apart over the range of 0.5 to 1.5 Hz (Fig. 11). The resulting covariance curve, shown in Figure 12, is damped because of the destructive and constructive interference introduced by superimposing the cosine functions. The energy density spectrum shown in Figure 13 is obtained when this covariance is transformed into the frequency domain. On inspection of the spectrum, we observe that, while the bandwidth of the output spectrum is identical with the input spectrum, the amplitude distribution of the output spectrum is not constant. This spectrum is correct.

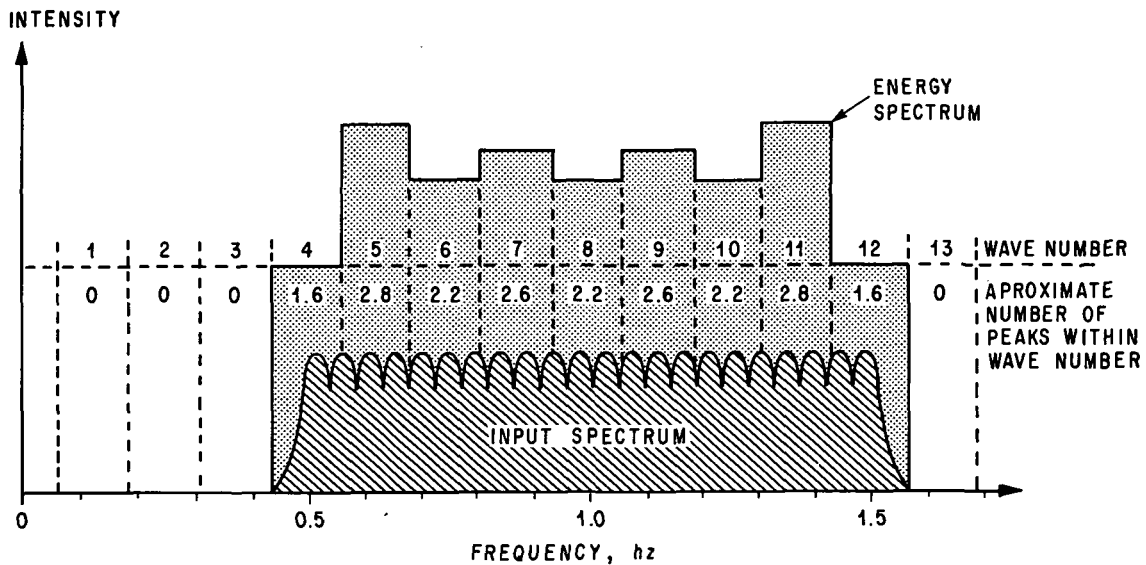


Figure 11. Graphical relation between input spectrum and energy density spectrum.

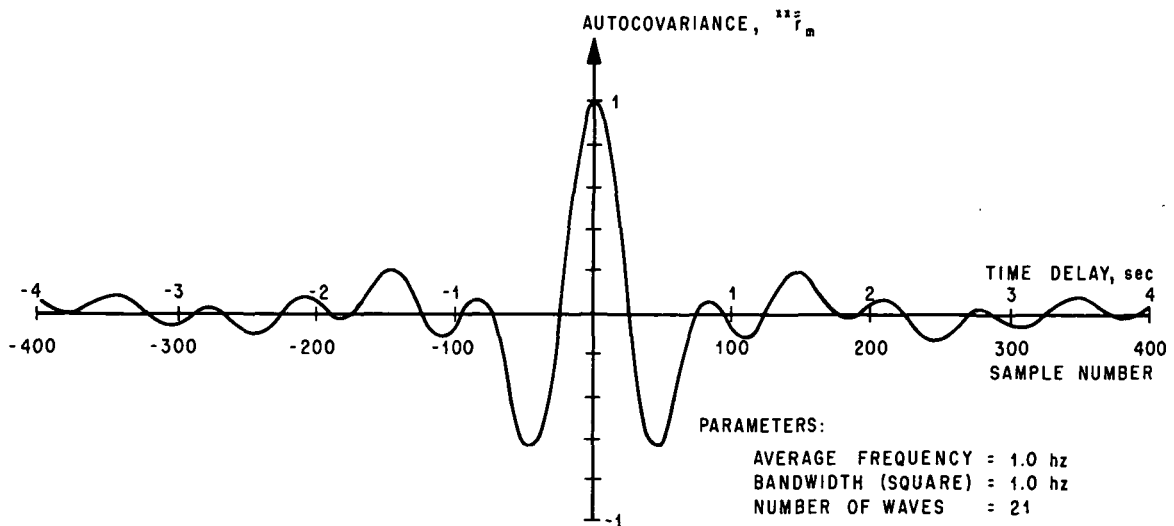


Figure 12. Autocovariance curve in time domain.

The explanation is as follows. The gain of the input energy density window was 4.77 percent for each of the 21 frequencies. The entire bandwidth of these data occupies only nine wave numbers in our energy space, implying a mean gain of 11.11 percent. Figure 11 shows the input in terms of the output spectrum obtained. This discrete

PARAMETERS:

AVERAGE FREQUENCY = 1.0 hz
BANDWIDTH = 1.0 hz
NUMBER OF WAVES = 21
FREQUENCY INTERVAL = 0.05 hz

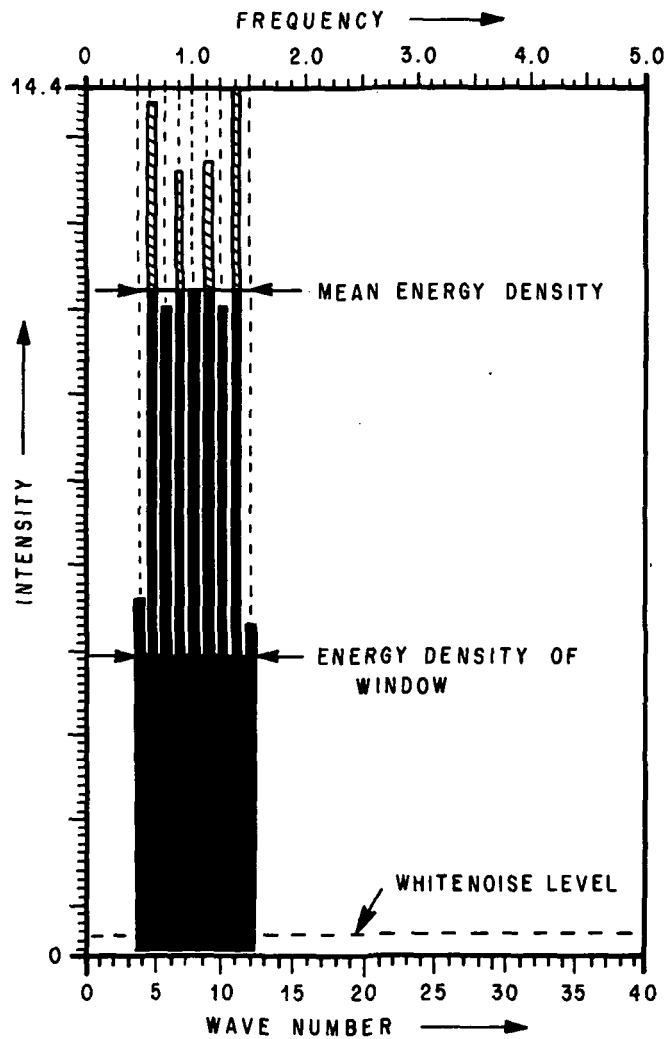


Figure 13. Energy density spectrum of a narrowband process.

spacing between the wave numbers, which is required for an orthonormal spectrum, causes an overlap and results in a distortion of the intensity distribution. (The wave number is that integer multiple of the inverse of the sampling interval that gives the frequency.) If there were integral multiples of wave numbers between frequencies, this would not happen. Thus, the price paid for obtaining the orthonormal frequency space is a loss in the resolution of the input spectrum. From this demonstration, we can conclude that the reproducibility of the actual frequency domain from the energy density spectrum, without either a foreknowledge of the desired results or a focusing of the spectrum, can be misleading. This forces us to seek a new parametric description that eliminates the masking effects of a Fourier analysis which resulted from the degree of uncertainty due to frequency quantization.

This new frequency description of the time domain will be reduced to a description of the size, density, and location of an average envelope about a wave packet. Since the frequency domain is subject to distortion, our analysis is performed in the time domain. An algorithm for this wave packet description will be generated as a function of the average frequency $\langle f \rangle$, the bandwidth B , and the number of frequencies N present (Fig. 14) in the wave packet. The superposition of N frequencies equally spaced and with the same amplitude, which is a boxcar distribution, is given by (for N -odd):

$$\frac{1}{N} \sum_{i=1}^N \cos \omega_i \tau = \frac{1}{N} \left[\sum_{i=1}^{\frac{N-1}{2}} \cos (\langle \omega \rangle \tau - \Delta \omega_i \tau) + \cos \langle \omega \rangle \tau + \sum_{i=1}^{\frac{N-1}{2}} \cos (\langle \omega \rangle \tau + \Delta \omega_i \tau) \right], \quad (41)$$

where

$$\omega_i = 2\pi f_i, \quad (42)$$

$$\langle f \rangle = \frac{\langle \omega \rangle}{2\pi} = \frac{1}{N} \sum_{i=1}^N \omega_i, \quad (43)$$

and

$$\Delta \omega_i = \langle \omega \rangle - \omega_i . \quad (44)$$

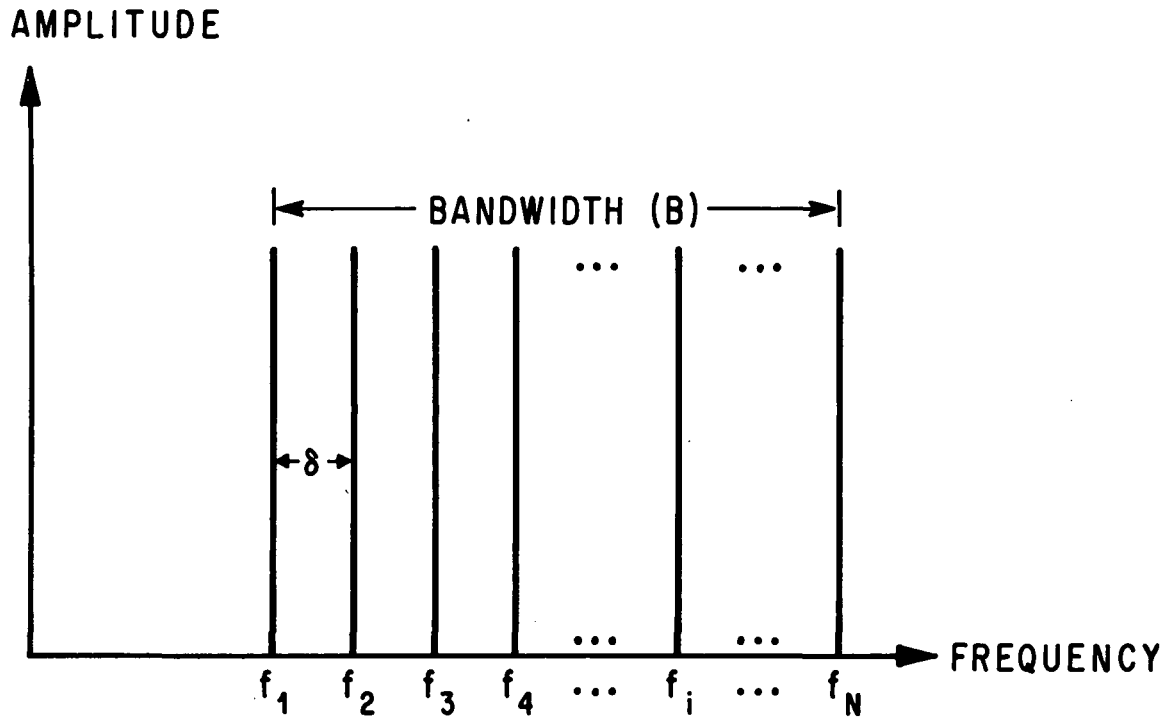


Figure 14. Spectrum of the wave packet algorithm.

Next, the cosine relationship for the difference and sum of angles gives

$$\begin{aligned} \frac{1}{N} \sum_{i=1}^N \cos \omega_i \tau = \frac{1}{N} & \left[\sum_{i=1}^{\frac{N-1}{2}} (\cos \langle \omega \rangle \tau \cos \Delta \omega_i \tau + \sin \langle \omega \rangle \tau \sin \Delta \omega_i \tau) \right. \\ & \left. + \cos \langle \omega \rangle \tau + \sum_{i=1}^{\frac{N-1}{2}} (\cos \langle \omega \rangle \tau \cos \Delta \omega_i \tau - \sin \langle \omega \rangle \tau \sin \Delta \omega_i \tau) \right] . \end{aligned} \quad (45)$$

Simplifying the above relationship, we obtain

$$\frac{1}{N} \sum_{i=1}^N \cos \omega_i \tau = \frac{1}{N} \cos \langle \omega \rangle \tau \left[1 + 2 \sum_{i=1}^{\frac{N-1}{2}} \cos \Delta \omega_i \tau \right] . \quad (46)$$

Now consider the summation in the above relationship:

$$\sum_{i=1}^{\frac{N-1}{2}} \cos \Delta \omega_i \tau = \sum_{k=1}^{\frac{N-1}{2}} \cos \left(\frac{2\pi k B \tau}{N-1} \right) , \quad (47)$$

where

$$2\pi B = \omega_N - \omega_1 \quad (48)$$

and k is an integer. To remove the summation, the following strategy is used:

$$\begin{aligned} \sum_{k=1}^{\frac{N-1}{2}} \cos \left(\frac{2\pi k B \tau}{N-1} \right) &= \cos \left(\frac{2\pi B \tau}{N-1} \right) + \cos \left(\frac{4\pi B \tau}{N-1} \right) \\ &+ \cos \left(\frac{6\pi B \tau}{N-1} \right) + \dots + \cos (\pi B \tau) . \end{aligned} \quad (49)$$

However, for the k th term,

$$2 \sin \left[\frac{\pi B \tau}{N-1} \right] \cos \left[\frac{2\pi k B \tau}{N-1} \right] = \sin \left[(2k+1) \frac{\pi B \tau}{N-1} \right] - \sin \left[(2k-1) \frac{\pi B \tau}{N-1} \right] ; \quad (50)$$

then, for the $(k + 1)$ th term,

$$2 \sin \left[\frac{\pi B \tau}{N-1} \right] \cos \left[\frac{2\pi(k+1) B \tau}{N-1} \right] = \sin \left[(2k+3) \frac{\pi B \tau}{N-1} \right] - \sin \left[(2k+1) \frac{\pi B \tau}{N-1} \right] . \quad (51)$$

That is, only the first and last terms in the summation remain, or

$$2 \sin \left[\frac{\pi B \tau}{N-1} \right] \sum_{k=1}^{N-1} \cos \left[\frac{2\pi k B \tau}{N-1} \right] = \sin \left[\frac{N\pi B \tau}{N-1} \right] - \sin \left[\frac{\pi B \tau}{N-1} \right] , \quad (52)$$

or

$$\sum_{k=1}^{N-1} \cos \left[\frac{2\pi k B \tau}{N-1} \right] = \frac{\cos \left[\left(\frac{N+1}{N-1} \right) \frac{2\pi B \tau}{4} \right] \sin \left[\frac{2\pi B \tau}{4} \right]}{\sin \left[\left(\frac{2}{N-1} \right) \frac{2\pi B \tau}{4} \right]} . \quad (53)$$

Returning to equation (47) and using the above results, we obtain

$$\frac{1}{N} \sum_{i=1}^N \cos \omega_i \tau = \frac{1}{N} \cos \langle \omega \rangle \tau \left\{ 1 + 2 \frac{\cos \left[\left(\frac{N+1}{N-1} \right) \frac{2\pi B \tau}{4} \right] \sin \left[\frac{2\pi B \tau}{4} \right]}{\sin \left[\left(\frac{2}{N-1} \right) \frac{2\pi B \tau}{4} \right]} \right\} . \quad (54)$$

This algorithm provides a wave description of a packet of sinusoidal waves as a function of the average frequency, bandwidth, and number density. This can be interpreted, in

accordance with the superposition theorem, as an autocovariance curve that is a time domain description of the wave packet; that is,

$$r(\tau) |_{\langle f \rangle, B, N} = \frac{1}{N} \cos 2\pi \langle f \rangle \tau \left\{ 1 + 2 \frac{\cos \left[\left(\frac{N+1}{N-1} \right) \frac{2\pi B \tau}{4} \right] \sin \left[\frac{2\pi B \tau}{4} \right]}{\sin \left[\left(\frac{2}{N-1} \right) \frac{2\pi B \tau}{4} \right]} \right\}. \quad (55)$$

Since this autocovariance curve is the result of the wave description in the frequency domain being transformed to the time domain, we shall refer to it as the wave packet algorithm. This algorithm can only be used to analyze a single wave packet description in the transport process. Where several different wave packets are occurring simultaneously, frequency discrimination techniques must be utilized to isolate the wave packet associated with each process. This relation is the wave description for the signatures of those fluid kinematics associated with the parametric fluctuations resulting from the dispersive transport process. The parameters $(\langle f \rangle, B, N)$ of this wave description are retrieved by the use of the least-squares fit of the wave packet algorithm to the autocovariance curve which is obtained from the suppression of the transit time information in the cross-covariance delineation of two spatially separate probes.

A more general form for the wave packet algorithm compresses the original three parameters into two, by redefining the time axis such that

$$\theta = \langle f \rangle \tau \quad (56)$$

and defining the bandwidth ratio to be

$$\beta = \frac{B}{\langle f \rangle} \quad (57)$$

These will be referred to as the similarity relations. Then, by this similarity transform, the wave packet algorithm, equation (55), becomes

$$r(\theta) \Big|_{\langle f \rangle, B, N} = \frac{1}{N} \cos(2\pi\theta) \left\{ 1 + \frac{2 \cos \left[\left(\frac{N+1}{N-1} \right) \frac{2\pi\beta\theta}{4} \right] \sin \left[\frac{2\pi\beta\theta}{4} \right]}{\sin \left[\left(\frac{2}{N-1} \right) \frac{2\pi\beta\theta}{4} \right]} \right\}, \quad (58)$$

which is the same as if the frequency were 1 Hz.

A computer comparison of the wave packet algorithm with the equivalent description obtained from the superposition theorem shows that more precise results were obtained with the algorithm, especially when the number density of sinusoidal functions was high. The discrepancy between the two descriptions (maximum of 2.19 percent) which occurred for small covariance coefficients in the wings of the curve was a result of truncation errors induced by summing large numbers of sinusoidal functions. It can be concluded from this analysis that the wave packet algorithm is not only a faster but a more sensitive means of attaining the wave description than by using superposition techniques.

C. The Wave Packet Interpretation for the Covariance Curve

The parametric effects of the wave packet on the shape of the covariance curve will now be considered.

Statistical processes are commonly grouped into three classifications: periodic, narrowband, and broadband processes [8]. Typical examples of the autocovariance curves associated with these processes, using data obtained from glow discharge experiments [4], are shown in Figure 15. The distinguishing characteristic between these different processes is the degree of damping associated with each process.

To interpret the mechanism responsible for the damping, the wave packet algorithm will be reexamined. We observe that, when the algorithm is written in the form

$$r(\tau) \Big|_{\langle f \rangle, B, N} = \cos(2\pi\langle f \rangle\tau) D(\tau), \quad (59)$$

where

$$D(\tau) = \frac{1}{N} \left\{ 1 + \frac{2 \cos \left[\left(\frac{N+1}{N-1} \right) \frac{2\pi B\tau}{4} \right] \sin \left[\frac{2\pi B\tau}{4} \right]}{\sin \left[\left(\frac{2}{N-1} \right) \frac{2\pi B\tau}{4} \right]} \right\}, \quad (60)$$

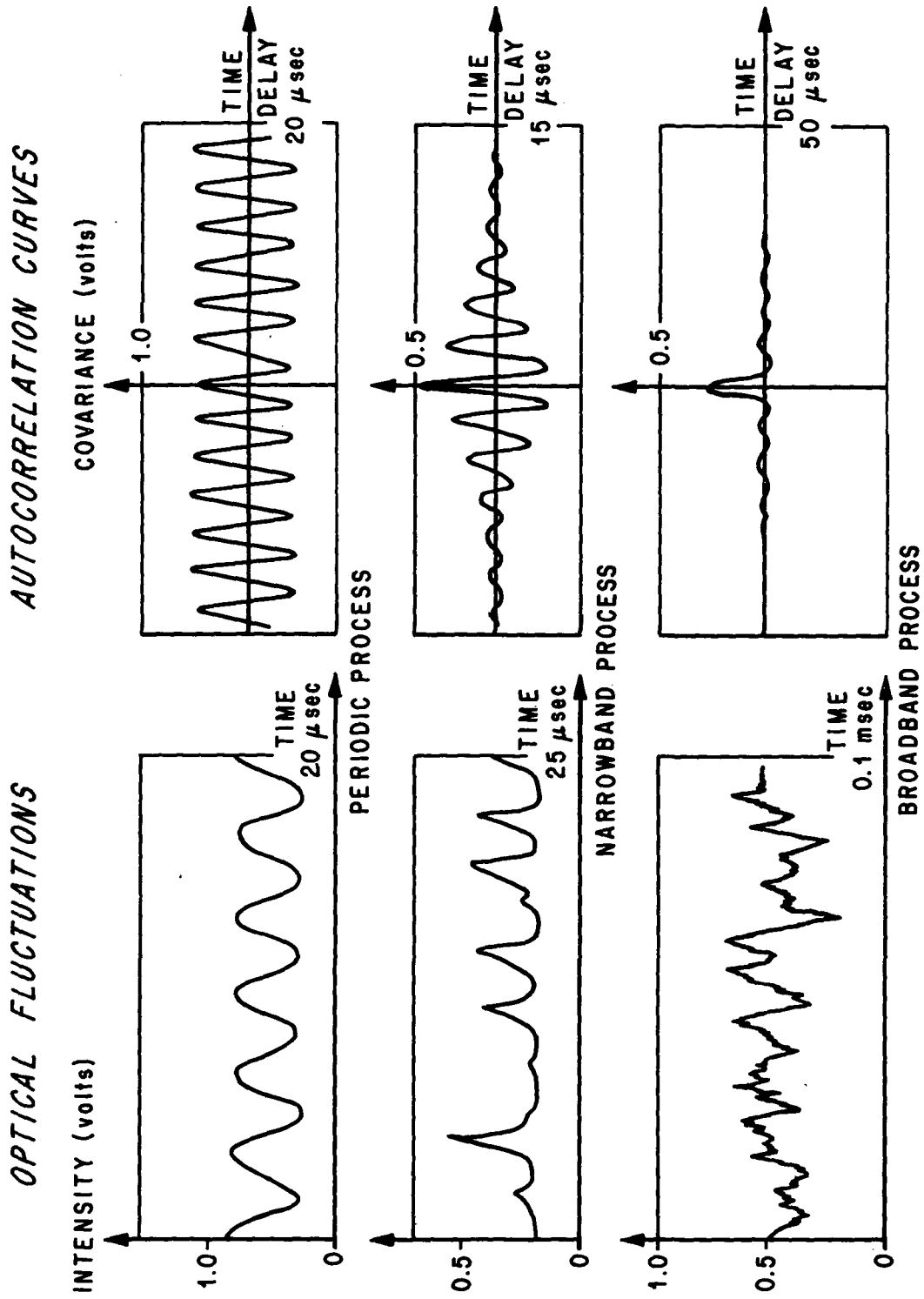


Figure 15. Autocorrelation curves for moving striations.

we obtain a periodic cosine function of the average frequency and a time delay dependent factor, $D(\tau)$, which is clearly the damping factor in the wave description.

Now consider the limiting case where the bandwidth of the wave packet is zero. Then the damping factor using l'Hôpital's rule is

$$D(\tau) \big|_{B \simeq 0} = 1 \quad (61)$$

for all time delays. This results in a periodic covariance curve of the average frequency, as we would expect. We can further conclude from an examination of the damping factor that the damping of the average frequency is a result of the number density and the bandwidth. In fact, to a first-order approximation, we can attribute the damping primarily to the bandwidth.

Obviously the damping factor is a suppressing agent of the cosine function of the average frequency such that the bounds for the cosine function are set by the damping envelope. Using the same parameters in the wave packet algorithm that were employed with the superposition theorem (Fig. 11) in generating the covariance curve (Fig. 12), we can generate the autocovariance curve in Figure 16. This covariance curve generated with the algorithm has an important analysis impact in that it affords us the opportunity to examine the effects of the damping envelope. By inspection of this covariance curve, we can observe that the damping envelope defines the level of suppression for the cosine function of the average frequency.

It is desirable to be able to obtain, by inspection, the average frequency of the wave packet directly from the autocovariance curve, as we would, for example, in the case of a periodic function. From an analysis of the wave packet algorithm, it follows that our freedom to retrieve the average frequency by inspection becomes more restricted as the bandwidth increases, because it will result in an increase in the suppression of the characteristics of the average periodicity. In fact, there is a point where the bandwidth suppression of the covariance is so strong that even the first quarter cycle of the average periodicity is suppressed, thereby preventing the retrieval by inspection of the average frequency associated with the wave packet.

It is thus necessary to establish a classification system which divides the statistical processes into those processes that are amenable to a direct information retrieval scheme and those processes that require a more sophisticated information retrieval scheme. This is the objective of the next section.

D. Classification of Covariance Curves

A procedure for the systematic classification of covariance delineations is developed that enables us to group statistical processes in accordance with the minimum data processing required for the retrieval of the wave packet description.

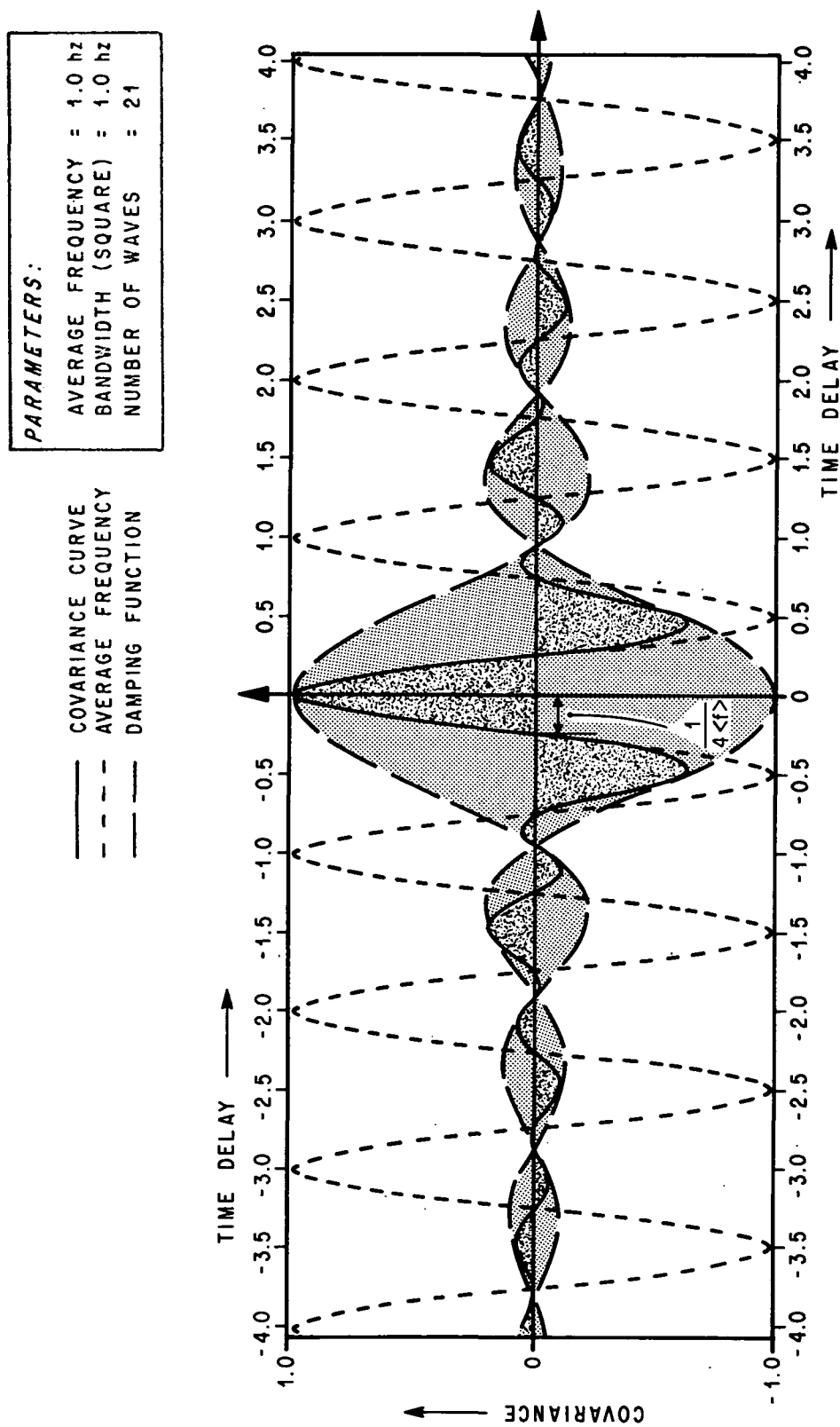


Figure 16. Covariance curve from the wave packet algorithm.

There is a classical system defining the classification of statistical processes, as pointed out in the last section. No damping implies a periodic process, some damping implies a narrowband process, and strong damping implies a broadband process – thus a heuristic definition. While this definition is an aid in grouping data, it lacks an analytic formalism. More specific definitions of the processes are to be found in optics [13], but they do not directly apply to our discussion.

The behavior of the damping envelope, as pointed out in the last section, is our primary concern. The principal factor governing the damping envelope is the bandwidth of the statistical process. From the similarity transform of the wave packet algorithm [equation (58)], we observe that a behavior pattern for the damping envelope also can be obtained in terms of the bandwidth ratio [equation (57)]. The beauty of the dimensionless bandwidth ratio lies in its ability to render a generalized damping model. Since we would like our classification system to have significance in the frequency domain as well as the time domain, we will initially direct our attention to the behavior of the spectral envelope as a function of the bandwidth ratio.

The range of the bandwidth ratio is from zero to two for the defined boxcar spectral envelope. If the bandwidth exceeds two, then the spectrum folds (Fig. 17) because of the even property associated with cosine functions. It follows that the three analytical classifications, from the spectral standpoint, of the correlation curve based on the bandwidth ratio, β , are:

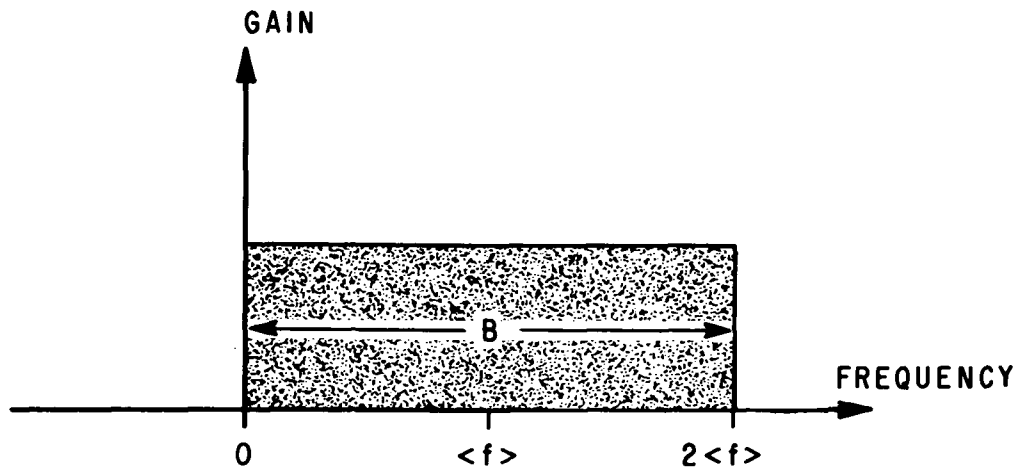
1. Periodic processes: $\beta = 0$.
2. Narrowband processes: $0 < \beta \leq 2$.
3. Broadband processes: $\beta > 2$.

With this proposed classification system as a guide, a closer examination of the time and frequency domains is in order.

To facilitate this examination, the computer program, whose flow diagram is given in Figure 18, was used to generate a set of covariance curves to demonstrate the effects of the bandwidth ratio on the damping envelope. Our objective is to illustrate that the classification system just defined not only has significance in the frequency domain, but that this system also groups covariance curves such that in periodic and narrowband processes the average frequency can be retrieved by inspection in accordance with

$$\langle f \rangle = \frac{1}{4 \tau_{FCP}} , \quad (62)$$

A. NARROWBAND LIMIT ($\beta = 2$)



B. BROADBAND ($\beta > 2$)

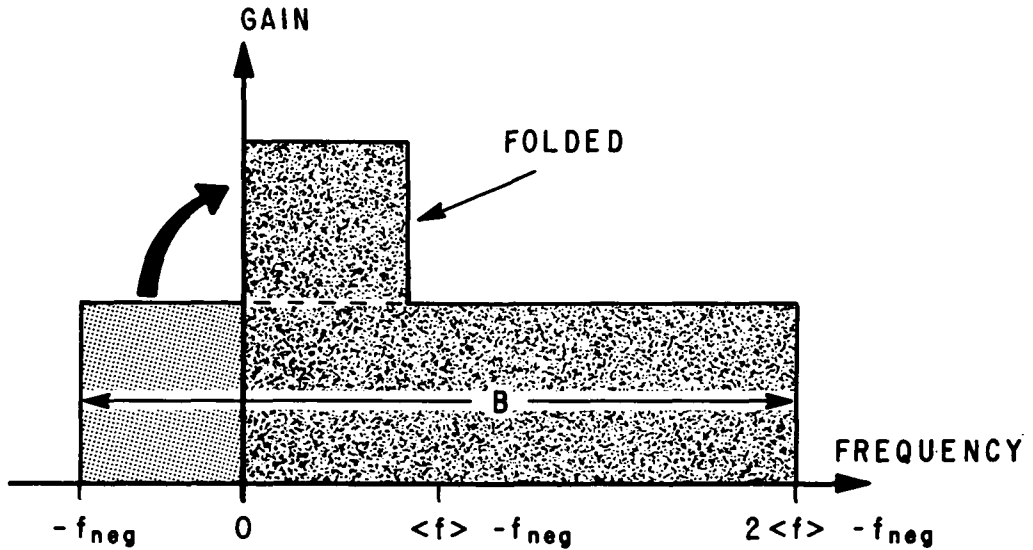


Figure 17. Schematic representation of the envelope for the spectrum from narrowband and broadband processes.

where τ_{FCP} is the delay time of the first crossing point which is taken as the delay corresponding to the initial zero value of the covariance coefficient. This relation [equation (62)] indicates that the first quarter cycle of the covariance curve corresponds with the first quarter cycle of a cosine wave of the average frequency.

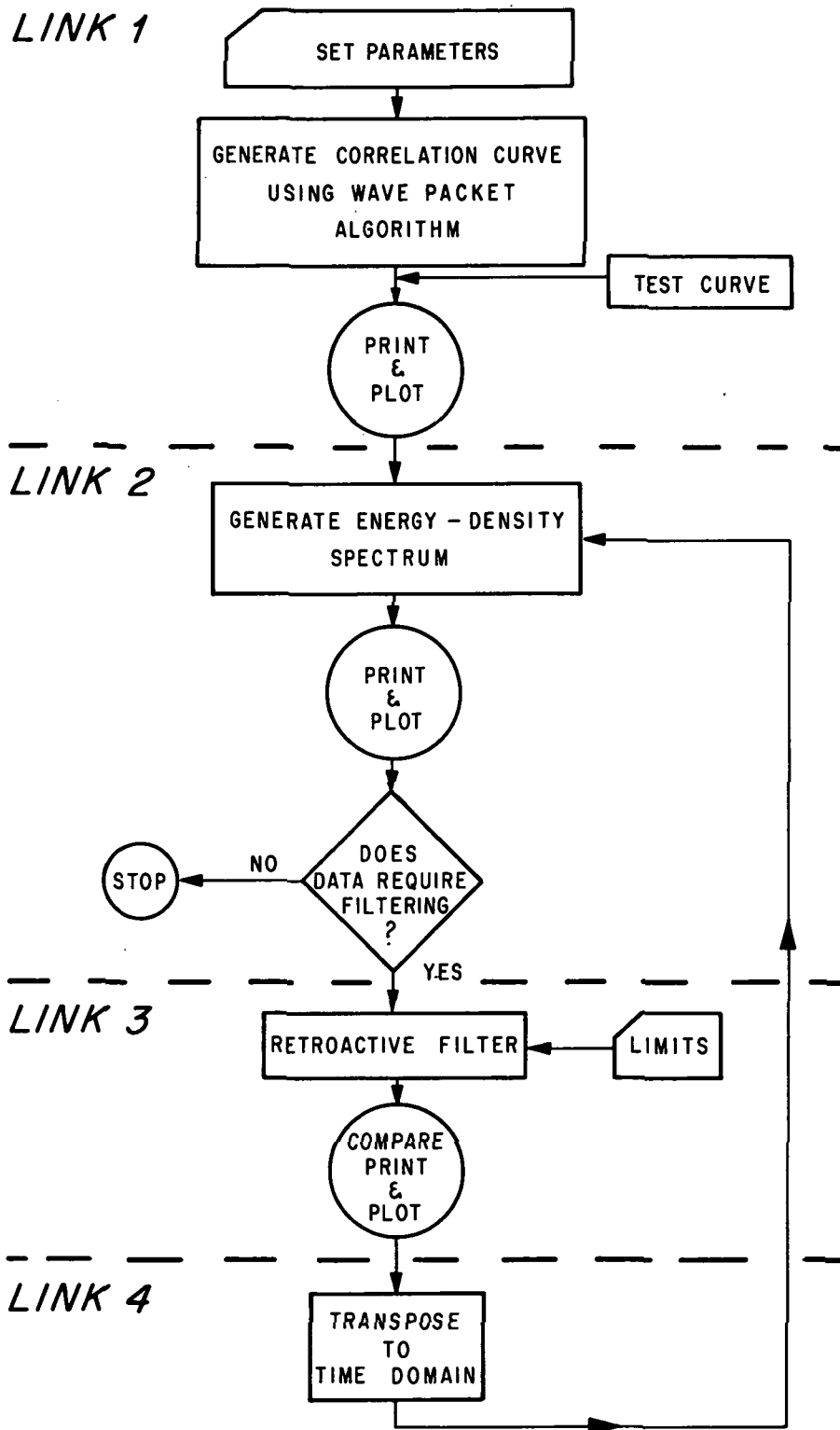


Figure 18. Flow diagram of spectral decomposition program.

The results for mappings of the autocovariance curve over the bandwidth ratio range of zero to eight, of which three typical results are given in Figure 19, clearly indicate that the average frequency can be retrieved by inspection in periodic and narrowband processes. However, in broadband processes, where the bandwidth ratio exceeds two, the damping envelope always suppresses the first quarter cycle of the average frequency, making information inspection retrieval impossible. This behavior is in accordance with our original classification model objectives in which we wanted to differentiate between the statistical processes where the average frequency could be retrieved by inspection from those processes where analytical techniques are required.

Analytical techniques for ascertaining the wave packet parameters include spectral decomposition (Appendix) and regression analysis of the wave packet algorithm. Link 2 of the computer program (Fig. 18) was used to test the information retrieval capabilities of the energy density spectrum. The covariance curves subjected to this spectral decomposition were generated by the wave packet algorithm. This means that the output spectrum should be identical to the boxcar input spectrum (Fig. 14). The boxcar spectrum is obtained when there is an integral wave number spacing between each of the input spectral frequencies (Fig. 20). This is a special case, and in general we would not have this integral spacing. Therefore, it is much more difficult to obtain the wave packet description directly from the spectrum. To demonstrate this point, observe the narrowband spectrum shown in Figure 21. In this example, the quantization effect caused by discrete sampling has suppressed the information regarding the distribution and the number density. It can be shown that the description of the time domain in the frequency domain is limited to the same number of unique representations, as pointed out in the explanation of the spectrum in Figure 12. Thus, in addition to the distortion illustrated in this figure, there is also an uncertainty associated with the spectrum which is equal to the wave number spacing. This uncertainty in the spectral description renders the spectrum unsuitable for the detection of small changes in the average frequencies between different covariance curves. Therefore, the application of change statistics of the average frequency for periodic and narrowband processes requires either inspection retrieval or wave packet regression analysis.

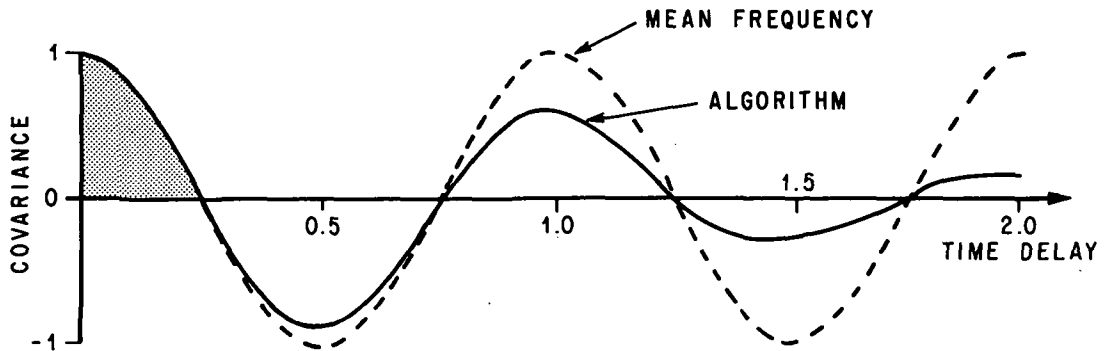
In broadband processes, the Fourier spectral description of the autocovariance curve will deteriorate. Using the same spectral input model as used in the narrowband discussion, but with a broader bandwidth, we obtain the integral wave number spectrum shown in Figure 22. We would expect a result similar to that shown in Figure 20, except it would be folded. Instead, we get a spectrum with a marked ringing signature in the folded region. The deterioration results from the fact that the Fourier spectrum, which is a correlation between the covariance curve and a sinusoidal function, is being calculated for a covariance curve which no longer has a dominant signature of the average frequency. This signature has been suppressed by the bandwidth damping. Naturally, the broadband nonintegral wave number spectrum of the autocovariance curve (Fig. 19c) results in even more deterioration for the output spectrum (Fig. 23). Unlike the nonintegral narrowband distribution, the average frequency of the wave packet will not tend to dominate the broadband spectrum, and must be retrieved in terms of a model. In fact, our whole analysis of a broadband process requires a model to interpret the wave packet parameters.

PARAMETERS:

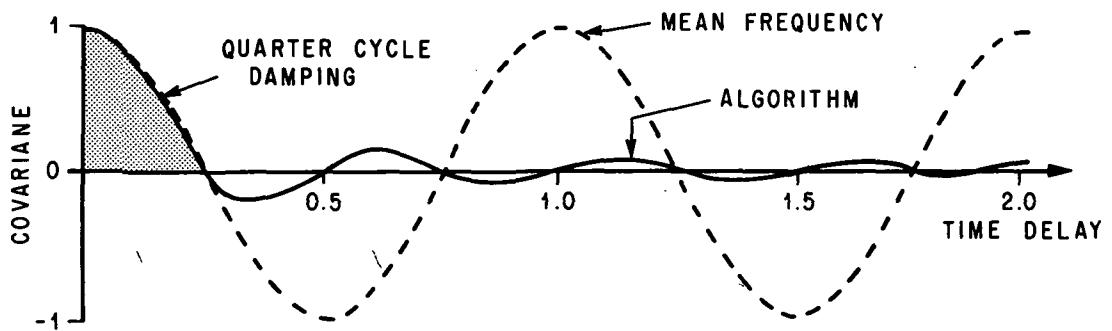
AVERAGE FREQUENCY = 1.0

NUMBER OF WAVES = 21

A. NARROWBAND PROCESS, $\beta = 0.5$



B. LIMIT BETWEEN NARROWBAND & BROADBAND PROCESSES, $\beta = 2.0$



C. BROADBAND PROCESS, $\beta = 6.0$

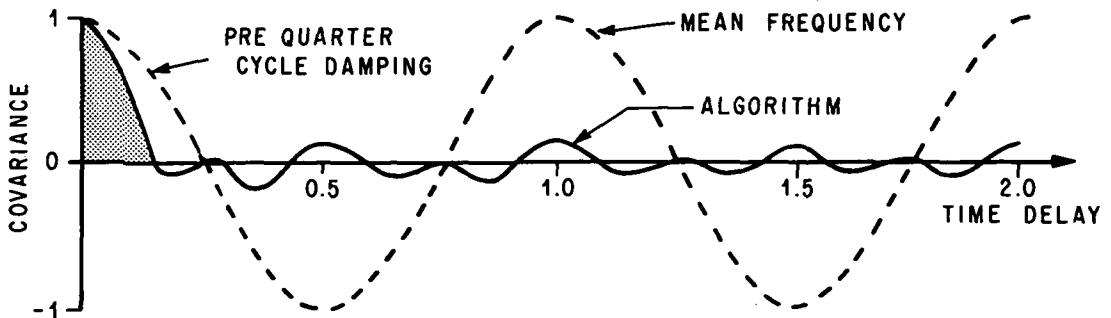


Figure 19. Autocovariance curves of narrowband and broadband processes.

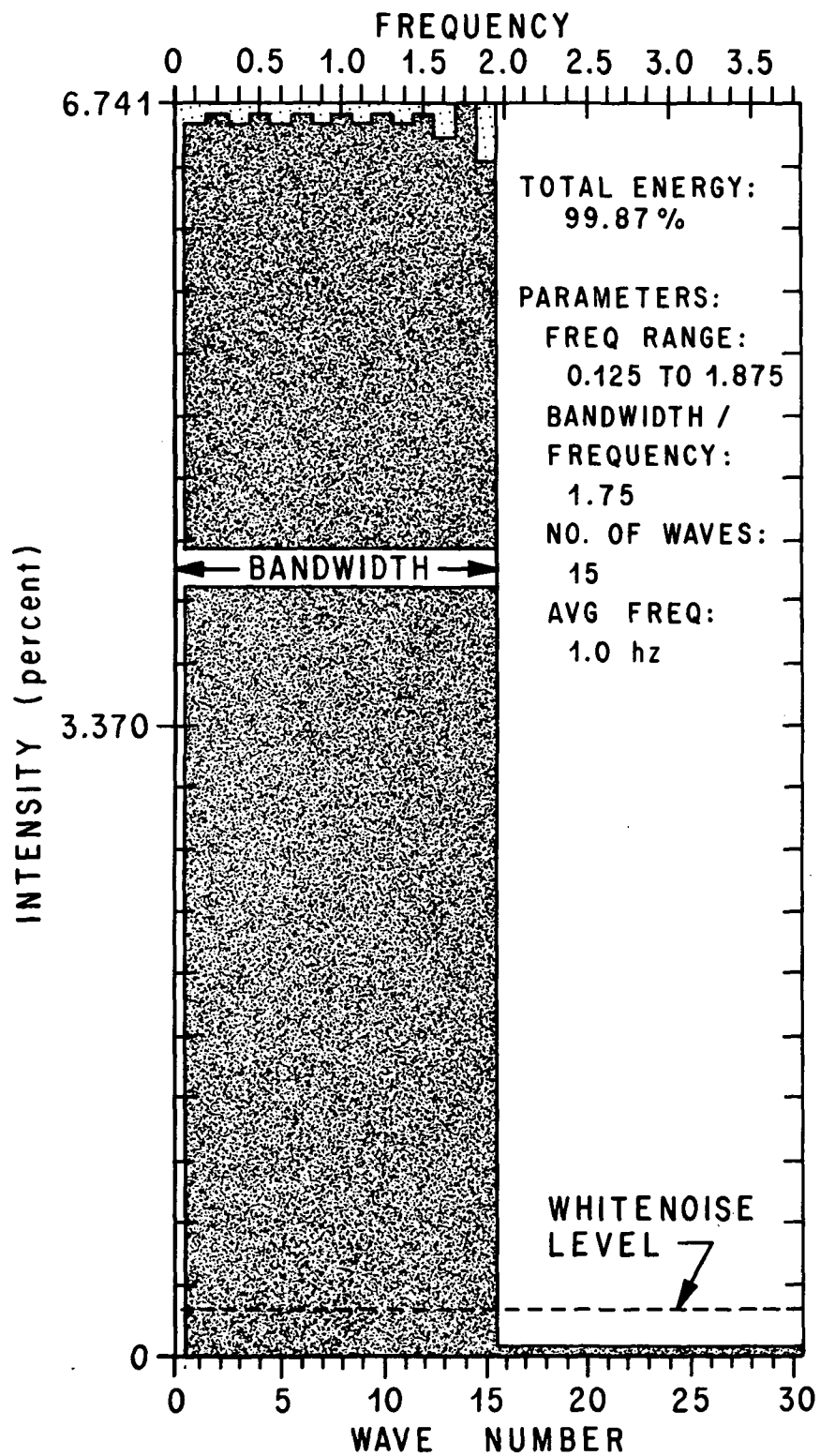


Figure 20. Transform of square input with integral spacing.

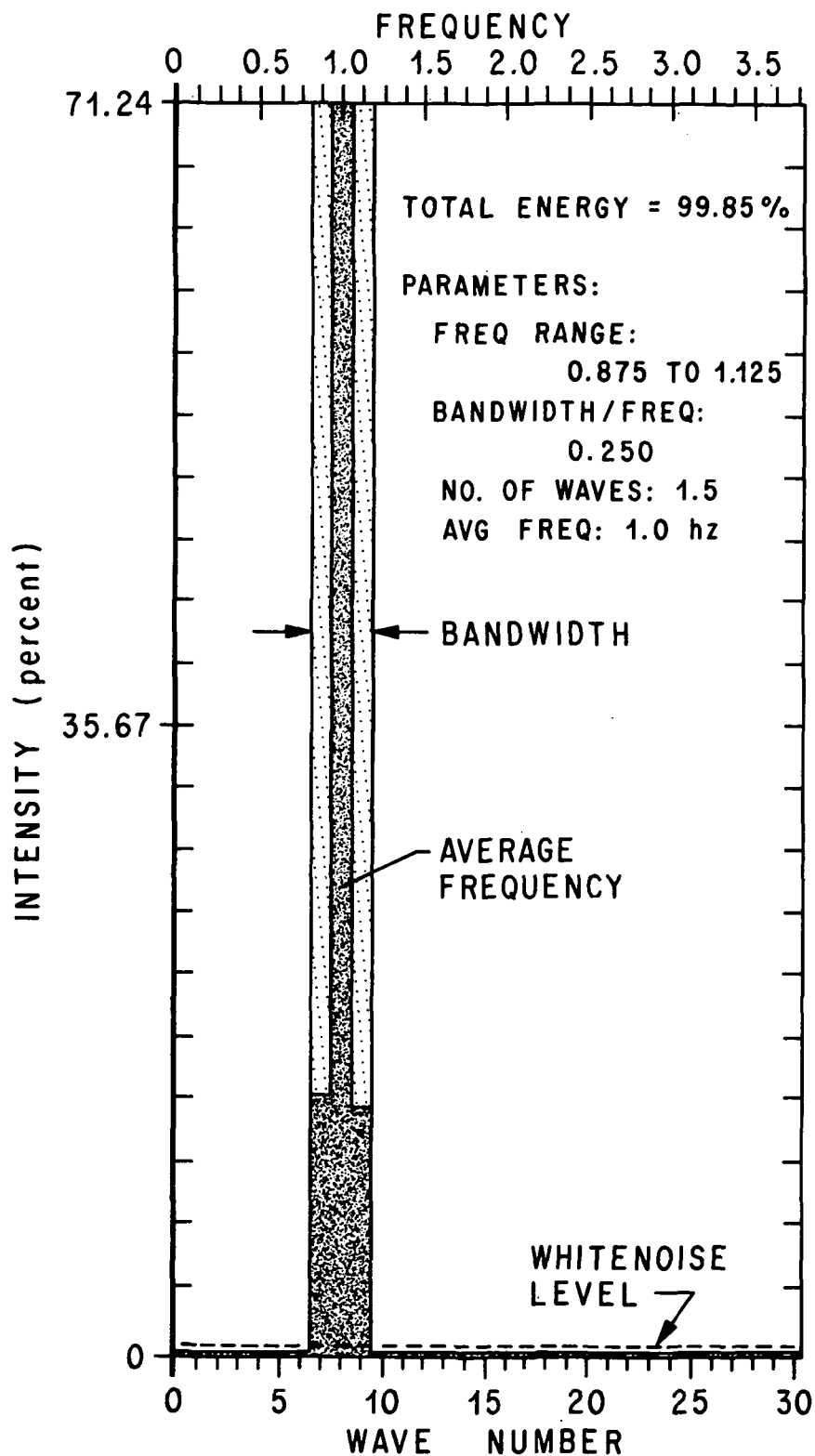


Figure 21. Compressed bandwidth.

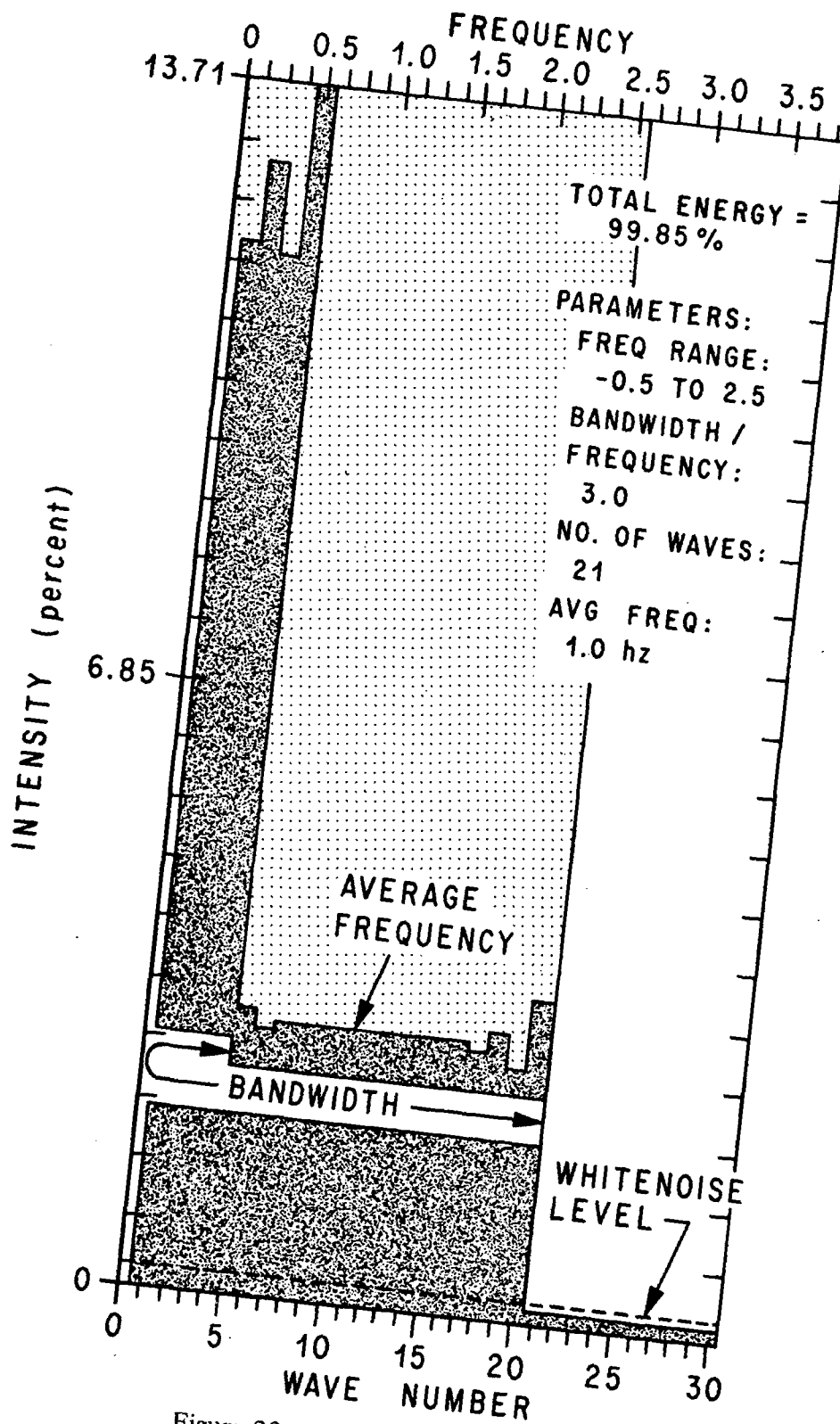


Figure 22. Broadband folding.

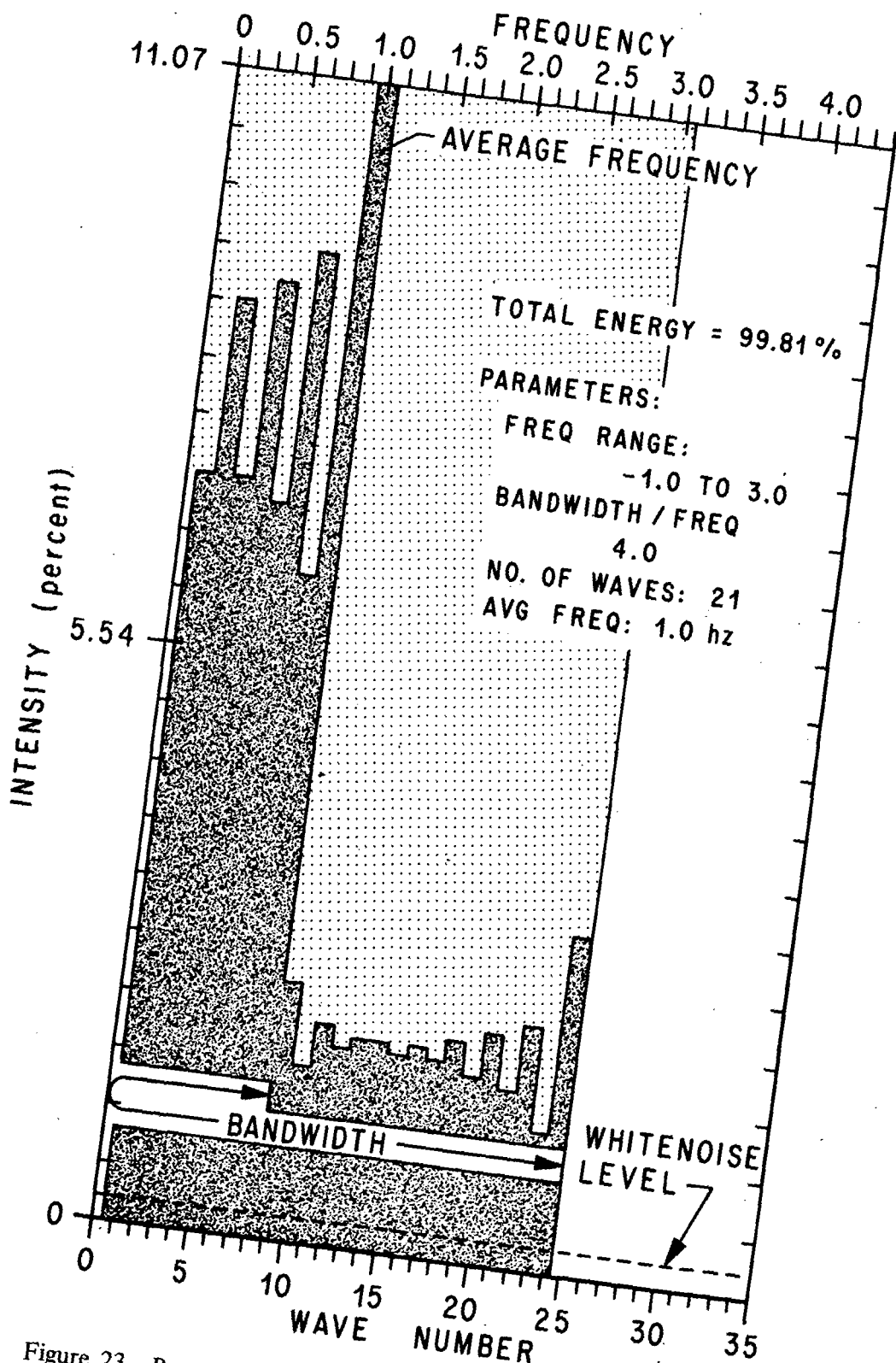


Figure 23. Broadband folding at average frequency.

To verify the validity of the wave packet description, we must examine both the phase diagram (Fig. 5) and the accumulative error (Fig. 7). The phase diagram affords an independent test for the average frequency of the wave packet, since the derivative is normalized by the average frequency. The effect of this normalization is to remove the oscillation in the radial vector resulting from the average frequency; therefore, only the proper frequency normalization removes the oscillations. The average frequency defined by the wave packet description is compatible with the restrictions imposed by the phase diagram. The effective bandwidth (Fig. 7) obtained from the accumulative error can be shown to be the equivalent of the bandwidth in the wave packet description. It can therefore be concluded that the wave packet description is compatible with our overall statistical model. Thus, it is a valid model for interpreting the spectra from any process.

Since our model for interpreting the spectrum is valid, our problem in broadband analysis is again the quantization uncertainty introduced by discrete data. To circumvent this problem, which is inherent to the frequency spectrum, the least-squares criterion for fitting the wave packet algorithm to the autocovariance curve was used. To demonstrate the effectiveness of this criterion, the residue error mapping of the algorithm fit to the covariance curve was made. A typical example of the residue mapping from fitting to the algorithm to covariance curves of boxcar spectral inputs is shown in Table 1. The wave packet algorithm retrieved the exact parameters for the average frequency, bandwidth, and number density in all cases. When the narrowband process was simulated using an elliptical input spectral window, the exact average frequency was retrieved and the bandwidth retrieved gave an equivalent area under the spectral curve (Fig. 24). Similar results were obtained for broadband processes (Fig. 25) using the algorithm. The greatest error in the parameters of the wave number algorithm was found in the number density, where a unique value was not always clearly determined. In spite of this limitation of the wave packet description, the results were always reproducible with the original covariance curve to less than 2.61-percent deviation for narrowband processes and less than 3.46-percent deviation for broadband processes. In general, the deviation between the known covariance curve and the one generated by the algorithm parameters occurred in the far wings of the curve. The number density can be viewed as a fine-tuning adjustment, since it only slightly affects the damping function. A comparison of results obtained with the wave packet algorithm provides the sensitivity and dependability required for transport analysis.

Thus, the classification system which has been just developed not only is an analytical guide to the statistical techniques applicable to the analysis, but it also affords an index to the spectral type. While Fourier analysis affords a parametric estimate for the wave packet description, it lacks the necessary precision for change detection which is obtained with either the direct inspection retrieval or the wave packet algorithm. A degree of care must be exercised with the direct retrieval of the average frequency because its application is limited to periodic and narrowband processes.

With this basis for the retrieval of the wave packet information, we can now examine the analysis of the transport process.

**TABLE 1. MAPPING OF ALGORITHM DEVIATION RESIDUE
FOR AN AVERAGE FREQUENCY OF 5 Hz**

NUMBER OF WAVES	BANDWIDTH (Hz)							
	5.400	5.600	5.800	6.000	6.200	6.400	6.600	6.800
22	0.00312	0.00217	0.00091	0.00050	0.00174	0.00273	0.00331	0.00363
24	0.00316	0.00225	0.00103	0.00033	0.00158	0.00259	0.00321	0.00356
26	0.00320	0.00232	0.00113	0.00020	0.00144	0.00247	0.00313	0.00351
28	0.00323	0.00237	0.00121	0.00009	0.00133	0.00237	0.00306	0.00346
30	0.00326	0.00242	0.00129	0.00000	0.00124	0.00229	0.00300	0.00342
32	0.00328	0.00247	0.00135	0.00008	0.00116	0.00222	0.00295	0.00339
34	0.00331	0.00250	0.00141	0.00015	0.00109	0.00215	0.00290	0.00335
36	0.00333	0.00254	0.00146	0.00021	0.00103	0.00219	0.00286	0.00333
38	0.00335	0.00257	0.00150	0.00026	0.00097	0.00205	0.00283	0.00330
40	0.00337	0.00259	0.00154	0.00031	0.00093	0.00200	0.00279	0.00328
42	0.00338	0.00262	0.00158	0.00036	0.00088	0.00196	0.00276	0.00326
STANDARD DEVIATION BETWEEN ALGORITHM AND TEST CURVE								
<f> = 5 Hz								
Parameters of Test Curve: B = 6.0 Hz								
N = 30 waves								

E. Separation of Convective and Dispersive Transport Phenomena

The various statistical techniques that have been discussed will now be unified to obtain a method of separating the convective and dispersive transport information from the signatures contained in the covariance curve.

Assume that the temporal histories of the fluctuations in the optical density of a flowing fluid have been retrieved at three points along the streamline (Fig. 26). Three cross-covariance curves can be obtained by cross-correlating the temporal information obtained from the x-probe with the temporal information retrieved from the three y_i -probes. This set of three curves provides a mapping along the streamline of the time-averaged transport. To establish the validity of this transport description, the accumulative error is examined to determine whether the process is stationary. If we have a stationary ensemble, then peak identification procedures are used to determine the

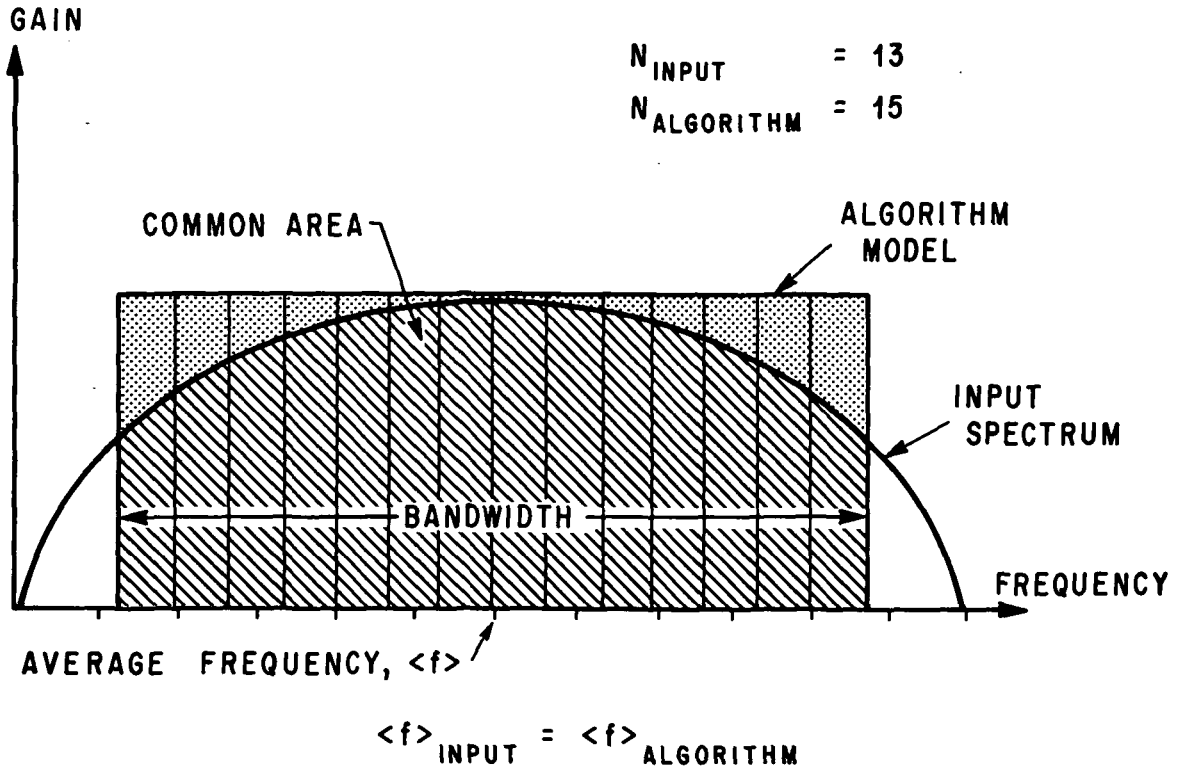


Figure 24. Wave packet algorithm fit of elliptical envelope.

probability of retrieving the transport and of isolating the transit time of the transport. The two transit times thus retrieved are plotted as a function of their transit distance. The slope of the straight line passing through these points is the average convection velocity along the streamline.

To obtain the dispersive signatures, it is necessary to transform the covariance curve from a fixed representation to a representation moving at the convective velocity. Two techniques can be used to obtain this transformation. The first is to suppress the convective information by transforming the gain spectrum into a fourth-order covariance curve. The second technique is to directly obtain a fourth-order covariance curve of the cross-covariance curve by the relation

$$(\overline{xy})_{\tau_m}^2 = \frac{\overline{xy}_{\tau_p - \tau_m} + \overline{xy}_{\tau_p + \tau_m}}{2}, \quad (63)$$

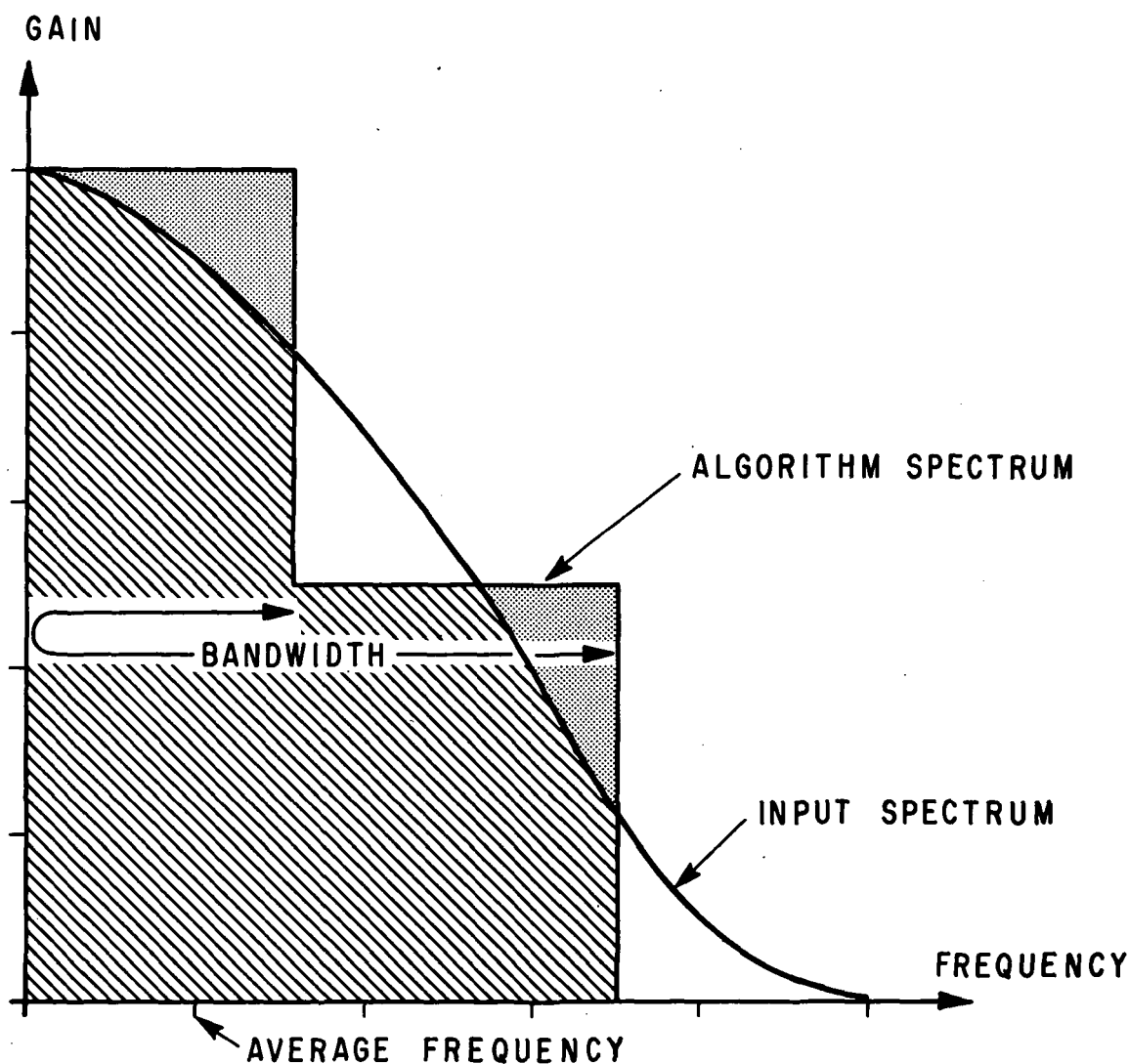


Figure 25. Wave packet algorithm fit of broadband process.

where τ_p is the transit time. This second suppression technique will be used in these discussions because of its simplicity. (The computer program in Figure 18 is designed to use the first technique.)

This fourth-order covariance curve contains only dispersive information since this suppression technique has effectively suppressed the transit time information concerning the convective process. The dispersive information is retrieved from the fourth-order covariance by fitting the wave packet algorithm to it and obtaining the parameters for the wave description.

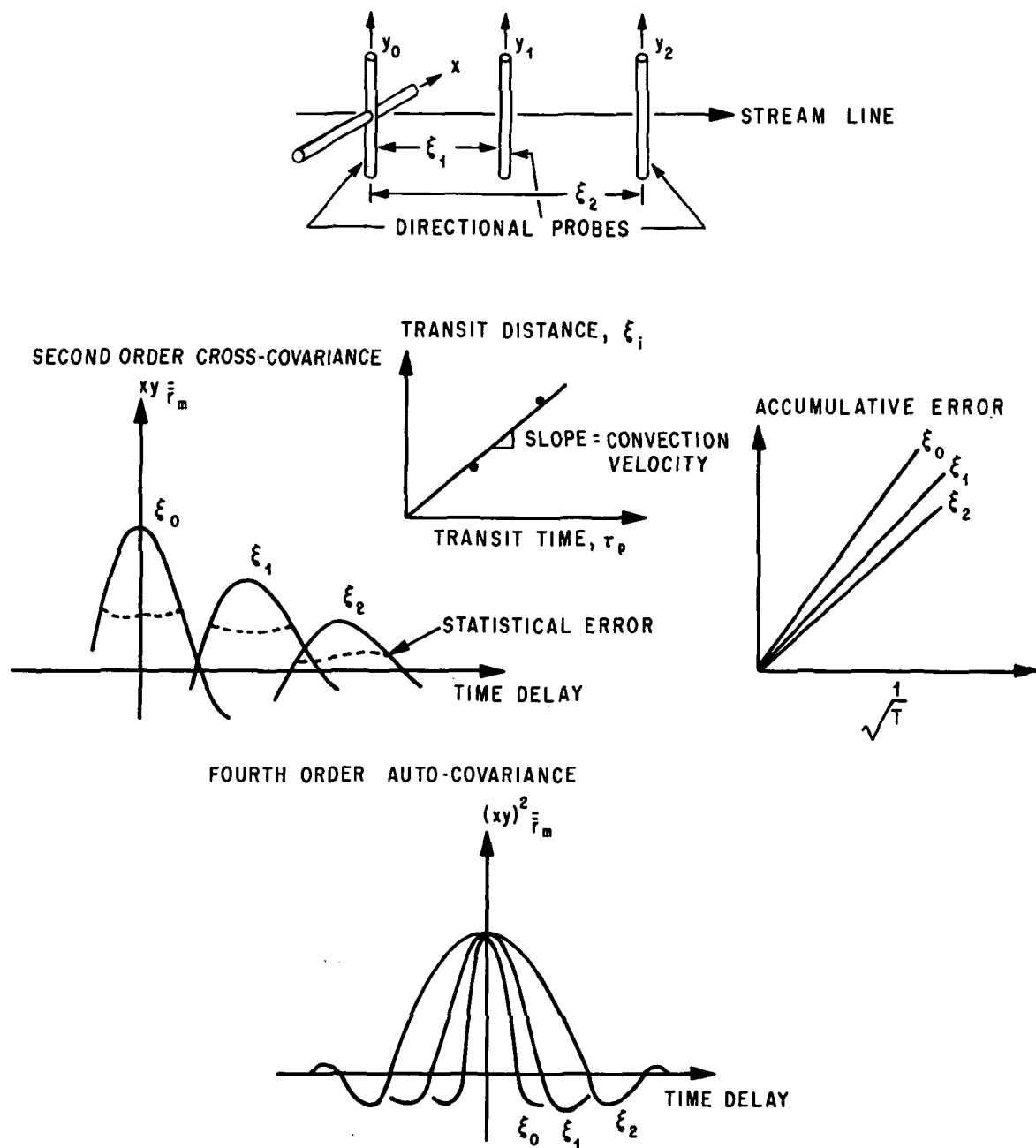


Figure 26. Retrieval of convective and dispersive transport.

The dispersive velocity, v_d , can be expressed in terms of the change in the average frequency of the wave packet, the convective velocity, v_c , and the transit distance. The following argument is used. The change in the packet size, Δs , due to dispersion is

$$\Delta s = \frac{1}{4} \left[\frac{1}{\langle f(\xi_i) \rangle} - \frac{1}{\langle f(\xi_j) \rangle} \right] v_c, \quad (64)$$

where the quarter cycle spread represents the change in the packet shape. The time interval, τ_p , over which this change occurs is

$$\tau_p = \frac{\xi_j - \xi_i}{v_c}. \quad (65)$$

It follows then from the elementary laws of kinematics that the dispersive velocity is

$$v_d = \frac{\left[\langle f(\xi_j) \rangle - \langle f(\xi_i) \rangle \right] v_c^2}{4 \langle f(\xi_i) \rangle \langle f(\xi_j) \rangle (\xi_j - \xi_i)}. \quad (66)$$

The convective and dispersive velocities can thus be separated by first retrieving the convection from the second-order cross-covariance curve, then suppressing the convective information and determining the wave description of the fourth-order autocovariance. The change of average frequency as a function of transit distance affords the dispersion. Returning to the continuity equation [equation (9)], the convection is the mean transport; whereas, the dispersion is the turbulent flux.

SECTION IV. APPLICATIONS TO REMOTELY SENSED DATA

A. Introduction

The empirical evidence of applicability of the statistical techniques, which have been discussed, to remotely retrieve the transport kinematics will now be demonstrated. Since heuristic arguments regarding the crossed-beam test arrangement have thus far been presented, we begin by presenting the analytical arguments that demonstrate the crossed-beam correlation technique's potential to remotely utilize detected optical modulations to obtain local information regarding the turbulent transport process.

The applicability of the kinematic description obtained with these techniques will be illustrated under three different environmental conditions. The analysis of moving striations in the glow discharge is an example of one-dimensional flow which illustrates ensemble grouping, process identification, and transport analysis. The analysis of the convective and dispersive transport associated with the plume of an air jet is used to show the applicability of these techniques to a stationary, two-dimensional turbulent flow in a fixed direction. The third illustration involves transport phenomena in the troposphere where the turbulence flow is nonstationary, and, because the flow direction is a variable, it is also three dimensional.

B. The Crossed-Beam Test Arrangement

The fundamental crossed-beam correlation method which was initially conceived by Krause et al. [1] can be perceived most readily by examining Figure 27. Assume that a region of turbulent flow is contained within the broken line and is being convected in the direction normal to the plane of the diagram. Two optical systems consisting of a radiation source and a radiometer are arranged so that collimated beams of radiation pass across the flow in two mutually perpendicular directions and the beams intersect at the point to be investigated. The wavelength of this radiation is selected so that it is modulated by one or more species of the flow, allowing fluctuations of the concentration or density of the selected species to be reflected in changes in the intensity of the radiometer [19]. Each beam alone reflects only an integral of the appropriate fluctuations along its entire path length; however, it will be shown that the covariance of the signals from the radiometers does yield local information about the point of investigation.

The retrieval of this local information can be explained intuitively as follows: The instantaneous signal at each detector is the resultant of all modulating influences along the path of the beam at a particular time. These modulations of the source radiation can be categorized into two groups:

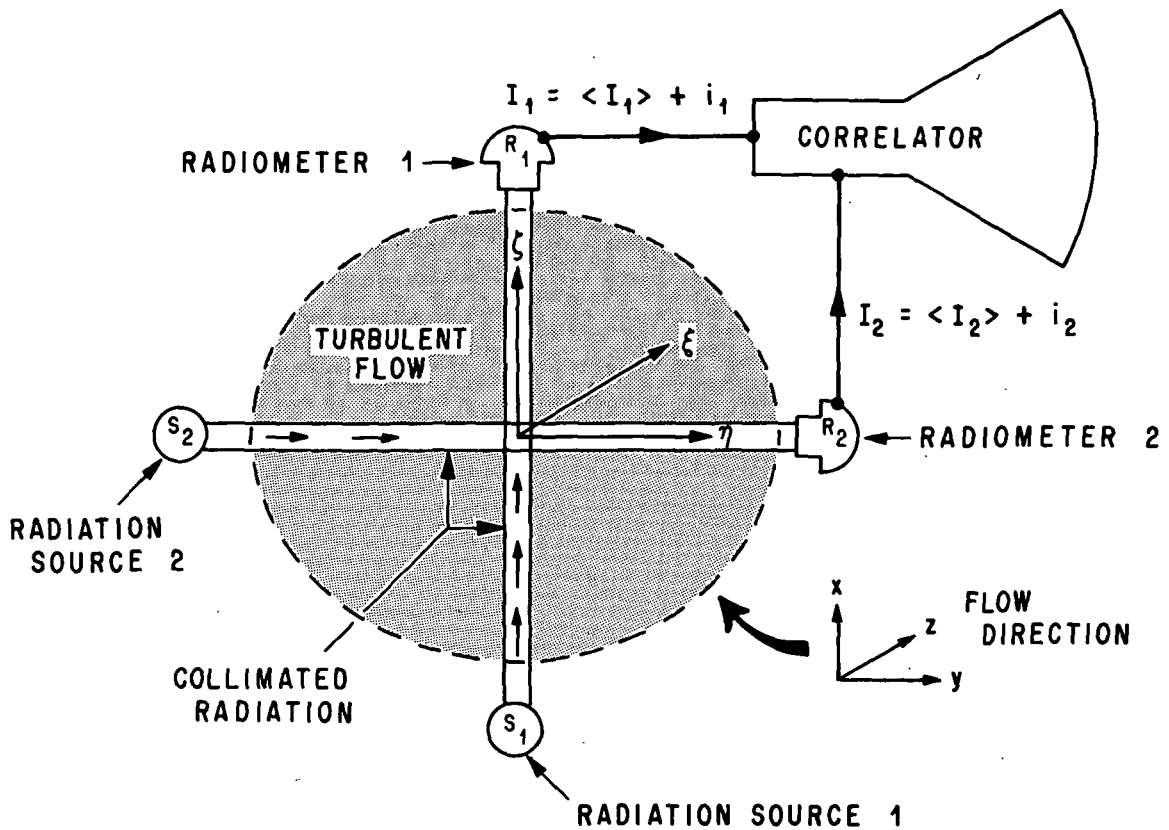


Figure 27. Schematic cross section for the crossed-beam monitoring system in a turbulent flow.

1. Those which occur sufficiently close to the point of beam intersection to introduce a related (i.e., correlated) modulation in both beams.
2. The remaining modulations that occur at a sufficient distance from this point and are uncorrelated because they introduce an unrelated effect on the beam intensities.

The correlation of the two signals will yield an average value of zero for those portions of the modulated signal created by the unrelated flow fluctuations; whereas, the related flow fluctuations will yield a finite average product. In principle, then, the measured covariance is a function of only those fluctuations that modulate the beams in the correlation area around the beam's intersection point.

To analytically demonstrate that the covariance of the two detected modulations yields a measure of required turbulent properties, we will introduce the following coordinate system. The point of beam intersection has the coordinates (x, y, z) where

the x and y axes are oriented parallel to beams one, $S_1 R_1$, and two, $S_2 R_2$, respectively. The distances measured from the point of beam intersection are denoted by ζ , η , and ξ in the x , y , and z directions, respectively.

For beam one, the intensity of the radiation recorded at detector R_1 at time t is

$$I_1 = I_0 \exp \left\{ - \int_{S_1}^{R_1} K(x + \zeta, y, z, t) d\zeta \right\} , \quad (67)$$

where I_0 denotes the initial intensity of the beam and K is the appropriate extinction coefficient. Here, "extinction" is any possible mode of beam attenuation. Two common forms of extinction are pure absorption by a flow constituent and scattering by particulate matter in the flow. The extinction coefficient, K , is also a function of both the wavelength of the radiation and of the thermodynamic parameters of the constituents [19]. Since this dependence does not add enlightenment to the present discussion, it will not be explicitly shown.

Whatever the actual mechanism of extinction, it should be selected such that the extinction depends on a required flow property. Since the flow properties are functions of both position and time in a turbulent flow, the extinction coefficient will be similarly dependent, and thus we can just refer to fluctuations or modulations of the extinction coefficient. Since these changes are linearly related to fluctuations of a flow property, statistical properties of the flow do represent statistical properties of the extinction coefficient.

The instantaneous extinction coefficient, K , can be written as

$$K(x + \zeta, y, z, t) = k(x + \zeta, y, z, t) + \overline{K(x + \zeta, y, z)} , \quad (68)$$

where k is the instantaneous fluctuation of the extinction coefficient about the mean value, \overline{K} . The detected intensity [equation (68)] can now be written as

$$I_1(t) = I_0 \exp \left\{ - \int_{S_1}^{R_1} \overline{K(x + \zeta, y, z)} d\zeta \right\} \exp \left\{ - \int_{S_1}^{R_1} k(x + \zeta, y, z, t) d\zeta \right\} . \quad (69)$$

If the extinction process is such that the integral of the fluctuations $[\int k(x + \zeta, y, z, t) d\zeta]$ is sufficiently small to permit linearization of that portion of the exponential, using the series expansion of an exponential to first-order approximation, the intensities can be written as

$$I_1(t) = I_0 \exp \left\{ - \int_{S_1}^{R_1} \overline{K(x + \zeta, y, z)} d\zeta \right\} \times \left[1 - \int_{S_1}^{R_1} k(x + \zeta, y, z, t) d\zeta \right] . \quad (70)$$

This assumption does not restrict the crossed-beam correlation technique to applications with small modulation of the optical beam because of the following:

1. The integral in question represents a sum of a number of statistically independent events, which will tend to reduce the value of the integral.

2. It was shown [20] that if the integral of the fluctuations is of the order of 10 percent of the mean integrated value or less, then an optimum value for the mean attenuation is given by

$$\int_{S_1}^{R_1} \overline{K(x + \zeta, y, z)} d\zeta = 1 . \quad (71)$$

For this magnitude of fluctuation, the linearization would be acceptably accurate.

3. If larger fluctuations relative to the mean value are experienced, it would be acceptable and indeed desirable to reduce the mean absorption, by reducing the gain, so that linearization is still possible.

If the intensity at the detector is now written as the sum of its time average \bar{I}_1 and a fluctuation component $i_1(t)$ relative to the average value, it can be shown that

$$i_1(t) = - \bar{I}_1 \int_{S_1}^{R_1} k(x + \zeta, y, z, t) d\zeta . \quad (72)$$

Within the limits of the above discussion, we obtain the expected result that the fluctuation of the intensity at the detector is proportional to the instantaneous integral of the modulations of intensity along the entire light path.

By inspection, we can write similar results for the other beam:

$$i_2(t) = - \bar{I}_2 \int_{S_2}^{R_2} k(x, y + \eta, z, t) d\eta \quad . \quad (73)$$

If we now take these two fluctuating intensities, $i_1(t)$ and $i_2(t)$, and determine their time-average product, we obtain the covariance in a piecewise form similar to equation (24); i.e.,

$$\begin{aligned} \frac{i_1 i_2}{\tau} &= \frac{\bar{I}_1 \bar{I}_2}{\sqrt{\bar{I}_1^2 \bar{I}_2^2}} \\ &\times \int_{S_1}^{R_1} \int_{S_2}^{R_2} \frac{1}{T} \int_0^T k(x + \zeta, y, z, t) k(x, y + \eta, z, t) dt d\eta d\zeta \quad , \end{aligned} \quad (74)$$

where the spatial and temporal integration has been reversed. This now gives us the covariance as a function of the modulations of the extinction coefficients, or in terms of the statistical flow parameters of the fluid.

To most conveniently understand how spatial resolution is obtained with the cross-covariance, we will initially consider just the temporal integration at $\tau = 0$:

$$\overline{\rho(x + \zeta, y + \eta, z)} \bigg|_{\tau=0} = \frac{1}{T} \int_0^T k(x + \zeta, y, z, t) k(x, y + \eta, z, t) dt. \quad (75)$$

This term clearly represents the covariance of the fluctuations occurring at the two points $(x + \zeta, y, z, t)$ and $(x, y + \eta, z, t)$. If one or both of these points are sufficiently far

from the beam intersection point in an inhomogeneous flow, the fluctuations will be mutually random and the resulting covariance will be zero. Only those points contained within the correlation area around the beam intersection point will contribute to the measured value of the covariance. Therefore, the value of the covariance, $i_1 i_2 \bar{r}$, does not change if these limits are replaced by those limits of the locally correlated area, although formally the limits of spatial integration in equation (74) extend from source to detector. Because of our prerogative in establishing the limits, we can view the measured quantity as reflecting only the local modulating information and thus providing spatial resolution.

To retrieve the transit time between beams, the two beams must be separated in the z -direction a distance ξ (Fig. 28). To the flow, there still appears to be an intersection point for the beams, which we shall refer to as a "virtual crossing point." This virtual point is the only point at which a particle moving in the z -direction can pass through both beams; therefore, the intersecting beam argument for spatial resolution still holds except that the information is correlated now at a time delay. The time delay τ_ρ , corresponding to the maximum covariance, is a measure of the transit time between the beams.

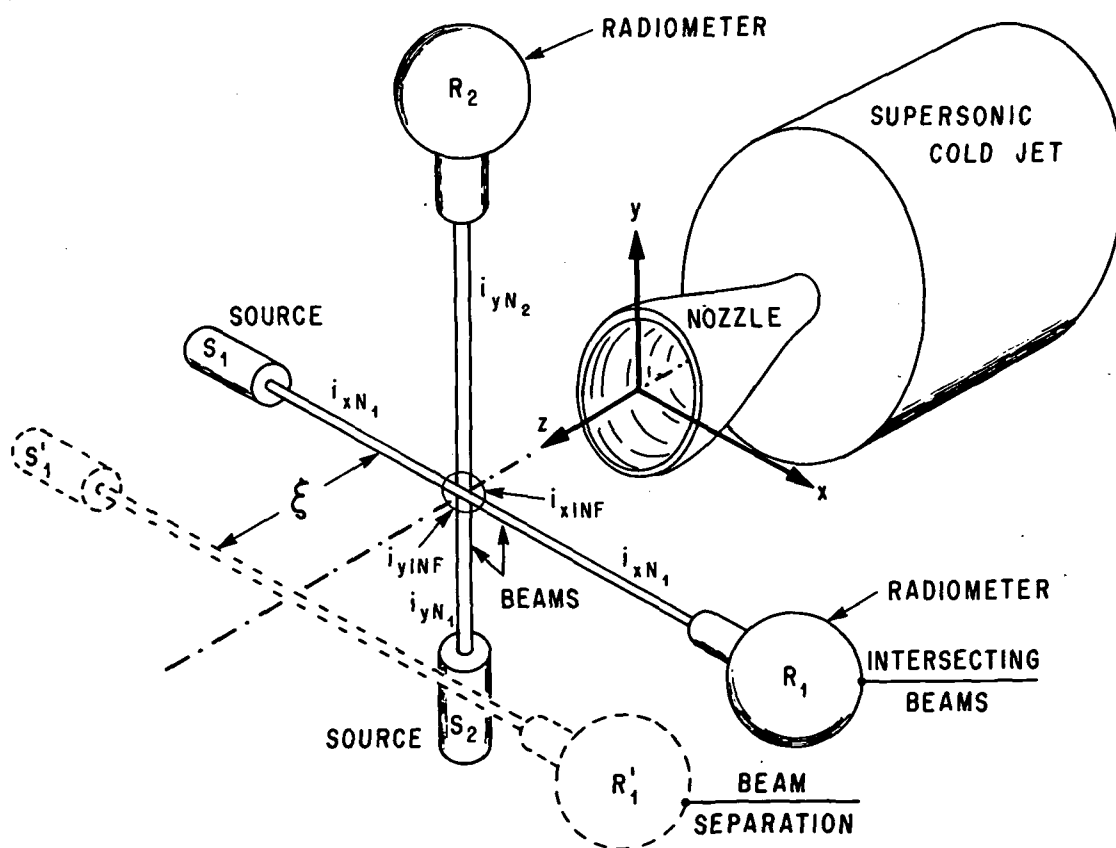


Figure 28. Crossed-beam test configuration for the cold jet.

This now provides an analytic association of the extinction coefficient with the crossed-beam correlation model. This model could be easily expanded to include spectroscopic emission and absorption [19], but for this discussion, our attention can be focused on just the kinematics of the flow.

C. Ion and Electron Transport in the Glow Discharge

To empirically demonstrate the feasibility of the retrieval and separation of convective and dispersive fluid transport, the application of the crossed-beam correlation technique to an investigation of moving striations in the flow discharge will be discussed.

The striation is the disc of ionized and excited gas found in the positive column of the glow discharge (Fig. 29). Since the ions normally give the striated gas a net positive charge, these striations, which we will call forward-moving striations, move toward the cathode (Fig. 30) [21,22]. This emission process is the signature for the ion transport.

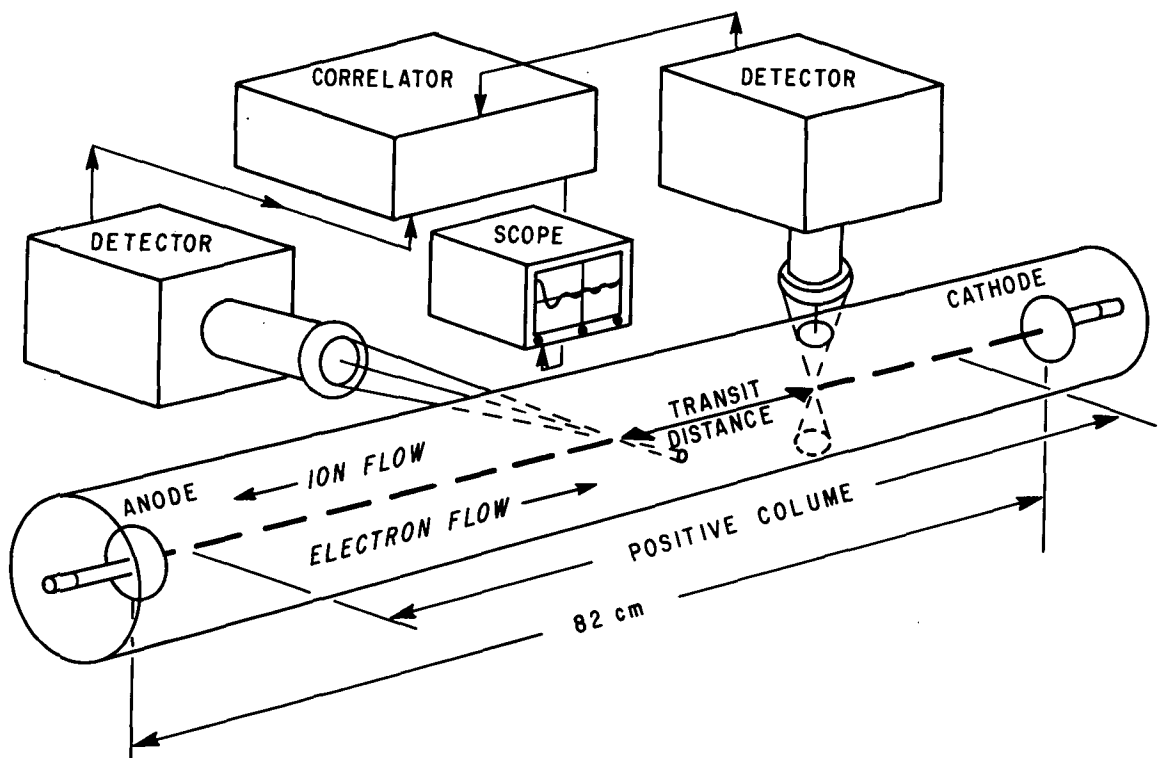


Figure 29. Experimental setup for glow discharge.

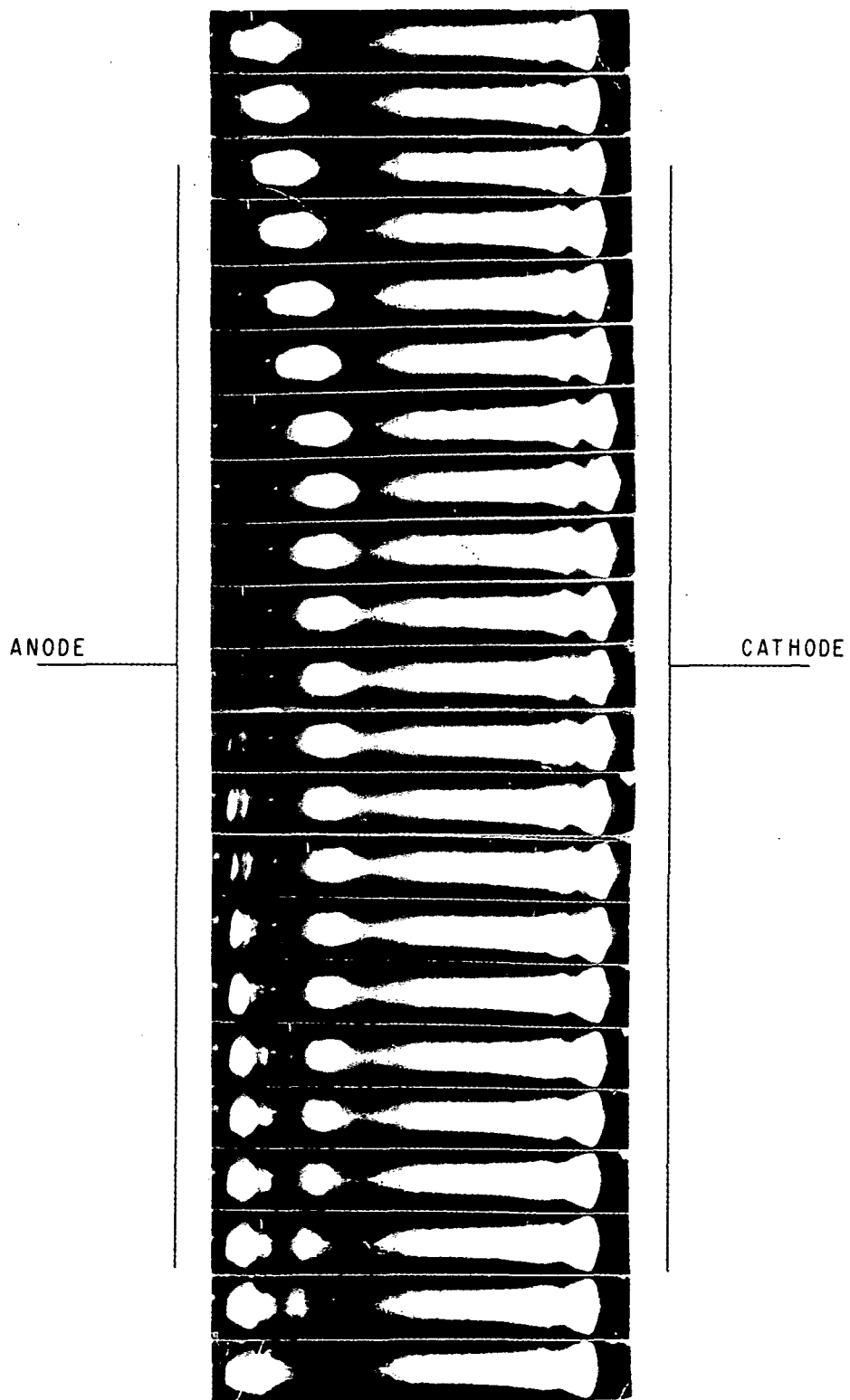


Figure 30. Forward-moving striation.

There exists in the glow discharge a second transport; namely, an electron flow from the cathode to the anode. The electron flow is an extinction process whose signature modulates the ionization and excitation of the striation resulting in detectable undulations in the emission. When the striations are weakly ionized compared to the electron flow, the backward-moving striation exists (Fig. 31). Other investigators have also made this observation [23,24]. The importance of the backward-moving striation lies in the fact that it demonstrates the dispersive and convective transport characteristics of the electron flow. The glow discharge consequently provides an excellent stationary one-dimensional data source to demonstrate the effectiveness of the statistical method and algorithms used for fluid transport analysis.

The transport process in the glow discharge was monitored by the crossed-beam configuration shown schematically in Figure 29. While a wide range of different kinds of transport was observed [4], our primary interest in these discussions is the data obtained when both electron and ion transport were simultaneously detected. A typical segment of such a data record is shown in Figure 32.

The initial step in the data analysis was to cross-correlate the data and obtain the accumulative covariance, the accumulative error, and the transport probability in accordance with the data reduction scheme shown in Figure 33 [25]. The accumulative error was used to determine when the discharge was in equilibrium. It was found that about a half-hour warmup time was required for the transport process to reach its first stage of equilibrium. Once this stage was reached, the data could be treated as stationary until there was a discrete transition to the next lower mode. These transitions continued until the ground mode was reached. The physical significance of these modes will be explained. For now it is important to recognize that the accumulative error did permit us to differentiate between the different modes and to group coherently the data in its proper mode.

The transport probability showed:

1. A high probability that two different transport processes were occurring simultaneously in different directions — one a high frequency transport, the other a low frequency transport. Retroactive filtering [26]¹ was used to separate these two transport processes.

2. A high probability that the fluctuations in the discharge current were related to the transport moving toward the anode. Spatial mappings of the backward-moving striations showed there was indeed a correlation between these striations and the current.

1. Essentially, retroactive filtering is where the covariance curve is transformed to the frequency domain. The gain of the frequencies to be filtered are suppressed by setting them to zero and transforming the remaining energy density spectrum back to the time domain. Thus, the covariance curve is filtered without reprocessing the data.

ANODE

CATHODE

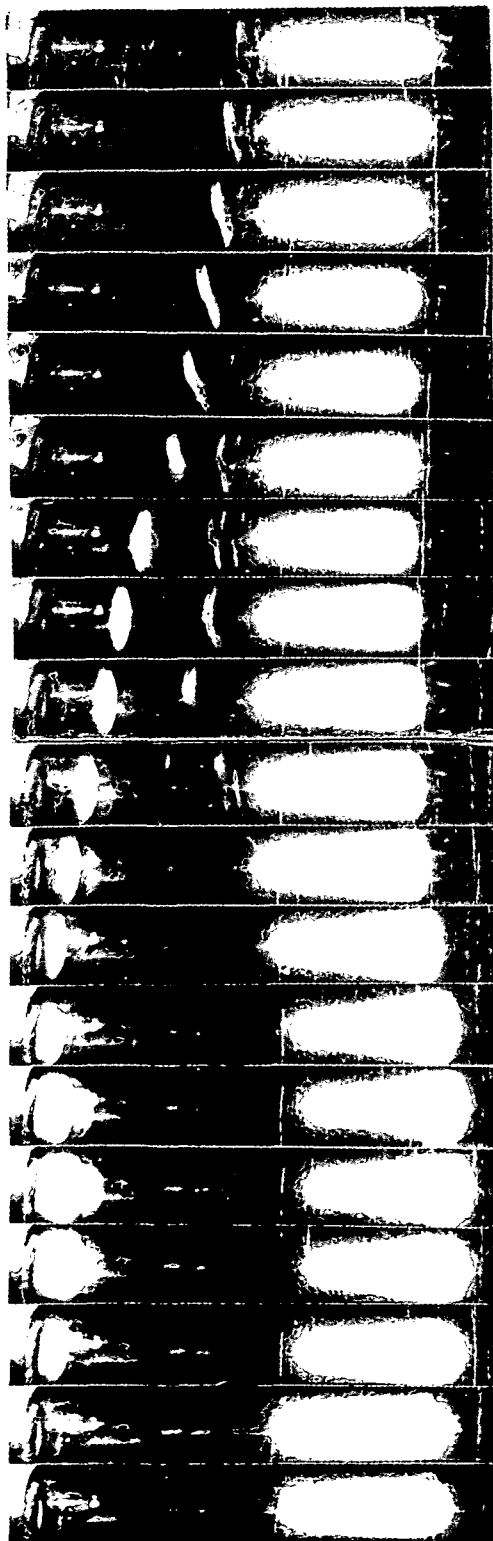


Figure 31. Backward-moving striation.

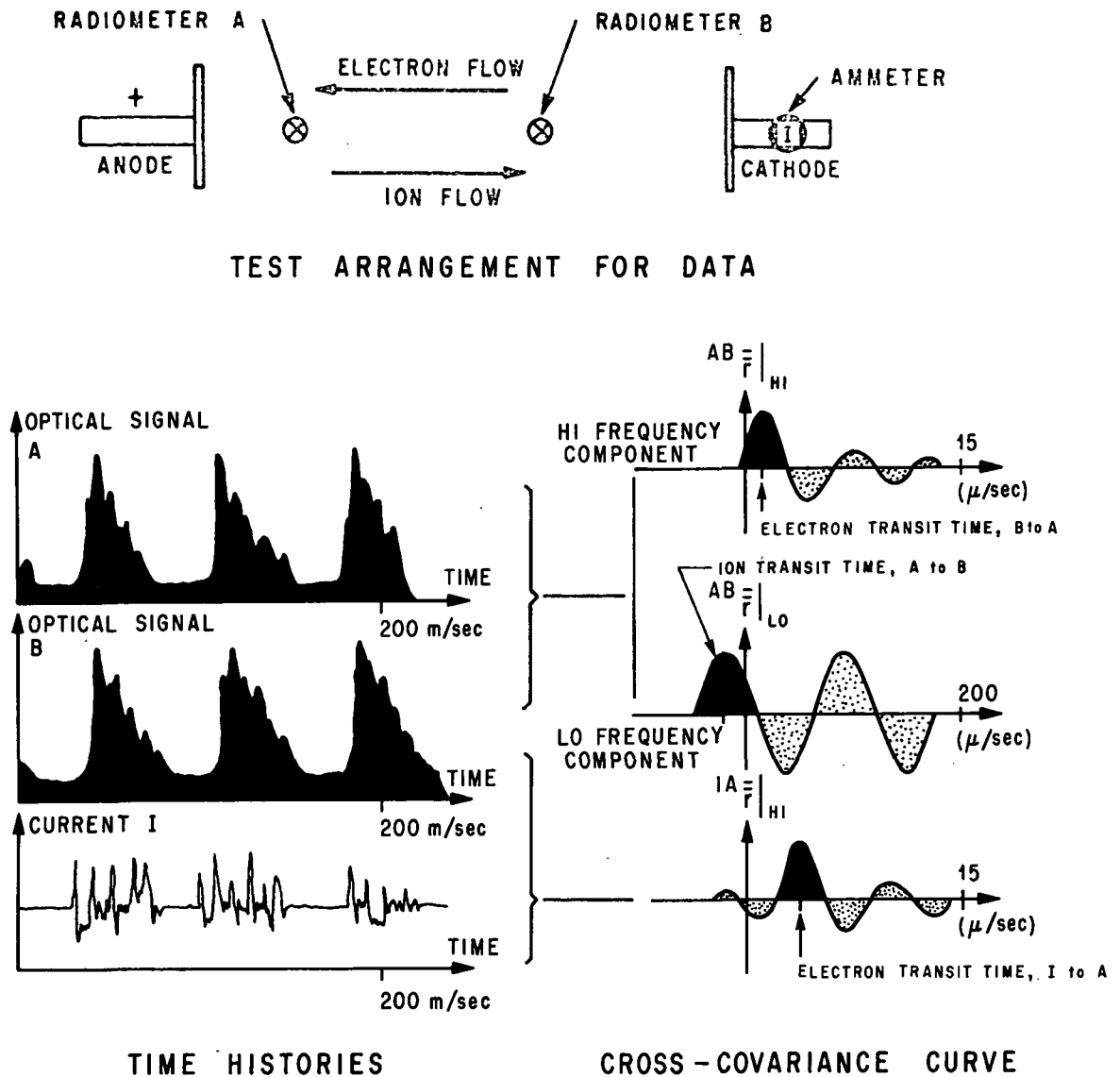


Figure 32. Separation of electron and ion transport.

fluctuations. Thus, the transport probability in these experiments served to isolate the different processes occurring in the glow discharge during a time interval which has been shown, using the accumulative error, to be stationary.

Based on the transport probability, if we retroactively suppress the high frequency information by filtering the processed results, we obtain a field description of striations moving toward the cathode. The results of the forward-moving striations are summarized in Figure 34. The spatial mapping of the covariance curves affords a representation of the

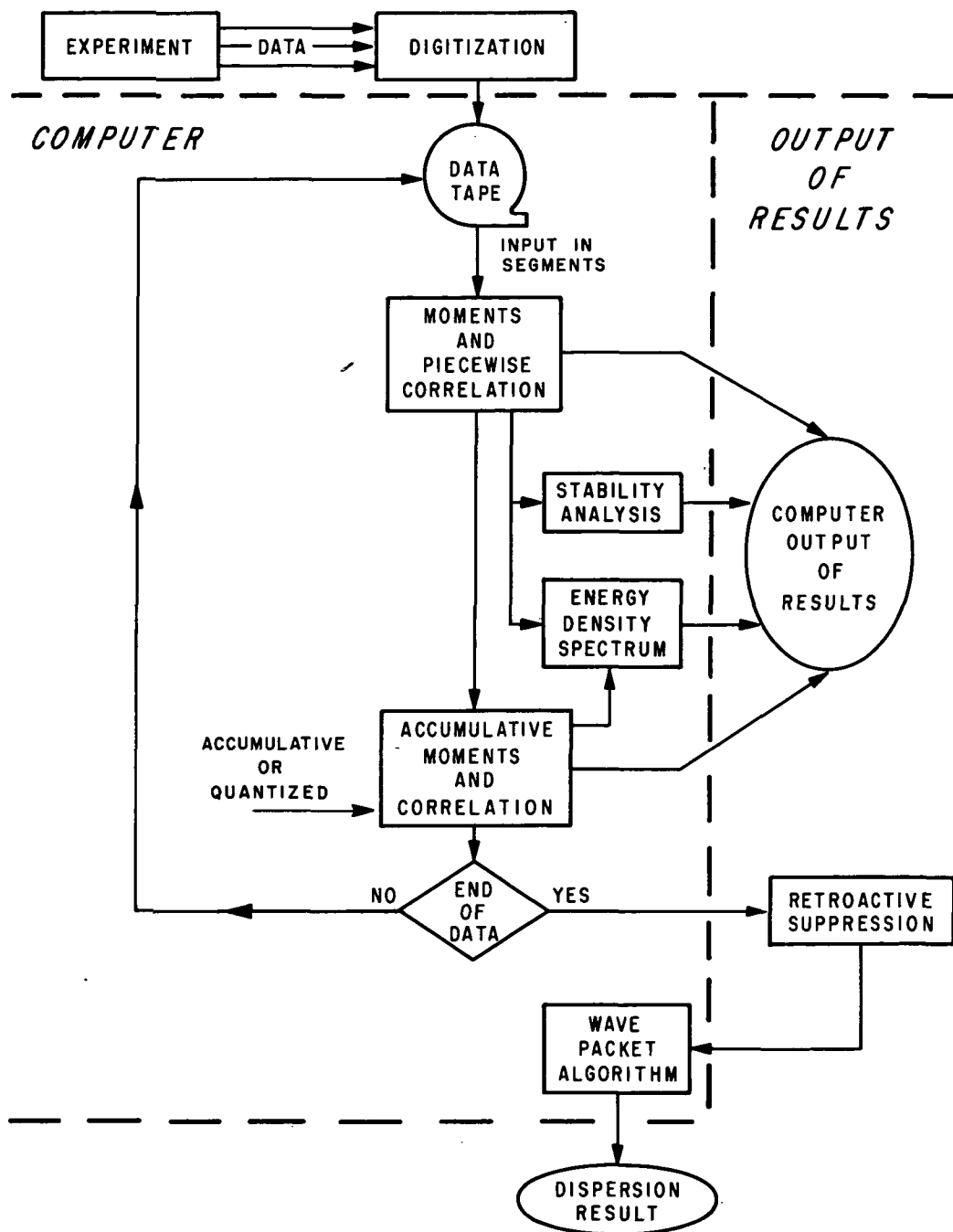


Figure 33. Data reduction block diagram for MLTCOR.

The fourth-order autocovariance mapping in which the observer is in a moving frame where the transit time information has been suppressed indicates that the longitudinal length scale of the forward-moving striation was invariant as it was propagated along the positive column of the discharge. The proof of this invariance is obtained from the spatial independence of the wave description. The longitudinal length of the ion striation is obtained from the relation

$$l_x = \frac{v_c}{2\langle f \rangle} \quad , \quad (76)$$

where v_c is the convection velocity and $\langle f \rangle$ is the average frequency obtained from the wave packet algorithm. The experimental results for this striation length varied from 5.3 to 10.2 cm as a function of the electrical energy supplied to the discharge. These length scales are in keeping with values obtained from high speed movies of the discharge.

The repetition frequency, which is the rate at which an event occurs at a point, can be retrieved either directly from the crosscovariance or from the frequency spectrum of this curve by retroactively suppressing the wave packet description. The remaining energy density spectrum is due to the rapidity of the process. (If no spectrum exists, then the average frequency is the repetition frequency.) Using the repetition frequency, f_r , and the convection velocity, v_c , the longitudinal wavelength is

$$\lambda_x = \frac{v_c}{f_r} \quad . \quad (77)$$

The longitudinal wavelength of the ion striation was always an integral multiple of the length of the positive column, l_{pc_x} ; i.e.,

$$l_{pc_x} = n\lambda_x \quad \text{where } n = 1, 2, 3, 4 \quad . \quad (78)$$

The highest mode measured was four. The most stable mode was $n = 1$ and will be referred to as the ground mode. Experimental observations revealed that there was always a discrete transition between the modes, which could be detected by changes in the accumulative error. These changes appeared when the power supplied to the discharge was changed, whereupon a nonground mode would occur. This higher mode would decay back to the ground mode in discrete transitions. For standing striations, the wavelength

relation changed such that the ground mode corresponded to a wavelength equal to the distance between like points of adjacent striations rather than the length of the positive column.

The signature of the electron transport was enhanced by suppressing the lower frequencies (Fig. 35). The analysis used for the ion striations was repeated for the electron transport. Since the test configuration has been reversed, the positive convection velocity (Fig. 36), which is obtained from the plot of the transit time as a function of transit distance, implies that the flow direction is from the cathode to the anode. This flow was identified as an electron transport by first obtaining a cross-covariance between the optical fluctuations in the ionized gas and the fluctuations in the discharge current, and then calculating the transport probability. Close analysis of the temporal histories of these fluctuations revealed that there was not a continuous flow but rather a discrete transport; therefore, the electron transport can be more accurately referred to as a flow of electron packets which are propagated toward the anode.

When the transit time information was suppressed [equation (63)], the mapping of the fourth-order autocovariance curves (Fig. 36) showed that the electron packet's shape was not invariant during its propagation toward the anode. This observation was supported by a change in the average frequency obtained from the wave packet algorithm. The electron packet's dispersion velocity [equation (66)] was calculated to be approximately 260 m/sec compared to the ion convection velocity of 16 km/sec. Using the relation for the longitudinal length scale [equation (76)], the electron packet size changed, on an average, from 1.0 to 1.5 cm over a transit distance of 30 cm. The major problem encountered in this work was that the dispersive effect required a resolution of one part in 10^7 per centimeter to retrieve the changes in the average frequency. Thus, only by the use of averaging techniques and the wave packet algorithm was it possible to obtain the consistent results required for this change detection.

These typical results demonstrate the feasibility of the analysis procedure used. Systematic analysis afforded by statistical techniques enhances the results and thereby reduces the amount of interpretation required. Since moving striations and turbulence eddies are both treated as moving packets of molecules, we can, in our next discussion of turbulent transport, conceptually approximate the turbulence eddies as being moving striations.

D. Convective and Dispersive Transport in a Supersonic Jet Shear Layer

The supersonic cold jet transport will be used as an empirical illustration of the applicability of the convective and dispersive transport model to stationary two-dimensional transport problems. To obtain a two-dimensional coordinate system, the axial streamline is assumed to be an axis of symmetry. This two-dimensional model is a direct extension of the one-dimensional description used with the glow discharge except that it accounts for lateral kinematics that could be neglected in the one-dimensional

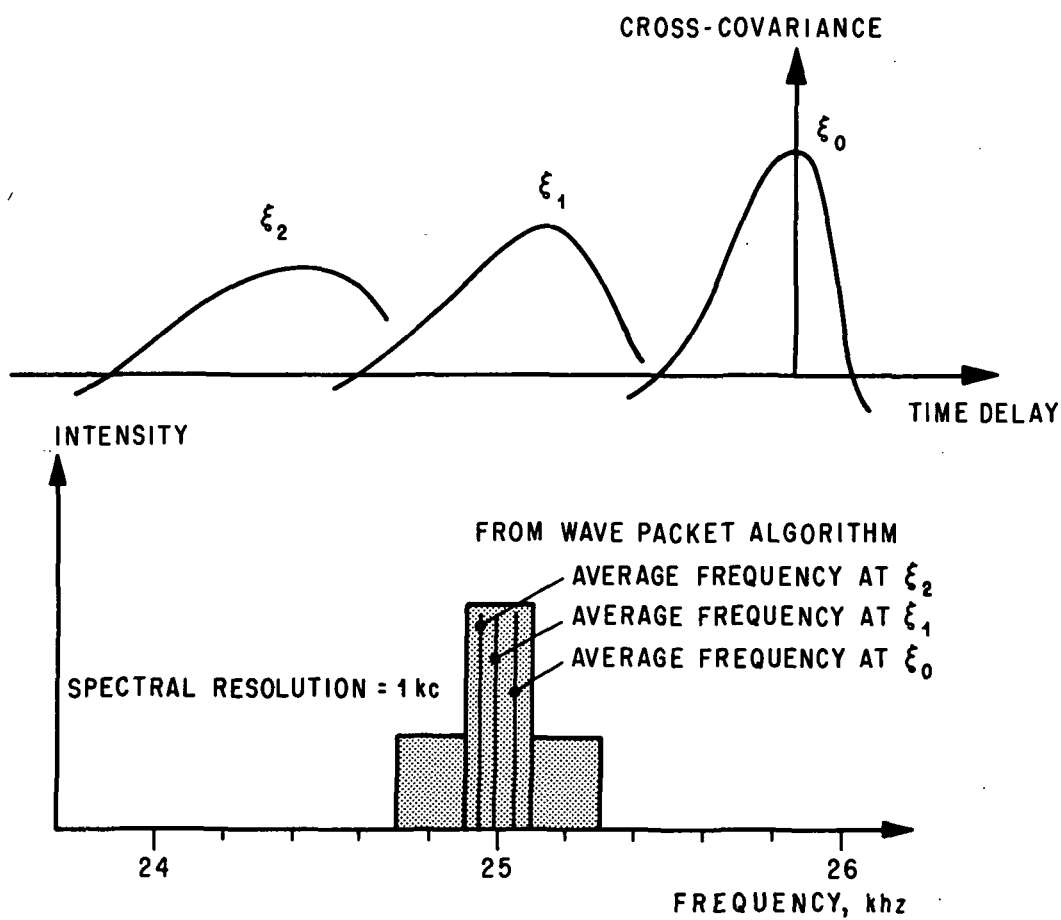
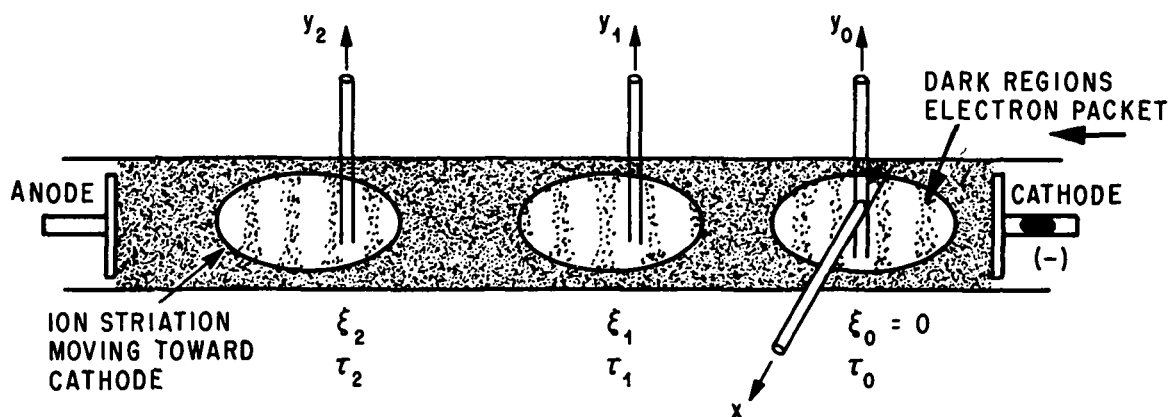


Figure 35. Electron packet flow in the glow discharge.

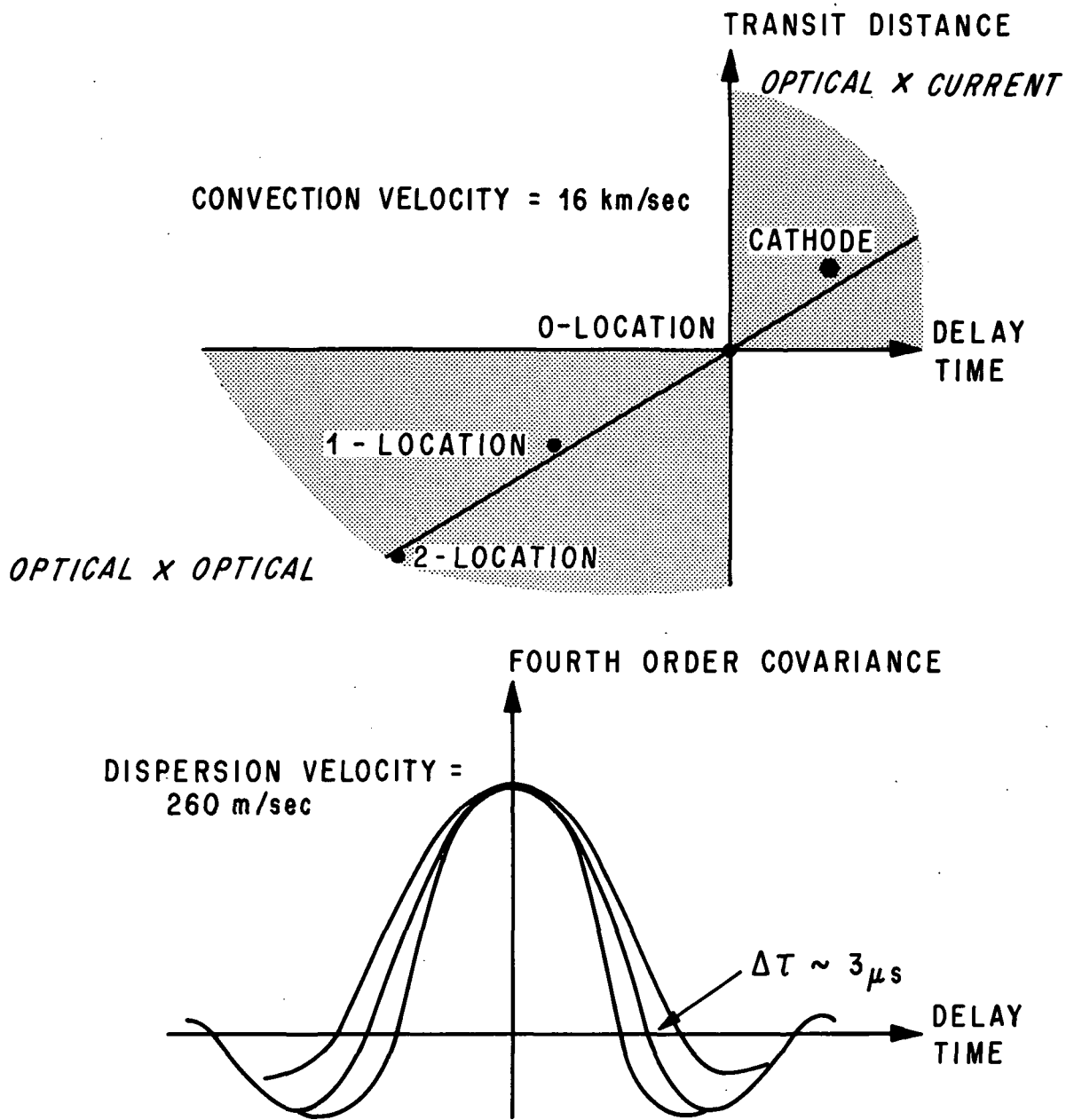


Figure 36. Convection and dispersion velocities for electron flow.

flow using the constraints of the system. Our conceptual view must become more sophisticated for transport processes which are not subjected to the constraints of a one-dimensional flow. The shadowgraph of the cold jet flow clearly shows the flow expansion, which must be accounted for in any complete description of the kinematics. To this end, Corrsin's spherical description is introduced to account for this transport behavior [27]. The applicability of the spherical model was demonstrated in the

discussion of the fluid model. The implications of this assumption are a discrete flow formed from a collection of expanding spheres emanating from a point source. These spheres are referred to as "turbulence eddies," and are assumed to be of constant mass with a changing volume due to thermodynamic and force gradients. The current state of the statistical information retrieved prohibits a detailed consideration of these gradients, thus limiting the predictability of any of the algorithms to a local description. This means that the long-range kinematics can be extrapolated only from a spatial mapping.

The cold jet is schematically shown in Figure 28. Again, we will assume a fan beam test arrangement, which is obtained by making a series of measurements along the streamline under similar test conditions. Using those data obtained along a streamline by Fisher and Johnston [2], the spatial mapping of the covariance curves shown in Figure 37 was obtained. When Fisher and Johnston plotted the transit time as a function of transit distance, they obtained a convection velocity of 347 m/sec. They further showed that the

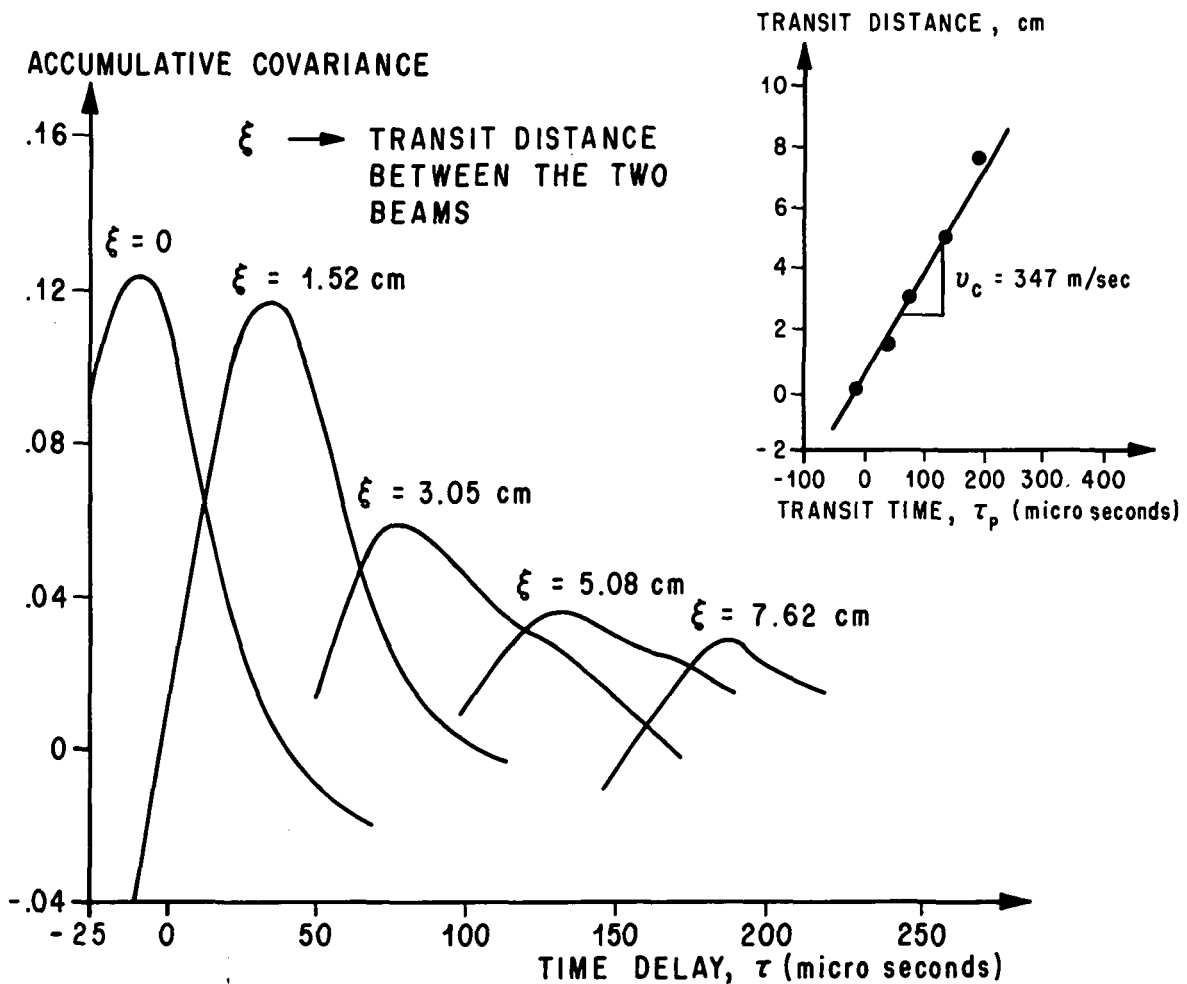


Figure 37. Space-time correlation curves for cold air jet.

data were stationary by using the accumulative error (Fig. 9) to establish the reliability of their results. The decay in the amplitude of the peaks of the covariance curves as a function of transit distance is a signature indicating the presence of a dispersive transport. To emphasize the need for a more sensitive wave description, we show the typical frequency spectrum of these covariance curves in Figure 38. Upon inspection of this spectrum, it is obvious that a resolution of one part in 10^7 per centimeter for the change in the average frequency, which is required to retrieve the dispersive transport, cannot be obtained. Thus, we are again, as with the glow discharge, forced to use regression analysis of the wave packet algorithm [equation (55)] for each of these covariance curves to retrieve the parameters for the wave description.

The bandwidth ratio did change as we moved radially outward across the shear layer from 1.47 to 1.92. While the plume of the jet involves a clearly narrowband process, we observe that, as we move out of the jet's flow, the process tends to approach a broadband process. This is the expected result since atmospheric turbulence is characteristically a broadband process.

Using the average frequency obtained with the wave packet algorithm, in the dispersion relation [equation (64)], an average radial dispersion velocity of 19.7 m/sec was obtained with a convection velocity of 347 m/sec. If we assume that there is spherical expansion from a point source, in accordance with Corrsin's model and our fluid model, then we can obtain a lateral mixing rate, L , given by

$$L = \frac{2 v_d}{v_c} \quad . \quad (79)$$

Applying this relationship to this data set, we obtain a lateral mixing rate of 0.1135. This rate implies a radial plume expansion of 11.35 cm/m downstream. This expansion rate is plotted on the shadowgraph of the jet plume, along with the locations of the points from where the local turbulent information was retrieved (Fig. 39). The outer plume cone is drawn so as to include all of the plume; whereas, the inner cylinder represents no plume expansion. It is clear from studying this shadowgraph that the cone defined by the rate of radial expansion is the average rate of expansion. This follows logically, as would be expected, since the source of the statistical information is obtained from the covariance curve, which is an averaging process, and is in accordance with the average turbulence flux [equation (12)]. Thus, the rate of dispersive transport obtained from the wave description affords an accurate analytical description of the physical situation associated with the cold jet plume.

It is recognized that this prediction of convective and dispersive transport is only short range, since long range prediction would require an accounting for shear and gravitational forces [6,28,29]. In spite of this limitation, this new description of

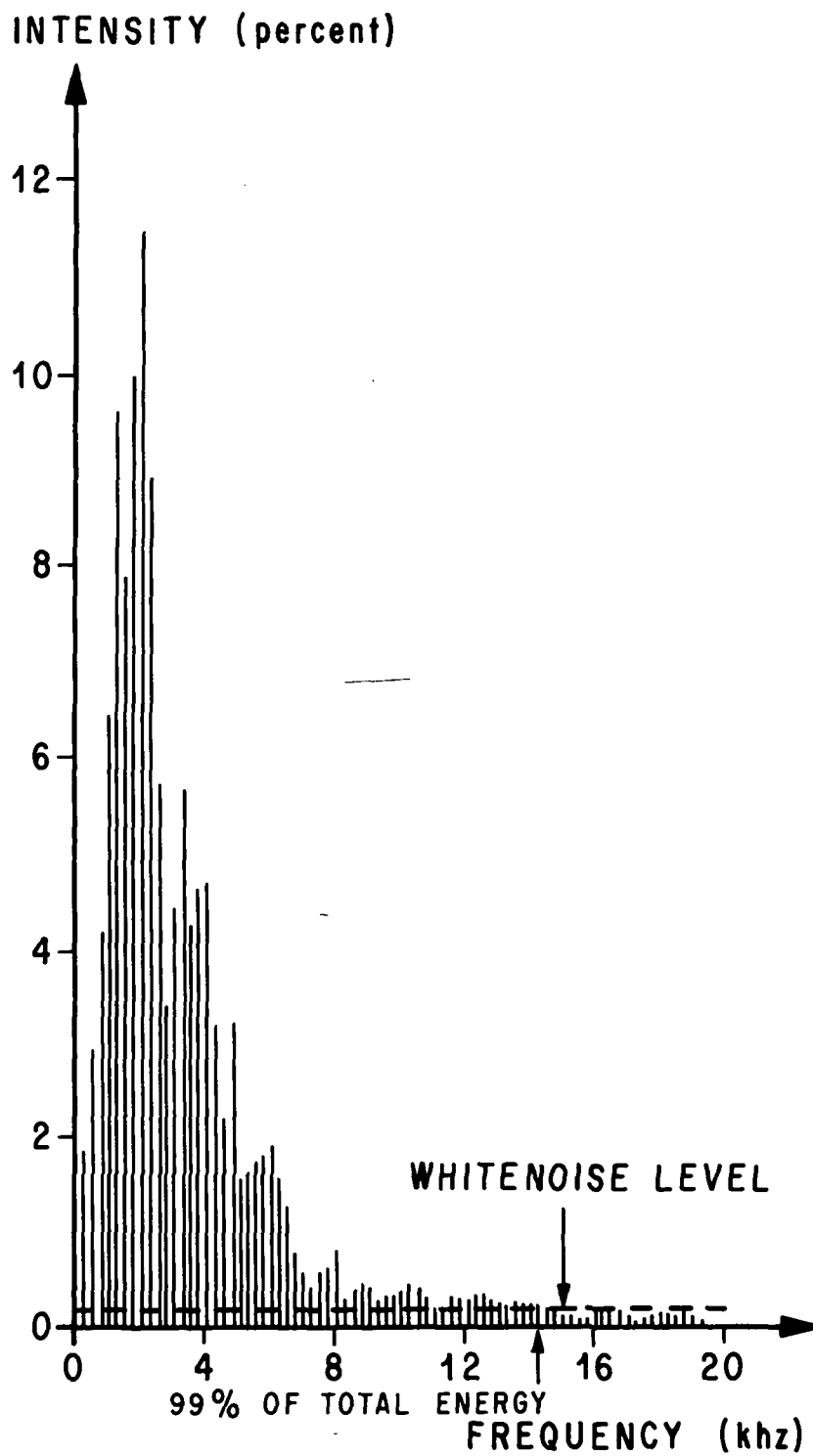


Figure 38. Typical energy density spectrum for cold air jet.

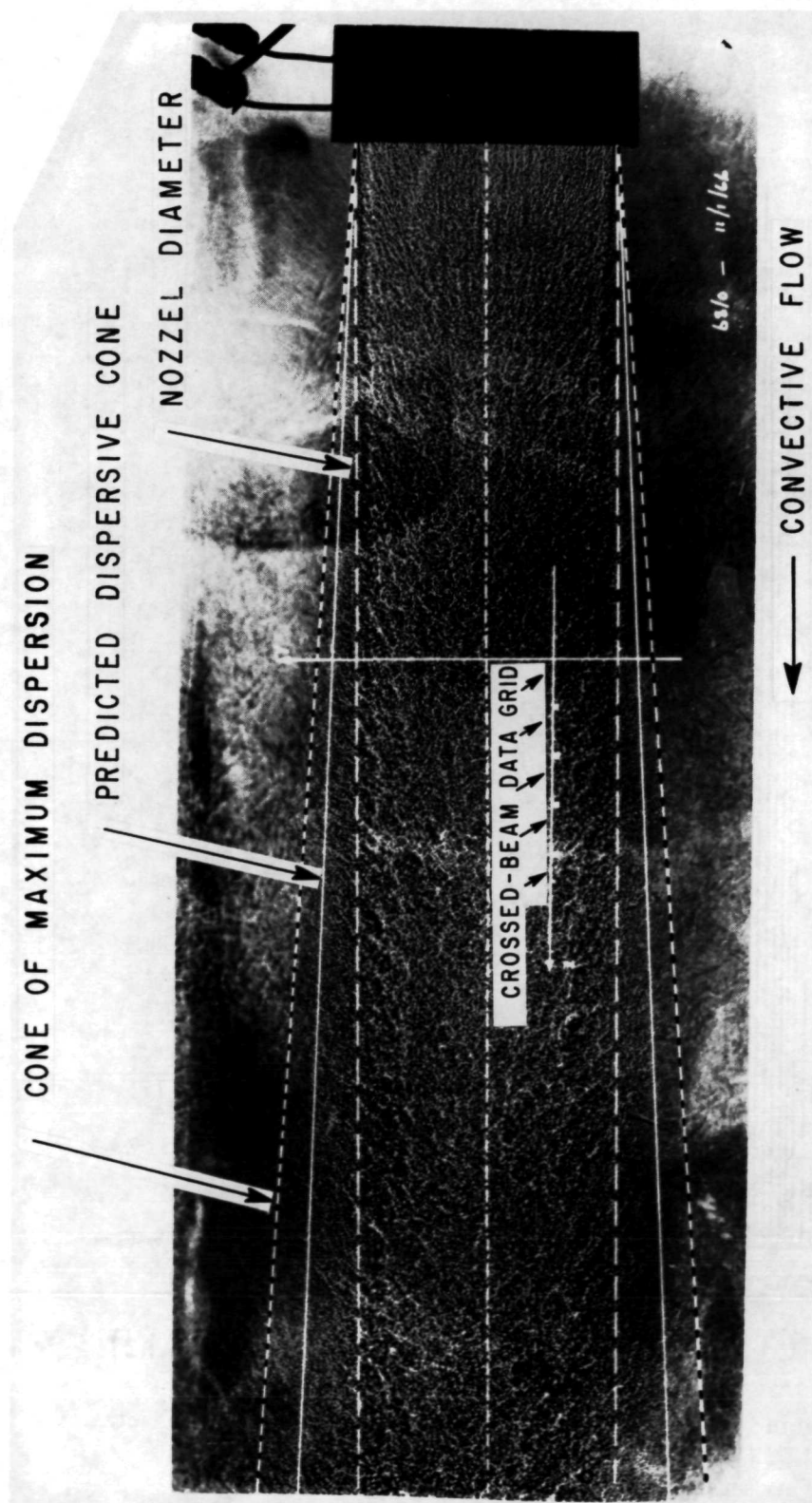


Figure 39. Prediction of lateral scales in cold jet.

turbulent transport is a significant contribution to turbulent investigations, because, for the first time, it accounts for the turbulent flux in the jet flow.

E. Convection and Dispersion in the Atmosphere

The crossed-beam correlation technique has been applied to the measurements of both clear air turbulence [3] and smoke stack emission.² The experiments involving the retrieval of clear-air turbulence convection velocities and scales served to establish the statistical models for recognizing and interpreting nonstationary data. The geometric constraint imposed by using just two single-beam radiometers (Fig. 40) prohibited the application of change statistics which are required for the retrieval of the dispersive transport [30,31]. This limitation was overcome in the smoke plume experiments by introducing a fan-beam radiometer which enables us to retrieve the local data at five different positions along the streamline.

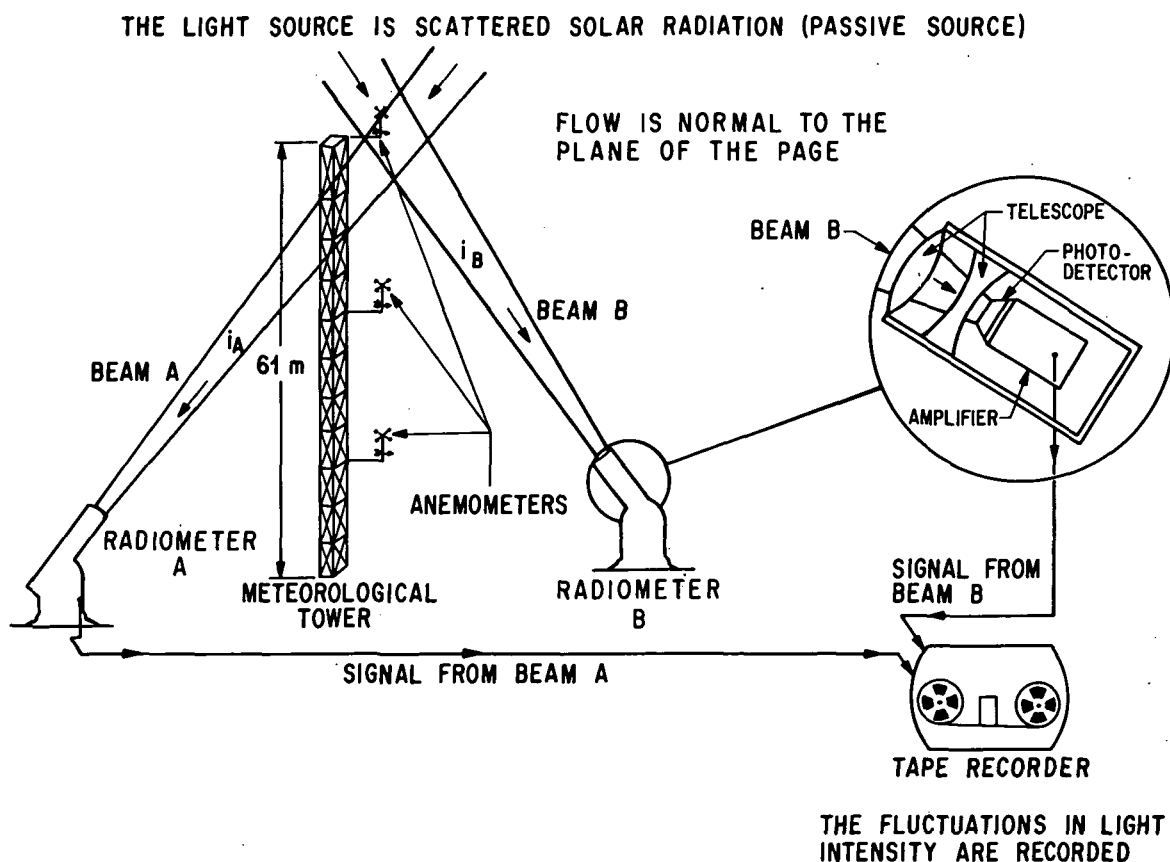


Figure 40. Atmospheric crossed-beam detection system for clear-air turbulence.

2. Bilbro, J.W., et al.: Passive Remote Detection of Smoke Plume Height and Velocity using Correlation Techniques. To be published as a NASA Technical Memorandum.

To apply the statistical techniques discussed for cold jet experiments, we must first obtain a covariance curve which affords a stationary description of the transport process. In the jet plume and the glow discharge experiments, the test for stationarity was done primarily as an aesthetic step to obtain completeness. Such is not the case for atmospheric transport phenomena, because the interval of stationarity in the atmosphere is usually less than an hour in duration [32]. Therefore, the accumulative error must always be checked to determine whether it remains within the error bounds set by the chi-square test. Normally, the accumulative covariance is checked for stationarity and is used when it meets this requirement. If the accumulative error curve indicates that accumulative covariance is nonstationary, then we normalize each piecewise covariance curve and average them to obtain the quantized covariance. The accumulative error of this quantized covariance curve is then checked for stationarity to determine where these results are reliable.

Since the duration for atmospheric stationarity is relatively short even when quantization techniques are used, the local information must be enhanced. Enhancement is obtained by using the statistical error to identify the significant transport information. Such results are shown in Figure 41, where the covariance is plotted as a function of the

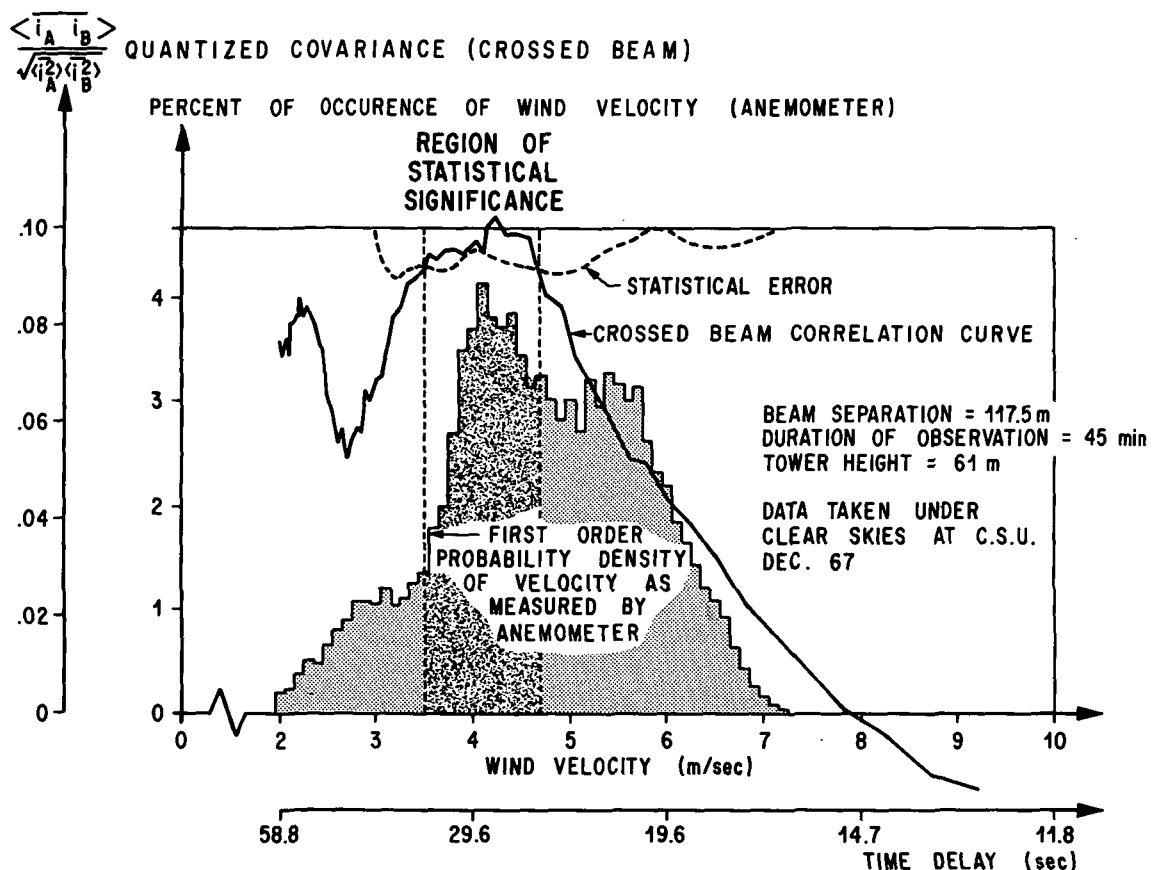


Figure 41. Crossed-beam and anemometer comparisons.

convection velocity and compared to the anemometer velocities taken at the point of beam intersection. To establish the reliability of these results, the probability of retrieving the transport information [equation (39)] is calculated. In this case the probability was 57 percent. In general, the probability of transport retrieval ranged from 50 to 58 percent in the clear-air turbulence experiments, where the transit distance ranged from 0 to 100 meters. The empirical results show that the transport probability decreases as the transit distance increases. These clear-air turbulence measurements were all broadband processes with bandwidth ratios ranging from 4.1 to 6.3 and with an average frequency ranging from 0.01 to 0.02 Hz. The eddy size was determined to range from 73 to 102 meters. The significance of these parameters for the clear-air measurements will become apparent when they are compared with the smoke transport in the atmosphere.

The smokestack emission experiments are similar to the clear-air turbulence experiments in that both are atmospheric experiments and, in addition, the clear-air turbulence experiments are the limiting case for the smoke plume. However, the smoke plume is a dominant source of optical modulations, at least in the near field, and the smoke plume can, like the cold jet, be treated as having a point source origin. These differences permit the baseline of the radiometers to be aligned parallel with the axis of the smoke plume (Fig. 42) rather than perpendicular to the flow, as is done in the clear-air turbulence experiments. As a result of this test configuration, the transit height of the local information being retrieved is a variable which is uniquely determined from the transit time of the convective transport for a given set of geometric parameters. The reason for the different test arrangement is that for clear-air turbulence, which occurs at all altitudes, we wanted to isolate the altitude at which the transport phenomena are being measured; whereas, in smoke-plume measurements, which occur at a unique height, we want the velocities of transport and the height of transport [12]. Outside of these transit height considerations, the statistical retrieval of the convection speed is the same for the smoke transport as for the clear-air turbulence transport.

Figure 43 shows a spatial mapping of the accumulative covariance curves resulting from smoke transport. The mean convective velocity was found to be about 3.2 m/sec at an altitude of 299 meters. Since we obtained a spatial mapping of these covariance curves along the streamline, we can obtain a dispersion velocity. In this case, the average frequency of the first covariance curve according to the wave packet algorithm was 0.0491 Hz and decreased to 0.029 Hz for the last covariance curve. The bandwidth ratio was approximately 1.9 to 3.6, which is clearly smaller than that obtained in clear-air turbulence measurements. The mean dispersion velocity was determined to be 0.6 m/sec which means a lateral mixing rate of 0.2102. The eddy size increases from 34 to 58 meters over a transit distance of 148 meters. This point of observation was about 360 meters from the point of emission. This information for the convective and dispersive transport was incorporated into the smoke plume picture shown in Figure 44. The dispersion cone shown in this figure is in agreement with the observed average rate of dispersion.

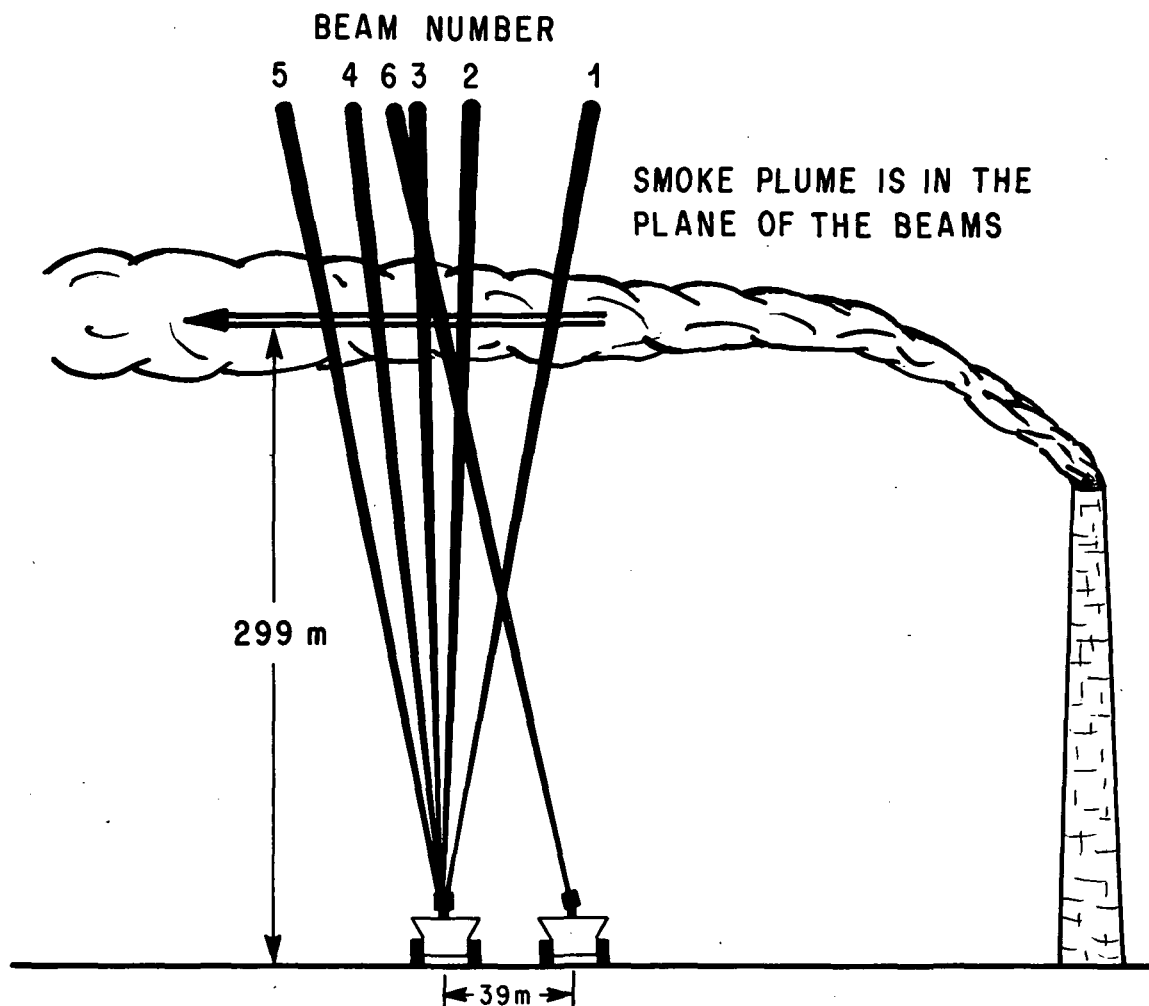


Figure 42. Crossed-beam test arrangement for fan system.

Comparing the smoke plume dispersive transport parameters for the average frequency and the eddy size with the parameters obtained for clear-air turbulence, we infer that the smoke plume is approaching the clear-air parameters. In fact, a linear estimate says that, at about 700 meters downstream of the source, the smoke plume should obtain comparable scales with the atmospheric turbulence.

Our transport probability has an additional function in these measurements, since it serves as a check to verify that the data are from a common streamline. The transport probability ranged between 64 percent for the shortest transit distance to 51 percent for the maximum transit distance. These data show that the probability of retrieving transport information always decreased as the transit distance increased. It is interesting to note that the probability of retrieving transport information is higher for intersecting

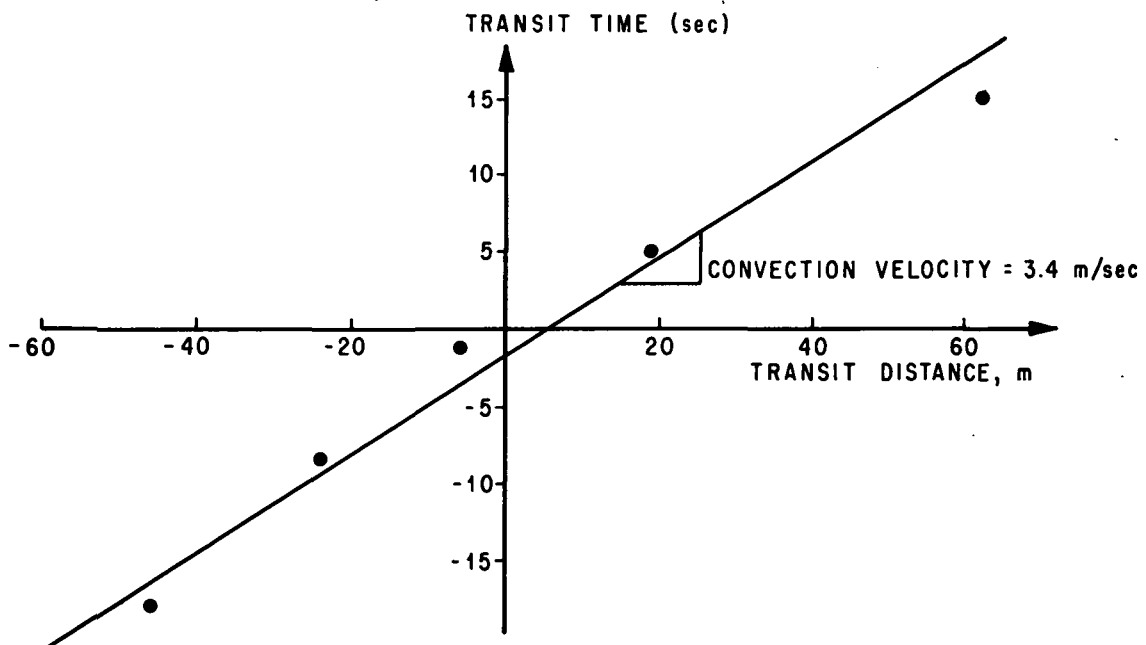
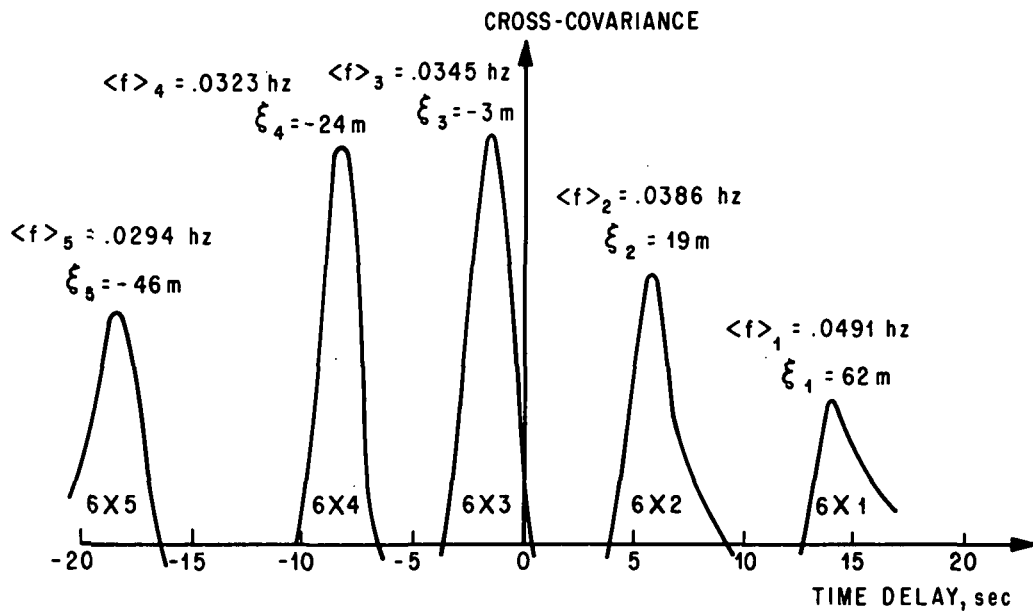


Figure 43. Smoke-plume convection and dispersion transport.

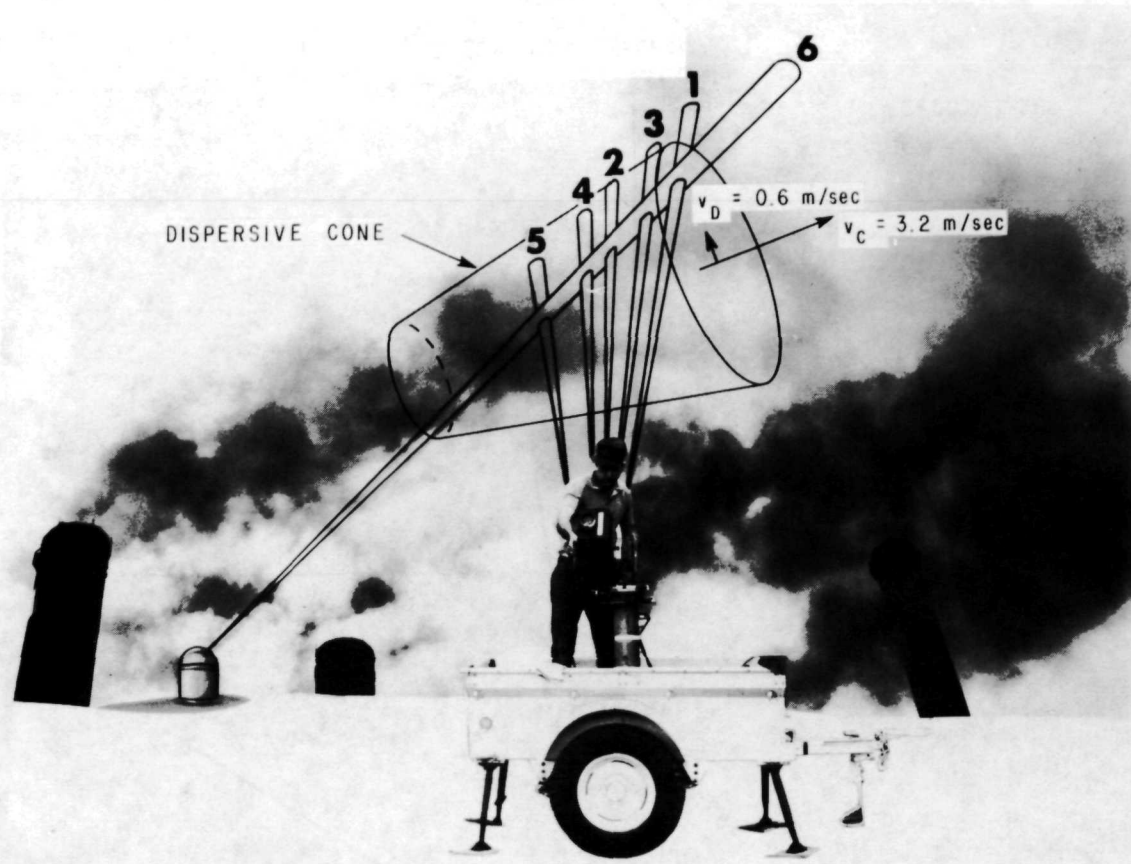


Figure 44. Remote mapping of high stack emissions.

beams in smoke plumes than in clear-air turbulence. This is logical since the smoke signatures are more intense. This higher probability means that the integration times required for correlating the smoke data can be shorter than those required for clear-air turbulence.

SECTION V. SUMMARY AND CONCLUSIONS

The present investigation is the first study of dispersion and convection patterns of fluid transport phenomena using the crossed-beam correlation technique for the analysis of both stationary and nonstationary fluids. This new analysis scheme, as has been demonstrated, permits the separation of the dispersive parameters without extending significantly the data retrieval requirements. This separation of fluid transport was achieved by associating changes in the time domain with convection and changes in the frequency domain with dispersion.

This new information retrieval scheme can be summarized as follows:

1. The data source is the crossed-beam data collection system, which collects the temporal history of the optical fluctuations occurring in the field of view from the beams where they are in sufficient number to ensure spatial mapping. While the retrieval of the convection velocity does not require a spatial mapping, this mapping is highly desirable because it improves the statistical reliability of the results. On the other hand, it is mandatory that a minimum two-point mapping exist for the retrieval of the dispersive parameters. This spatial mapping is the only additional data collection requirement imposed by this analysis.

2. This temporal history of the optical fluctuation is compressed into a correlation curve, from which the convection velocity and scales are directly obtained. To establish the stability levels and to employ statistical discrimination, it is necessary to subdivide the data record into pieces and to use the piecewise accumulative covariance technique. If the data tend to be of a nonstationary nature — that is, if short data recorders are used and thus rapid convergence is required — then it is advantageous to obtain piecewise independence by using the quantized accumulative covariance technique. This technique prevents any segment of the short data record from dominating the accumulative result. The stability tests were extended by the new concept of a transport probability, which affords an integral estimate for the minimum acceptable probability level for the retrieval of significant transport information and a check to determine whether the information is from a common streamline.

3. The second-order cross-covariance is then analyzed for gradients in the average frequency composition. The gradients are the dispersive signature. This analysis is performed by suppressing the temporal information associated with the convective transport, which is the equivalent of changing from a fixed to a moving reference frame. In this way, the second-order covariance curve is transformed into a fourth-order covariance curve. The fourth-order covariance curve is curve-fitted, using regression analysis with the wave packet algorithm to obtain the frequency content in terms of the average frequency, the bandwidth, and the number density. This wave description is then used to obtain the dispersive transport, the lateral mixing scale, and the mixing rate characterizing the transport process.

4. The ratio of the bandwidth to the average frequency affords a systematic procedure for the classification of the various transport processes in accordance with their bandwidth ratio.

This new information retrieval scheme was successfully applied to the analysis of transport phenomena in the glow discharge, cold jet plumes, and air quality investigations, where it was demonstrated that this procedure could meaningfully retrieve the dispersive and convective characteristic of the transport process. The most significant contributions of this analysis procedure are:

1. The dispersion and convection phenomena were precisely defined from the equations of motion in terms of the normal and parallel fluxes of the stream tubes in the average velocity field.

2. In the glow discharge, the ability to associate the longitudinal length scale of a moving striation to the length of the positive column, and the longitudinal length scale of a standing striation with the distance between striations was achieved. This length scale was also an index to the equilibrium of the discharge.

3. The dispersion rate and the lateral mixing scales of the plume in the cold jet were predicted analytically. It was shown that this was in accordance with the empirical observations.

4. In clear-air turbulence measurements, the procedures of suppression of nonstationarity and of peak identification were demonstrated, which resulted in the enhancement of the covariance curve.

5. In the smoke plume studies, the convection and dispersion transport information was again retrieved from the crossed-beam data and was in agreement with the experimental conditions.

From these demonstrations, we can conclude that this information retrieval procedure has successfully made an original contribution to the recognition and interpretation of dispersive and convective transport phenomena in both stationary and nonstationary fluid transport processes.

APPENDIX

THE ENERGY DENSITY WAVE NUMBER SPECTRUM

The objective of this appendix is to establish the requirements for a conservative wave number spectrum, which will be referred to as the energy density wave number spectrum.

It can be shown [33] that the orthogonal form for the Fourier amplitude coefficients about the mean is

$$\begin{aligned} \bar{a}_{jm} &= 2 \sum_{i=0}^m \bar{r}_m \left(\delta_{j, \text{ odd}} \cos \frac{2\pi ki}{n} + \delta_{j, \text{ even}} \sin \frac{2\pi ki}{n} \right) \\ m &= n - 1 \\ j &= 1, 2, 3, \dots, m \\ k &= \frac{j}{2} + \frac{1}{2} \delta_{j, \text{ odd}} \end{aligned} \quad (\text{A.1})$$

where i is the time delay index, j is the amplitude index, k is the wave number, and $\delta_{j,xxxx}$ is the Kronecker delta used to switch between the sinusoidal functions.

The Fourier transpose from the frequency domain to the time domain is

$$[\bar{r}_m] = \sum_{j=1}^m \bar{a}_{jm} \left(\delta_{j, \text{ odd}} \cos \frac{2\pi ki}{n} + \delta_{j, \text{ even}} \sin \frac{2\pi ki}{n} \right), \quad (\text{A.2})$$

where the brackets indicate the frequency transpose of the covariance coefficient. The last two equations form a Fourier transform pair, which permits the interchange of information between the time and frequency domains.

The odd presubscripted amplitude coefficients are commonly referred to as the cospectra (real part),

$$\bar{C}_m = j \rightarrow \text{odd} \bar{a}_m, \quad (\text{A.3})$$

while the even presubscripted amplitude coefficients are referred to as the quadspectra (imaginary part),

$$k_{\bar{Q}}^{\bar{Q}}_m = j \rightarrow \text{even } \bar{a}_m \quad . \quad (\text{A.4})$$

These amplitudes are normally converted to a polar coordinate system whose radius vector, the gain, is

$$k_{\bar{G}}^{\bar{G}}_m = \sqrt{k_{\bar{C}}^{\bar{C}}_m^2 + k_{\bar{Q}}^{\bar{Q}}_m^2} \quad , \quad (\text{A.5})$$

and the phase angle is

$$k_{\bar{\phi}}^{\bar{\phi}}_m = \arctan \frac{k_{\bar{Q}}^{\bar{Q}}_m}{k_{\bar{C}}^{\bar{C}}_m} \quad , \quad (\text{A.6})$$

whose function is similar to that of the time delay in the time domain.

The restrictions imposed on the frequency description of a finite, discrete correlation curve by the orthogonal wave number representation are a bandwidth and a number density. Specifically, the lower frequency limit is set by the total time interval subject to the transformation, while the upper frequency limit is set by the interval of time, $\Delta\tau$, between the covariance coefficients in accordance with the Nyquist uncertainty principle. The number of covariance coefficients, n , that describe the correlation curve sets the number of parameters in the frequency description. Since one parameter is required for the mean value of the correlation curve, there must be less than $n-1$ equally spaced amplitude coefficients.

Next, we shall establish suitable requirements for the spectral normalization. To achieve this, consider the significance of the variance of the covariance

curve, $\langle \Delta_{\tau}^{xy} \bar{r}_m \rangle^2$, in terms of the amplitude coefficients $j\bar{a}_m$, of the Fourier series.

Let us observe that the variance under consideration is not the data variance, $(\Delta x)_m^2$ [equation (19)], commonly used in spectral normalization [8, 34], but is the variance of the correlation curve that is actually being transformed into the frequency domain:

$$\left\langle \Delta_{\tau \bar{r}_m}^{xy} \right\rangle^2 = \frac{1}{n} \sum_{i=0}^n \left(\bar{r}_m^i - \left\langle \Delta_{\tau \bar{r}_m}^{xy} \right\rangle \right)^2 . \quad (A.7)$$

In accordance with equation (A.2), the quantity in parentheses can be expressed as

$$\bar{r}_m^i - \left\langle \Delta_{\tau \bar{r}_m}^{xy} \right\rangle = \sum_{j=2}^n \bar{a}_m^j \left[\delta_{j, \text{ even}} \cos \frac{\pi j i}{n} + \delta_{j, \text{ odd}} \sin \frac{\pi (j-1) i}{n} \right] , \quad (A.8)$$

which is the Fourier transpose. The above result is now substituted into equation (A.7), and the resulting matrix is reduced. When the arguments of the sinusoidal products are different, the uncorrelated terms are zero; thus, we obtain a diagonal matrix of the form

$$\left\langle \Delta_{\tau \bar{r}_m}^{xy} \right\rangle^2 = \sum_{j=2}^n \frac{j \bar{a}_m^2}{n} \sum_{i=0}^n \left[\delta_{j, \text{ even}} \cos^2 \frac{\pi j i}{n} + \delta_{j, \text{ odd}} \sin^2 \frac{\pi (j-1) i}{n} \right] , \quad (A.9)$$

where the summations have been interchanged.

Since a squared sinusoidal function over an integral number of waves is one-half, it follows that equation (A.9) reduces to the form

$$\left\langle \Delta_{\tau \bar{r}_m}^{xy} \right\rangle^2 = \frac{1}{2} \sum_{j=2}^n j \bar{a}_m^2 . \quad (A.10)$$

Obviously, the same result is obtained when the time lag range is extended to include negative time delays. Equation (A.10) enables us to define an orthonormal wave number spectrum:

$$1 = \frac{1}{2 \left\langle \Delta_{\tau}^{xy} \right\rangle_m^2} \sum_{j=2}^n j \bar{a}_m^2 \quad . \quad (A.11)$$

We can now define the terms describing the spectrum. When the amplitude coefficients are squared, they will be called intensity coefficients (same terminology as in geometric optics). Since the intensity coefficients describe the relative energy content in the covariance curve as a function of wave number, this spectrum is referred to formally as the energy density wave number spectrum. This is a conservative spectrum.

The maximum number of linearly independent wave numbers in the representation for the frequency domain is $(n-1)/2$, where n is the number of covariance coefficients being transformed. This can be demonstrated by the following argument. The amplitude of the gain is

$$k^G = \frac{1}{n+1} \sum_{j=0}^n j^r \exp \left\{ i \frac{2\pi k j}{n+1} \right\} \quad (A.12)$$

$k = 1, 2, 3, \dots, n-1, \dots$

where i stands for the square root of minus one. In complex notation, the amplitude of the gain can be expressed in terms of the cospectra and quad-spectra as

$$k^G = k^C + i k^Q \quad . \quad (A.13)$$

The amplitude of the gain [equation (A.12)] can then be expressed in trigonometric form as

$$k^G = \frac{1}{n+1} \sum_{j=0}^n j^r \left(\cos \frac{2\pi k j}{n+1} + i \sin \frac{2\pi k j}{n+1} \right) \quad . \quad (A.14)$$

For manipulative ease, we now write this equation [equation (A.14)] in terms of the real and imaginary parts:

$$k^C = \frac{1}{n+1} \sum_{j=0}^n j^r \cos \left(\frac{2\pi k j}{n+1} \right) \quad (\text{A.15})$$

$$k^Q = \frac{1}{n+1} \sum_{j=0}^n j^r \sin \left(\frac{2\pi k j}{n+1} \right) \quad . \quad (\text{A.16})$$

Observe that when the wave number is zero ($k = 0$), then the amplitude gain is

$$k=0^G = \frac{1}{n+1} \sum_{j=0}^n j^r \quad , \quad (\text{A.17})$$

which is the mean. This is why the wave number spectrum starts at one and has only $n-1$ terms; i.e., one parameter of the spectrum is used for the mean value of the covariance curve.

Next, consider the cospectra [equation (A.15)]. The cospectra for the n th wave number is

$$n^C = \frac{1}{n+1} \sum_{j=0}^n j^r \cos \left(\frac{2\pi n j}{n+1} \right) \quad . \quad (\text{A.18})$$

Using the trigonometric angle-sum relation, the above equation can be written

$$n^C = \frac{1}{n+1} \sum_{j=0}^n j^r \left[\cos(2\pi j) \cos \left(\frac{2\pi j}{n+1} \right) + \sin(2\pi j) \sin \left(\frac{2\pi j}{n+1} \right) \right] \quad , \quad (\text{A.19})$$

where

$$\cos 2\pi j = 1 \quad (\text{A.20})$$

and

$$\sin 2\pi j = 0 \quad .$$

Substituting the last result into equation (A.19), we obtain

$${}_nC = \frac{1}{n+1} \sum_{j=0}^n j^r \cos \frac{2\pi}{n+1} j, \quad (A.21)$$

which is simply

$${}_{k=n}C = {}_{k=1}C \quad . \quad (A.22)$$

It logically follows then that, in general,

$${}_kC = {}_{n-k+1}C, \quad 1 \leq k \leq \frac{n}{2} \quad . \quad (A.23)$$

The quadspectra [equation (A.16)] has the same interrelationship as the cospectra. This is readily seen upon examination of the n th term that results from the application of the trigonometric angle-sum relation:

$$\begin{aligned} {}_nQ = \frac{1}{n+1} \sum_{j=0}^n j^r & \left[\cos(2\pi j) \sin \frac{2\pi j}{n+1} \right. \\ & \left. + \sin(2\pi j) \cos \frac{2\pi j}{n+1} \right] \quad . \end{aligned} \quad (A.24)$$

Again using the relations given in equation (A.20), we obtain the fact that

$${}_{k=n}Q = {}_{k=1}Q \quad (A.25)$$

or in general that

$$k^Q = {}_{n-k+1}^Q, \quad 1 \leq k \leq \frac{n}{2}. \quad (\text{A.26})$$

This derivation just proves the limits placed on the wave number representation.

Incorporating the normalization and limits just derived, we can write the Fourier transform for the wave number spectrum for the amplitude density and intensity density representations as:

1. Amplitude density representation.

a. Cospectral amplitude density:

$$k^{\bar{\bar{c}}}_m = \frac{2}{(2n+1) \left\langle \Delta_{\tau}^{\bar{\bar{r}}}_m \right\rangle} \left[{}_0^{\bar{\bar{r}}}_m + \sum_{j=1}^n \left({}_j^{\bar{\bar{r}}}_m + {}_{-j}^{\bar{\bar{r}}}_m \right) \cos \frac{2\pi k j}{n} \right]. \quad (\text{A.27})$$

b. Quadspectral amplitude density:

$$k^{\bar{\bar{q}}}_m = \frac{2}{(2n+1) \left\langle \Delta_{\tau}^{\bar{\bar{r}}}_m \right\rangle} \left[\sum_{j=1}^n \left({}_j^{\bar{\bar{r}}}_m + {}_{-j}^{\bar{\bar{r}}}_m \right) \sin \frac{2\pi k j}{n} \right] \quad (\text{A.28})$$

where $k = 1, 2, 3, \dots, n/2$.

The lower case spectral coefficients indicate the normalization of the coefficients; whereas, the capital spectral coefficients are the unnormalized coefficients. The rectangular coordinate system discussed above has the following counterpart in the polar coordinate system:

c. Gain amplitude density:

$$\overline{g}_m = \sqrt{\overline{c}_m^2 + \overline{q}_m^2} \quad . \quad (A.29)$$

d. The phase:

$$\overline{\phi}_m = \arctan \frac{\overline{q}_m}{\overline{c}_m} \quad . \quad (A.30)$$

2. Energy density representation.

a. Cospectral intensity density:

$$\overline{\chi}_m = \overline{c}_m^2 \quad . \quad (A.31)$$

b. Quadspectral intensity density:

$$\overline{\psi}_m = \overline{q}_m^2 \quad . \quad (A.32)$$

c. Gain intensity density (in polar form):

$$\overline{\gamma}_m = \overline{\chi}_m + \overline{\psi}_m \quad . \quad (A.33)$$

d. Phase:

$$\overline{\theta}_m = \arctan \frac{\overline{\psi}_m}{\overline{\chi}_m} \quad . \quad (A.34)$$

The energy density gain has the property that

$$\sum_{k=1}^{n/2} \bar{\gamma}_m = 1 \quad . \quad (A.35)$$

It should be recognized that the averaging notation and the post subscript are carried over from the covariance coefficient to indicate the way this coefficient was obtained.

These formulations for the spectra were tested by transforming the correlation curve in Figure 12 into the frequency domain. The results are shown in Tables A-1 through A-4 (the details of the calculations will be discussed later). From an inspection of these results, we can see that the majority of the calculations are insignificant. The next objective is to reduce the calculations of these insignificant coefficients.

By using the properties inherent to the energy-density representation, a criterion for the minimum level of acceptable spectral intensity can now be developed. The spectral energy of the correlation curve in Figure 12 was concentrated in 9 of the 400 wave numbers in this description, while the remaining 391 wave numbers contained less than 1 percent of the energy associated with the covariance. From a comparison of the known input parameters with these results, it is obvious that these 391 wave numbers represent the intensity level of calculation noise affording no insight into the behavior of the phenomena; therefore, a set of criteria to discriminate the significant energy bearing wave numbers from the noise bearing wave number is essential.

The term "noise" is the key to the establishment of this cutoff level. A white noise process is a purely random one characterized by a time series, consisting of random impulses, that results in a cross-covariance curve of zero magnitude at all time lags and an autocovariance curve with a delta function at zero time delay. Since a preferred frequency would not result in this kind of correlation curve, the intensity of the gain must therefore be of the same magnitude for all wave numbers. Because the energy density representation has the property that the sum of the gain intensities is one [equation (A.35)], it then, intuitively, follows that the intensity of the white noise gain is

$$\gamma_{\text{white noise}} = \frac{1}{n} \quad . \quad (A.36)$$

This result represents the white noise level which is composed of an equal distribution of energy between all wave numbers; therefore, an energy less than the white noise level can be viewed as a lack of significant energy. Thus, the intensities that are less than the white noise level can be legitimately rejected as being below the intelligence cutoff.

-----INPUT SPECTRUM-----FREQUENCY RANGE = 0.500 HZ TO 1.500 HZ
 -----NUMBER OF EQUAL AMPLITUDE COSINE WAVES = 21
 -----FREQUENCY INTERVAL BETWEEN WAVES = 0.05 HZ

RESULTING OUTPUT SPECTRUM

MINIMUM ACCEPTABLE GAIN INTENSITY = 0.25031

WAVE NUMBER	FREQUENCY	COORDINATE SYSTEM				POLAR	PERCENT OF ACCUMULATIVE ENERGY	
		CARTESIAN		POLAR				
		COSPECTRA		QUADSPECTRA				
		AMPLITUDE	INTENSITY	AMPLITUDE	INTENSITY	AMPLITUDE	INTENSITY	PHASE DEGREE
1	1.12500	0.0003599	0.0011	0.0003599	0.0011	0.0003599	0.0011	0.0011
2	1.17500	0.0004779	0.0022	0.0004779	0.0022	0.0004779	0.0022	0.0022
3	1.22500	0.0008461	0.0062	0.0008461	0.0062	0.0008461	0.0062	0.0062
4	1.27500	0.0013254	0.0094	0.0013254	0.0094	0.0013254	0.0094	0.0094
5	1.32500	0.00129157	0.0093	0.00129157	0.0093	0.00129157	0.0093	0.0093
6	1.37500	0.00112684	0.0076	0.00112684	0.0076	0.00112684	0.0076	0.0076
7	1.42500	0.00124283	0.0078	0.00124283	0.0078	0.00124283	0.0078	0.0078
8	1.47500	0.00114251	0.0074	0.00114251	0.0074	0.00114251	0.0074	0.0074
9	1.52500	0.00124498	0.0078	0.00124498	0.0078	0.00124498	0.0078	0.0078
10	1.57500	0.00112502	0.0076	0.00112502	0.0076	0.00112502	0.0076	0.0076
11	1.62500	0.00129691	0.0093	0.00129691	0.0093	0.00129691	0.0093	0.0093
12	1.67500	0.0005059	0.0025	0.0005059	0.0025	0.0005059	0.0025	0.0025
13	1.72500	0.0008472	0.0062	0.0008472	0.0062	0.0008472	0.0062	0.0062
14	1.77500	0.00124285	0.0078	0.00124285	0.0078	0.00124285	0.0078	0.0078
15	1.82500	0.0012724	0.0079	0.0012724	0.0079	0.0012724	0.0079	0.0079
16	1.87500	0.00114251	0.0074	0.00114251	0.0074	0.00114251	0.0074	0.0074
17	1.92500	0.00114454	0.0075	0.00114454	0.0075	0.00114454	0.0075	0.0075
18	1.97500	0.0011159	0.0073	0.0011159	0.0073	0.0011159	0.0073	0.0073
19	2.02500	0.0010946	0.0071	0.0010946	0.0071	0.0010946	0.0071	0.0071
20	2.07500	0.0009799	0.0061	0.0009799	0.0061	0.0009799	0.0061	0.0061
21	2.12500	0.00081673	0.0050	0.00081673	0.0050	0.00081673	0.0050	0.0050
22	2.17500	0.0007581	0.0045	0.0007581	0.0045	0.0007581	0.0045	0.0045
23	2.22500	0.0006928	0.0040	0.0006928	0.0040	0.0006928	0.0040	0.0040
24	2.27500	0.0006049	0.0034	0.0006049	0.0034	0.0006049	0.0034	0.0034
25	2.32500	0.0005043	0.0028	0.0005043	0.0028	0.0005043	0.0028	0.0028
26	2.37500	0.0003959	0.0020	0.0003959	0.0020	0.0003959	0.0020	0.0020
27	2.42500	0.0003324	0.0017	0.0003324	0.0017	0.0003324	0.0017	0.0017
28	2.47500	0.0002959	0.0015	0.0002959	0.0015	0.0002959	0.0015	0.0015
29	2.52500	0.0002625	0.0013	0.0002625	0.0013	0.0002625	0.0013	0.0013
30	2.57500	0.0002247	0.0011	0.0002247	0.0011	0.0002247	0.0011	0.0011
31	2.62500	0.0001927	0.0009	0.0001927	0.0009	0.0001927	0.0009	0.0009
32	2.67500	0.0001641	0.0008	0.0001641	0.0008	0.0001641	0.0008	0.0008
33	2.72500	0.0001395	0.0007	0.0001395	0.0007	0.0001395	0.0007	0.0007
34	2.77500	0.0001181	0.0006	0.0001181	0.0006	0.0001181	0.0006	0.0006
35	2.82500	0.0001069	0.0005	0.0001069	0.0005	0.0001069	0.0005	0.0005
36	2.87500	0.0000918	0.0004	0.0000918	0.0004	0.0000918	0.0004	0.0004
37	2.92500	0.0000814	0.0004	0.0000814	0.0004	0.0000814	0.0004	0.0004
38	2.97500	0.0000731	0.0003	0.0000731	0.0003	0.0000731	0.0003	0.0003
39	3.02500	0.0000631	0.0003	0.0000631	0.0003	0.0000631	0.0003	0.0003
40	3.07500	0.0000542	0.0002	0.0000542	0.0002	0.0000542	0.0002	0.0002
41	3.12500	0.0000477	0.0002	0.0000477	0.0002	0.0000477	0.0002	0.0002
42	3.17500	0.0000411	0.0002	0.0000411	0.0002	0.0000411	0.0002	0.0002
43	3.22500	0.0000355	0.0002	0.0000355	0.0002	0.0000355	0.0002	0.0002
44	3.27500	0.0000303	0.0002	0.0000303	0.0002	0.0000303	0.0002	0.0002
45	3.32500	0.0000259	0.0002	0.0000259	0.0002	0.0000259	0.0002	0.0002
46	3.37500	0.0000224	0.0002	0.0000224	0.0002	0.0000224	0.0002	0.0002
47	3.42500	0.0000196	0.0002	0.0000196	0.0002	0.0000196	0.0002	0.0002
48	3.47500	0.0000172	0.0002	0.0000172	0.0002	0.0000172	0.0002	0.0002
49	3.52500	0.0000150	0.0002	0.0000150	0.0002	0.0000150	0.0002	0.0002
50	3.57500	0.0000130	0.0002	0.0000130	0.0002	0.0000130	0.0002	0.0002
51	3.62500	0.0000112	0.0002	0.0000112	0.0002	0.0000112	0.0002	0.0002
52	3.67500	0.0000095	0.0002	0.0000095	0.0002	0.0000095	0.0002	0.0002
53	3.72500	0.0000080	0.0002	0.0000080	0.0002	0.0000080	0.0002	0.0002
54	3.77500	0.0000066	0.0002	0.0000066	0.0002	0.0000066	0.0002	0.0002
55	3.82500	0.0000054	0.0002	0.0000054	0.0002	0.0000054	0.0002	0.0002
56	3.87500	0.0000043	0.0002	0.0000043	0.0002	0.0000043	0.0002	0.0002
57	3.92500	0.0000036	0.0002	0.0000036	0.0002	0.0000036	0.0002	0.0002
58	3.97500	0.0000030	0.0002	0.0000030	0.0002	0.0000030	0.0002	0.0002
59	4.02500	0.0000025	0.0002	0.0000025	0.0002	0.0000025	0.0002	0.0002
60	4.07500	0.0000021	0.0002	0.0000021	0.0002	0.0000021	0.0002	0.0002
61	4.12500	0.0000018	0.0002	0.0000018	0.0002	0.0000018	0.0002	0.0002
62	4.17500	0.0000015	0.0002	0.0000015	0.0002	0.0000015	0.0002	0.0002
63	4.22500	0.0000013	0.0002	0.0000013	0.0002	0.0000013	0.0002	0.0002
64	4.27500	0.0000011	0.0002	0.0000011	0.0002	0.0000011	0.0002	0.0002
65	4.32500	0.0000009	0.0002	0.0000009	0.0002	0.0000009	0.0002	0.0002
66	4.37500	0.0000008	0.0002	0.0000008	0.0002	0.0000008	0.0002	0.0002
67	4.42500	0.0000007	0.0002	0.0000007	0.0002	0.0000007	0.0002	0.0002
68	4.47500	0.0000006	0.0002	0.0000006	0.0002	0.0000006	0.0002	0.0002
69	4.52500	0.0000005	0.0002	0.0000005	0.0002	0.0000005	0.0002	0.0002
70	4.57500	0.0000004	0.0002	0.0000004	0.0002	0.0000004	0.0002	0.0002
71	4.62500	0.0000003	0.0002	0.0000003	0.0002	0.0000003	0.0002	0.0002
72	4.67500	0.0000003	0.0002	0.0000003	0.0002	0.0000003	0.0002	0.0002
73	4.72500	0.0000002	0.0002	0.0000002	0.0002	0.0000002	0.0002	0.0002
74	4.77500	0.0000002	0.0002	0.0000002	0.0002	0.0000002	0.0002	0.0002
75	4.82500	0.0000002	0.0002	0.0000002	0.0002	0.0000002	0.0002	0.0002
76	4.87500	0.0000002	0.0002	0.0000002	0.0002	0.0000002	0.0002	0.0002
77	4.92500	0.0000002	0.0002	0.0000002	0.0002	0.0000002	0.0002	0.0002
78	4.97500	0.0000002	0.0002	0.0000002	0.0002	0.0000002	0.0002	0.0002
79	5.02500	0.0000002	0.0002	0.0000002	0.0002	0.0000002	0.0002	0.0002
80	5.07500	0.0000002	0.0002	0.0000002	0.0002	0.0000002	0.0002	0.0002
81	5.12500	0.0000002	0.0002	0.0000002	0.0002	0.0000002	0.0002	0.0002
82	5.17500	0.0000002	0.0002	0.0000002	0.0002	0.0000002	0.0002	0.0002
83	5.22500	0.0000002	0.0002	0.0000002	0.0002	0.0000002	0.0002	0.0002
84	5.27500	0.0000002	0.0002	0.0000002	0.0002	0.0000002	0.0002	0.0002
85	5.32500	0.0000002	0.0002	0.0000002	0.0002	0.0000002	0.0002	0.0002
86	5.37500	0.0000002	0.0002	0.0000002	0.0002	0.0000002	0.0002	0.0002
87	5.42500	0.0000002	0.0002	0.0000002	0.0002	0.0000002	0.0002	0.0002
88	5.47500	0.0000002	0.0002	0.0000002	0.0002	0.0000002	0.0002	0.0002
89	5.52500	0.0000002	0.0002	0.0000002	0.0002	0.0000002	0.0002	0.0002
90	5.57500	0.0000002	0.0002	0.0000002	0.0002	0.0000002	0.0002	0.0002
91	5.62500	0.0000002	0.0002	0.0000002	0.0002	0.0000002	0.0002	0.0002
92	5.67500	0.0000002	0.0002	0.0000002	0.0002	0.0000002	0.0002	0.0002
93	5.72500	0.0000002	0.0002	0.0000002	0.0002	0.0000002	0.0002	0.0002
94	5.77500	0.0000002	0.0002	0.0000002	0.0002	0.0000002	0.0002	0.0002
95	5.82500	0.0000002	0.0002	0.0000002	0.0002	0.0000002	0.0002	0.0002
96	5.87500	0.0000002	0.0002	0.0000002	0.0002	0.0000002	0.0002	0.0002
97	5.92500	0.0000002	0.0002	0.0000002	0.0002	0.0000002	0.0002	0.0002
98	5.97500	0.0000002	0.0002	0.0000002	0.0002	0.0000002	0.0002	0.0002
99	6.02500	0.0000002	0.0002	0.0000002	0.0002	0.0000002	0.0002	0.0002
100	6.07500	0.0000002	0.0002	0.0000002	0.0002	0.0000002	0.0002	0.0002

-FREQUENCY RANGE = 0.500 HZ TO 1.500 HZ
NUMBER OF EQUAL AMPLITUDE COSINE WAVES = 21
FREQUENCY INTERVAL BETWEEN WAVES = 0.05 HZ

MINIMUM ACCEPTABLE GAIN INTENSITY = 0.25031

91

RESULTING OUTPUT SPECTRUM

MINIMUM ACCEPTABLE GAIN INTENSITY = 0.2531

92

RESULTING OUTPUT SPECTRUM

MINIMUM ACCEPTABLE GAIN INTENSITY = 0.25031

```

WAVE * FREQUENCY ** COORDINATE SYSTEM ** POLAR ** PERCENT OF
NUMBER * ** ** ** ** ** ** ** ** ** ** ** ** ** ** ** **   ACCUMULATIVE
= ** CUSPECTRA ** QUASPECTRA ** GAIN ** PHASE ** ENERGY

```

[illegible]

The intelligence cutoff criteria, along with the conservative property associated with the energy density representation, are the ingredients for a spectral intelligence bandwidth which prevents blind data ingurgitation. When the sum of the gain intensities is

$$\sum_{k=1}^k \text{cut-off} \quad \bar{\gamma}_m = 1 - \gamma_{\text{white noise}} ; \quad (\text{A.37})$$

then, by the conservative property [equation (A.35)] afforded by this representation, we know that the remaining gain intensities will not afford any additional significant intelligence. This implies that we have found the upper limit of the intelligence bandwidth, and that the spectral calculations can be safely terminated without a possible loss of significant information. The lower limit of the intelligence bandwidth is set by where the spectral intensities first exceed the intelligence cutoff.

Applying the concepts developed in this appendix to the transformation of a correlation curve obtained from atmospheric turbulence data, we obtained the energy density spectrum shown in Figure A-1. Use of the traditional Fourier spectrum analysis

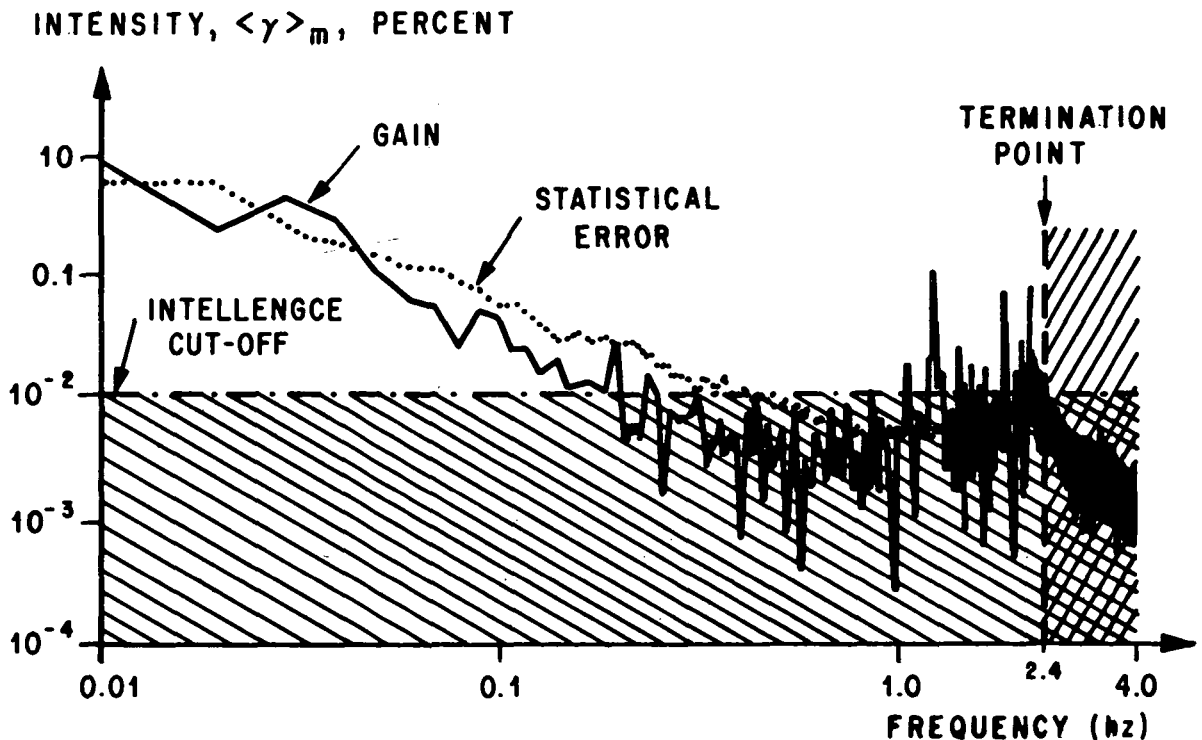


Figure A-1. Atmospheric energy density spectrum.

techniques [8,34] would require an explanation of the entire spectrum. Use of the intelligence cutoff criteria isolates the spectrum into two regions: from 0.01 to 0.26 Hz and from 1.0 to 2.4 Hz.

The significant point which has been established is that the intelligence cutoff criterion affords a systematic noise suppression which enhances the spectral intelligence. The intelligence termination point, on the other hand, is just a labor-saving scheme, permitting us to reduce the amount of wasted time and energy in searching regions in wave number space void of significant information. In this example, computational time could be reduced by one-third if we stop calculating the spectral coefficients after we reach the intelligence termination point.

George C. Marshall Space Flight Center

National Aeronautics and Space Administration

Marshall Space Flight Center, Alabama, October 20, 1972

REFERENCES

1. Fisher, M.J.; and Krause, F.R.: The Crossed-Beam Correlation Technique. J. Fluid Mech., vol. 28, part 4, 1967.
2. Fisher, M.J.; and Johnston, K.D.: Turbulence Measurements in Supersonic, Shock-Free Jets by the Optical Crossed-Beam Method. NASA TN D-5206, February 1970.
3. Stephens, J.B.; Sandborn, V.A.; and Montgomery, A.J.: Remote Wind Detection with the Crossed-Beam Method at Tower Heights. NASA TM X-53782, October 1968.
4. Stephens, J.B.; and Thomison, J.B.: Optical Detection of Moving Striations with the Cross-Correlation Technique. NASA TM X-64505, March 1970.
5. Thomison, J.B.; and Stephens, J.B.: Feasibility of Crossed-Beam Applications to Combustive Flows. NASA TM X-64505, March 1970.
6. Krause, F.R.; and Fisher, M.J.: A Unified Treatment of Turbulent Fluxes in Multi-component and Hot Flows. NASA TM X-53189, October 1964.
7. Lin, C.C., ed.: Turbulent Flows and Heat Transfer, Vol. 5, High Speed Aerodynamics and Jet Propulsion. Princeton University Princeton University Press, 1959.
8. Bendat, J.S.; and Piersol, A.G.: Measurement and Analysis of Random Data. John Wiley & Sons, Inc., 1966.
9. Crandall, S.H.; and Mark, W.D.: Random Vibrations in Mechanical Systems. Academic Press, 1963.
10. Krause, F.R.; and Hablutzel, B.C.: Noise Elimination by Piecewise Cross-Correlation of Photometer Outputs. NASA TM X-53782, October 15, 1968.
11. Jayroe, R.R., Jr.; and Su, M.Y.: Optimum Averaging Time of Meteorological Data with Time Dependent Means. NASA TM X-53782, 1968.
12. Su, M.Y.; Stephens, J.B.; and Phillips, M.: The Theory for the Determination of Wind Velocity and the Associated Altitude by the Cross-Beam Technique. NASA TM X-53782, 1968.
13. Born, M.; and Wolf, E.: Principles of Optics. The Macmillian Co., 1964.

REFERENCES (Continued)

14. Stephens, J.B.: Selected Stationary and Nonstationary Applications of the Correlation Technique. Specialist Paper, Physics Department, Oklahoma University, March 1971.
15. Johnson, G.; and Montgomery, A.J.: Survey of Detectors and Dynamic Calibration Methods for Remote Sensing Systems. NASA CR-751, April 1967.
16. Stephens, J.B.; and Hablutzel, B.C.: The Reliability Coefficient for Cross-Covariance. NASA TM X-64505, March 1970.
17. Korn, G.A.; and Korn, T.M.: Mathematical Handbook for Scientists and Engineers. McGraw-Hill Book Company, 2nd Edition, 1968.
18. Damkevala, R.J.; and Kadrmas, K.A.: Turbulence Measurements with an Infrared Crossed-Beam System Near 4.3 Microns. AIAA 8th Aerospace Sciences Meeting, New York, New York, January 1970, AIAA Paper 70-235.
19. Krause, F.R.; and Stephens, J.B.: Remote Detection of Local Temperatures and Local Partial Pressures with Crossed-Beam Spectroscopy. NASA TM X-5371, October 1967.
20. Fisher, M.J.; and Damkevala, R.J.: Fundamental Considerations of the Crossed-Beam Correlation Technique. NASA CR-61252, 1969.
21. Cobine, J.D.: Gaseous Conductors, Theory and Engineering Applications. Dover Publications, Inc., 1958.
22. Von Engel, A.: Ionized Gases. Oxford University Press, 1965.
23. Donahue, T.; and Dieke, G.H.: Striation Velocities. Phys. Rev., vol. 81, no. 248, 1951.
24. Garscadden, A.; and Lee, D.A.: Forward and Backward Moving Striations in the Constricted Discharge. Int. J. Electronics, vol. 20, no. 6, 1966, pp. 567-581.
25. Wachowski, A.; and Phillips, M.R.: Computer Program for Crossed-Beam Studies of Clear Air Turbulence Program Description (MLTCOR). Appendices C and D by F.R. Krause, NASA CR-61314, September 1969.
26. Stephens, J.B.; and Locklin, J.M.: Correlation Curves of Retroactively Filtered Data. NASA TM X-64505, March 1970.

REFERENCES (Concluded)

27. Corrsin, S.; and Kistler, A.L.: The Free-Stream Boundaries of Turbulent Flows. NACA Report 1244, 1955.
28. Chapman, S.; and Cowling, T.G.: The Mathematical Theories of Non-Uniform Gases. 2nd Edition, Cambridge, The University Press, 1960.
29. Hinze, J.O.: Turbulence. McGraw-Hill Book Co., Inc., 1959.
30. Krause, F.R.; LaFrance, J.C.; Parajape, S.V.; and Stephens, J.B.: Feasibility and Potential of Atmospheric Crossed-Beam Experiments. NASA TM X-53568, 1966.
31. Heybey, W.H.: The Use of a Ground-Based Multiple-Beam Detector in Crossed-Beam Atmospheric Experimentation. NASA TM X-53782, January 1969.
32. Neuberger, H.H.; and Stephens, F.B.: Weather and Man. Prentice Hall, Inc., 1948.
33. Stephens, J.B.; Locklin, J.M.; and Pooley, J.C.: Cross-Power Spectral Analysis for Atmospheric Cross-Beam Data. NASA TM X-64505, March 1970.
34. Jenkins, G.M.; and Watts, D.G.: Spectral Analysis and its Applications. Holden-Day, Inc., 1969.



POSTMASTER: If Undeliverable (Section 158
Postal Manual) Do Not Return

"The aeronautical and space activities of the United States shall be conducted so as to contribute . . . to the expansion of human knowledge of phenomena in the atmosphere and space. The Administration shall provide for the widest practicable and appropriate dissemination of information concerning its activities and the results thereof."

—NATIONAL AERONAUTICS AND SPACE ACT OF 1958

NASA SCIENTIFIC AND TECHNICAL PUBLICATIONS

TECHNICAL REPORTS: Scientific and technical information considered important, complete, and a lasting contribution to existing knowledge.

TECHNICAL NOTES: Information less broad in scope but nevertheless of importance as a contribution to existing knowledge.

TECHNICAL MEMORANDUMS: Information receiving limited distribution because of preliminary data, security classification, or other reasons. Also includes conference proceedings with either limited or unlimited distribution.

CONTRACTOR REPORTS: Scientific and technical information generated under a NASA contract or grant and considered an important contribution to existing knowledge.

TECHNICAL TRANSLATIONS: Information published in a foreign language considered to merit NASA distribution in English.

SPECIAL PUBLICATIONS: Information derived from or of value to NASA activities. Publications include final reports of major projects, monographs, data compilations, handbooks, sourcebooks, and special bibliographies.

TECHNOLOGY UTILIZATION PUBLICATIONS: Information on technology used by NASA that may be of particular interest in commercial and other non-aerospace applications. Publications include Tech Briefs, Technology Utilization Reports and Technology Surveys.

Details on the availability of these publications may be obtained from:

SCIENTIFIC AND TECHNICAL INFORMATION OFFICE

NATIONAL AERONAUTICS AND SPACE ADMINISTRATION
Washington, D.C. 20546